AN ABSTRACT OF THE THESIS OF

WILLIAM ALPHONSUS MANNION for the Ph. D.
(Name) (Degree)

in CHEMISTRY presented on May 5, 1969
(Major) (Date)

Title: A STUDY OF THE Mn^{+2} AND Pb^{+2}-Mn^{+2} IMPURITY SYSTEMS IN ALKALI CHLORIDES

Abstract approved: Redacted for Privacy
Dr. William J. Fredericks

The diffusion of manganese ion in sodium and potassium chloride was studied. The NaCl:Mn^{+2} diffusion can be represented by

$$D_s = 5.87 \times 10^{-4} \text{ cm}^2/\text{sec } e^{-20,500 \text{ cal}/RT}$$

between the temperatures of 449 and 656°C. The free energy of association of the manganese-vacancy complex is

$$-\Delta G(ev) = -1.090 + 5.0 \times 10^{-4} T.$$

The KCl:Mn^{+2} diffusion proved to be more complicated than NaCl:Mn^{+2}. Between the temperatures of 457 and 482°C the impurity-vacancy diffusion coefficient can be represented by

$$D_s = 1.3 \times 10^{10} \text{ cm}^2/\text{sec } e^{-63,000 \text{ cal}/RT}.$$

From 512 to 653°C D_s is given by

$$D_s = 1.16 \times 10^{-2} \text{ cm}^2/\text{sec } e^{-24,300 \text{ cal}/RT},$$

and in this temperature range the free energy of association is

$$-\Delta G(\text{ev}) = -1.598 + 1.06 \times 10^{-3} T.$$

A "phase change" theory has been postulated to account for the abrupt change in D_s vs. $1/T$ and a preliminary agreement of experiment with a theory of next nearest neighbor association is discussed.

The variation of activation energy for impurity ion movement with size in both NaCl and KCl is discussed and a theory of "directed relaxation" is advanced to account for this. The variation of the entropy of association with impurity ion radius is also discussed but only for the KCl matrix.

The luminescence of NaCl:Pb:Mn and KCl:Pb:Mn phosphors was studied. It was found that the size of a side band of the normal manganese emission grows upon annealing. The manganese emission in NaCl:Pb:Mn was found at 2.05 ev at room temperature and at 1.91 ev at 90 ± 3°K. In KCl:Pb:Mn it was found at 2.02 ev at room temperature and at 1.95 ev at 90 ± 3°K.

The quantum efficiency of NaCl:Pb:Mn was studied as a function of manganese concentration. The samples were quenched to insure that the impurities were randomly distributed and the luminescence due to precipitated phases and impurity pairs was minimized. The

theory of Dexter for dipole-quadrupole resonance energy transfer was followed to a concentration of 1.5×10^{-4} mole fraction of manganese for which the quantum efficiency was found to be 0.1. This led to the deduction that the energy absorbed in the 4.28 ev band of lead is transferred to the manganese from the 2.76 ev emission band of lead with an overlap of about $1/2\ ev^{-1}$. The luminescence of NaCl:Pb:Mn is at 2.05 ev for a total Stokes' shift of about 2.2 ev.

The theory of Dow in which the energy is thought to be transferred from impurity A to impurity B by means of excitons was examined here. Transfer of energy by excitons was found to be not very probably in NaCl:Pb:Mn or KCl:Pb:Mn because of the large energy separation between the lead absorption band and the lowest host exciton band.

A Study of the Mn^{+2} and Pb^{+2}-Mn^{+2} Impurity Systems in Alkali Chlorides

by

William Alphonsus Mannion

A THESIS

submitted to

Oregon State University

in partial fulfillment of
the requirements for the
degree of

Doctor of Philosophy

June 1969

APPROVED:

Redacted for Privacy

Professor of Chemistry
in charge of major

Redacted for Privacy

Chairman of Department of Chemistry

Redacted for Privacy

Dean of Graduate School

Date thesis is presented May 5, 1969

Typed by Marion F. Palmateer for William Alphonsus Mannion

ACKNOWLEDGMENT

I would like to thank Dr. W. J. Fredericks for his suggestions in writing this thesis and for his aid, intellectual and financial, during my stay here.

Thanks are due to my colleagues also, particularly Dr. Charles A. Allen, for interesting and informative discussions. I also thank Mr. Robert Chaney for proofreading my thesis.

TABLE OF CONTENTS

LIST OF TABLES

LIST OF FIGURES

A STUDY OF THE Mn^{+2} AND Pb^{+2}-Mn^{+2} IMPURITY SYSTEMS IN ALKALI CHLORIDES

I. INTRODUCTION

This research was begun with the intention of studying the luminescence of doped alkali chlorides. Sodium and potassium chloride phosphors have the advantage of a regular well defined crystal structure. These materials were also a convenient choice since this laboratory is equipped to grow pure single crystals of sodium and potassium chloride.

The systems chosen for study were KCl:Pb:Mn and NaCl: Pb:Mn. These materials have been shown to exhibit luminescence involving resonance transfer of energy from the sensitizer, lead, to the activator, manganese. In a theoretical consideration of the mechanism of the energy transfer between impurities, Dexter related the quantum efficiency of luminescence to concentration of the activator in the crystal. Thus it became obvious quite early that a study of the luminescent properties of the sodium and potassium chloride phosphors would have to include a determination of impurity concentration in the phosphor.

For several years this laboratory has been studying the diffusion of divalent cations into single crystals of sodium and potassium chlorides by means of radiotracers. It was thought that this

technique could be applied here to obtain information about the diffusion paramters of manganese in these crystals. Accordingly, information on the diffusion of manganese into single crystals of sodium and potassium chloride was taken and forms a rather substantial part of this work. As it turned out later, it was more convenient and accurate to grow single crystals doped with the impurities, grind them to make powder samples and then measure the activator concentration by polarography.

The diffusion of manganese into single crystals of sodium and potassium chloride is interesting in itself. Dipositive manganese ion is quite a bit smaller than either the sodium or potassium ion, whose lattice position it occupies, and it is also smaller than most of the other dipositive ions heretofore diffused into these salts. It's possible that the high charge density on the manganese II ion would have some rather interesting effects.

This work then is a combination of two rather separate investigations on the properties of manganese in single crystals of sodium and potassium chloride. There certainly is a fair amount of overlap and where possible the information derived from one form of measurement is applied and correlated with that found from the other, however, it seems more convenient to treat this study as composed of two separate sections. Hence the diffusion and luminescence sections will be kept separated throughout the body of the thesis.

II. BACKGROUND AND THEORY

Diffusion

Introduction of divalent cation impurities into an alkali halide lattice produces an equal number of cation vacancies, since the total number of anion and cation sites must be equal. Stasiw and Teltow (70) postulated that, because of the net negative charge on the vacancy, the vacancies will combine with the net positively charged divalent cations. This combination is called an impurity-vacancy complex. Because this complex is electrically neutral and will not move preferentially in an electric field, Etzel and Maurer (20) used this concept to interpret their results on the condutivity of NaCl doped with $CdCl_2$. Further experimental evidence for the existence of an interaction between divalent cation and cation vacancy was supplied by Mapother, Crooks and Maurer (52) in a study of self diffusion of Na in NaBr and NaCl.

It would seem reasonable to suppose that diffusion of an associated divalent impurity ion would be greater than that of the host cation, which must depend on the chance encounter of a vacancy for movement. Lidiard (46) has developed this line of thought into a quantitative theory of divalent cation diffusion obtaining equations which relate the diffusion coefficient of the impurity to its

concentration and the free energy of association of the complex. He has developed a theoretical model for diffusion of a divalent metal impurity in a lattice containing monovalent cations such as the alkali chlorides. An impurity can only move when there is a vacancy in the nearest neighbor position. Since a divalent cation impurity has a net charge of $+1$ when referred to the lattice and the cation vacancy has a net charge of -1, there is a certain electrostatic attraction between these two entities. Charge conservation requires that if the concentration of the divalent impurity is c, the concentration of cation vacancies will be c, when thermal contributions can be ignored. The electrostatic attraction between divalent cations and vacancies can produce a one to one complex.

A degree of association, p, is defined so that cp is the molar fraction of complexes. Then application of the mass action law to the pseudo-chemical reaction

$$\underset{\substack{\text{unassociated impurity}\\ \text{ion}}}{M^{+1}} + \underset{\substack{\text{unassociated}\\ \text{vacancy}}}{\boxed{+}^{-1}} \rightleftharpoons \underset{\substack{\text{impurity-vacancy}\\ \text{complex}}}{M\boxed{+}}$$

gives

$$\frac{cp}{c^2(1-p)^2} = K(T) \tag{2.1}$$

The mass action constant, K, depends only on temperature. In the simplest case in which the impurity ion and vacancy are regarded as

associated only when in nearest neighbor positions, a statistical thermodynamical treatment of the association reaction gives

$$\frac{p}{c(1-p)^2} = 12 \exp(-\frac{\Delta G}{kT}). \tag{2.2}$$

In the above equation 12 is the number of distinct orientations of an impurity-vacancy complex in a NaCl type lattice, and $-\Delta G$ is the free energy of association between the impurity and vacancy.

Lidiard has further shown that if the impurities move by the vacancy mechanism, i. e., jumping into a vacancy in the nearest neighbor position, the impurity diffusion coefficient is given by

$$D(c) = D_s \frac{d(pc)}{dc} \tag{2.3}$$

where D_s is the diffusion coefficient of the complex.

Lidiard has also shown in another section that

$$D_s = 1/3\, a^2 w_2 f \tag{2.4}$$

where a is the anion cation separation, w_2 is the jump frequency for exchange of positions between an impurity ion and its associated vacancy and f is a correlation factor. f is defined by Howard and Lidiard (31) as

$$f = \frac{w_1 + 7w_3/2}{w_1 + w_2 + 7w_3/2} \tag{2.5}$$

where w_1 is the jump frequency for a vacancy in an associated position moving to another associated position and w_3 is the jump frequency for a movement carrying the associated vacancy away from the impurity ion. These movements of the associated vacancy are illustrated in Figure (2. 1).

Now using equations (2. 2) and (2. 3) the concentration dependent diffusion coefficient can be found as

$$D(c) = D_s[1 - (1 + 48c\, e^{-\frac{\Delta G}{kT}})^{-1/2}] \qquad (2.6)$$

Note in this equation that as c increases $D(c)$ tends to a maximum value of D_s. D_s then is the saturation value of the diffusion coefficient. This equation can be used to determine D_s at particular temperatures and if log of D_s is plotted vs. $1/T\ (^\circ K^{-1})$, a value for U_o may be found from the slope of the line. U_o is the activation energy required for a divalent cation and an associated vacancy to exchange places in the lattice. Thus

$$D_s = D_o e^{-U_o/RT} \qquad (2.7)$$

where R is the gas constant, T is expressed in degrees Kelvin and D_o is a pre-exponential term.

The previous treatment leading to the development of equation (2. 6) rested on the assumption that the concentration of thermal

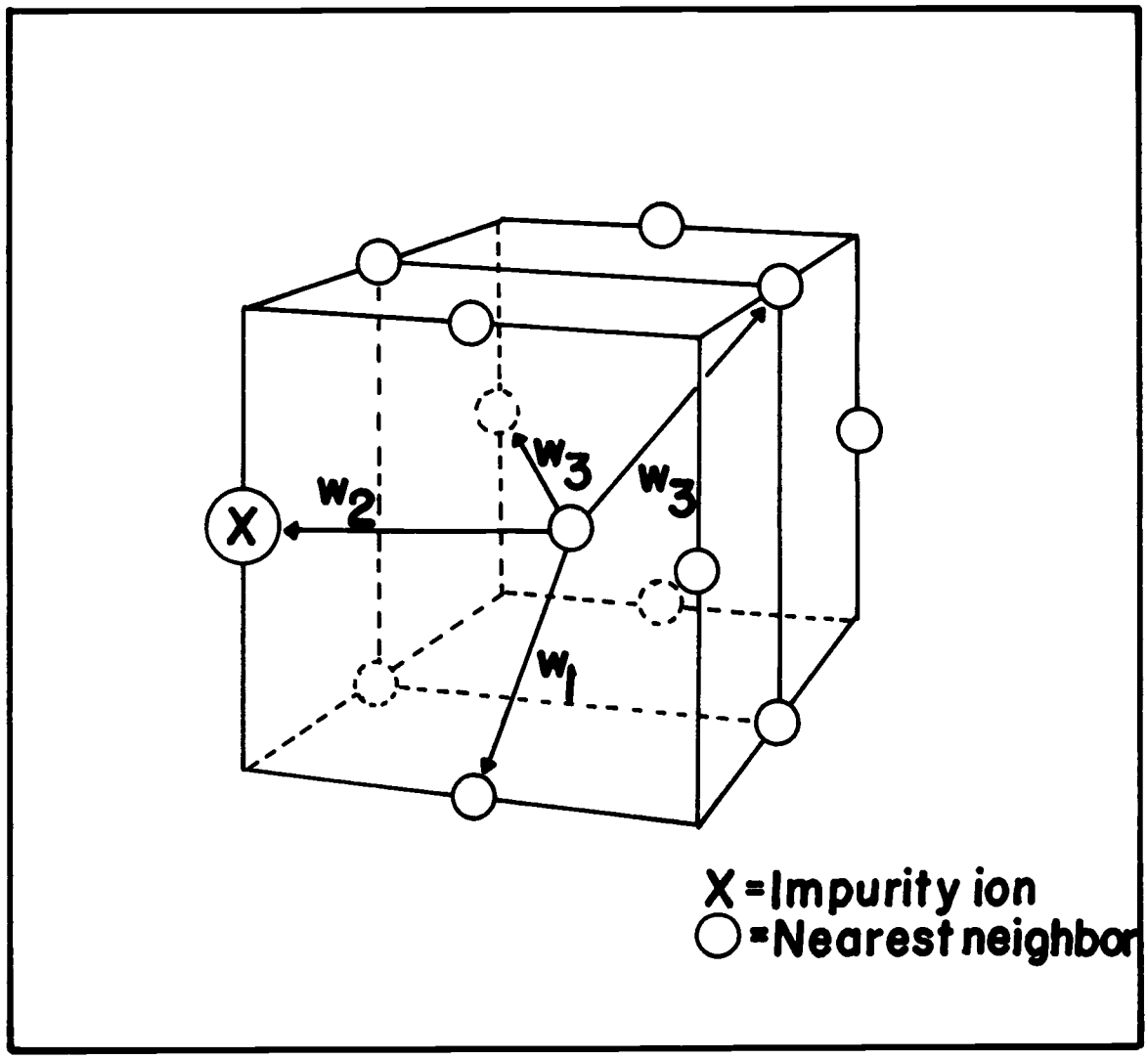

Figure 2.1 Diagram describing notation of jump probabilities. From Howard and Lidiard (30).

cation vacancies, c_v, was much smaller than the concentration of cation vacancies introduced with the divalent impurity, c_b, i. e., $c_v << c_b$. Howard and Lidiard (31) have considered the case where this condition does not apply. They have shown the mass action law analogous to equation (2. 2) as

$$\frac{c_p}{(c_v - c_p)(c_b - c_p)} = 12e^{(-\frac{\Delta g}{kT})} \qquad (2.8)$$

where c_p, c_v and c_b are the atomic fractions of pairs, vacancies and impurities respectively. They then develop a rather complicated expression for the diffusion coefficient of the impurity ions that simplifies considerably when either c_v or c_b are present in great excess. For the systems studied in this work $c_v << c_b$ and the diffusion coefficient is adequately described by equation (2. 6).

In both developments described here only vacancies in the nearest neighbor position were considered associated. The effects of the coulomb attraction were assumed to fall off so fast that no association in the next nearest neighbor position would occur. ΔG for Mn^{+2} is quite high in both sodium and potassium chloride and it was thought that there might be some next nearest neighbor association. Studying Mn^{+2} in NaCl and KCl by E. S. R. Watkins (27) found that the difference in binding energy (not free energy) was small and in KCl the vacancy in the next nearest site was actually more stable.

If this is true, then an adequate theoretical treatment ought to include the association energy of the vacancy in the next nearest neighbor site, since this would enhance diffusion by having vacancies more available for movement into nearest neighbor positions. Rothman et al. (61) and Lidiard (46) indicate that a way to account for this effect is through the use of a Debye-Hückel treatment of the attraction between unassociated impurity cations and cation vacancies.

As implied before, the diffusion of divalent manganese into sodium and potassium chlorides was studied because of its possible application later to luminescent systems and also because of its intrinsic interest. The diffusion of manganese into sodium chloride has been studied by Lure, Murin, and Brigevich (47) using radiotracer techniques and by Stewart and Reed (71) using EPR. Lure et al. found $-\Delta G = 0.55$ e. v. at 500° C and $U_o = 0.66$ e. v. while Stewart and Reed found $U_o = 0.954 \pm 0.037$ e. v.. No information regarding the diffusion of manganese into potassium chloride has been reported.

Divalent manganese in an alkali halide is interesting because of its electronic configuration, $3d^5$, and also because of its size, 0.80 A. (12, p. 43; 57, p. 518). Watkins (73, 74) has investigated the electron spin resonance structure of Mn^{+2} in sodium chloride and made some assessments of the states of aggregation of Mn^{+2} in the crystal. The ionic radius, 0.80 A , is quite a bit smaller than

most of the other ions heretofore introduced into sodium or potassium chlorides and this fact could lead to some interesting results; for instance, the higher charge density would lead one to expect a more tightly bound complex.

Radiotracer techniques have been used to study the diffusion of several ions into alkali chlorides, among them are: Pb^{+2} into KCl (35), Cd^{+2} into KCl (34), Cd^{+2} into NaCl (2), Pb^{+2} in NaCl (3, 50), Co^{+2} and Ni^{+2} into NaCl (32), Ca^{+2} into NaCl (56), Zn^{+2} into NaCl (61) and Hg^{+2} in KCl (1). Information about the divalent cation-vacancy association may also be obtained from conductivity and dielectric loss experiments.

Luminescence

The phenomena of sensitized luminescence has been studied for at least 20 years. Sensitized luminescence is a process whereby energy absorbed in an impurity, S, is transferred to an impurity, A, and is emitted as luminescence characteristic of A. In the more interesting cases A and S are different impurities.

Most of the earliest investigations were made on systems of simple structure such as calcite (63) and the alkali chlorides (29, 55, 62, 65). It was hoped that the simplicity of the structure would facilitate the elucidation of the mechanism of energy transfer between S and A. However, because of the low solubility of activators, A,

or sensitizers, S, in these matrices the work soon turned to more complicated systems such as, $Ca_3(PO_4)_2$:Ce:Mn, $Sr_3(PO_4)_2$:Sn:Mn, $Ca_2P_2O_7$:Sn:Mn (6), CaF_2:Ce:Mn (30), and silicates such as $CaSiO_3$:Pb:Mn (7). Interest was also shown in tungstates. Russian experimentalists soon became interested in the phenomena and they, along with some American workers, again focused attention on the alkali halides. Single impurities in sodium and potassium chloride were investigated (39, 48). Luminescence in doubly activated phosphors was studied in the case of KCl:Pb:Mn (68), NaCl:Pb:Mn (38), NaCl:Ag:Cu (11), KCl:Tl:Pb, KCl :Eu:Mn, KCl:Sn:Mn, NaCl:Eu:Mn, NaCl:Sn:Mn, and NaCl:In:Mn (69). Khalilov et al. (38) have collected much of the data on singly and doubly activated alkali chlorides. A rather complete review of luminescence has been made by Klick and Schulman (41, p. 97-172).

Transfer of energy between two impurity centers may occur by a cascade or a resonant process. In the cascade process a photon is absorbed by the sensitizer, S, and is emitted as a photon with an energy in the emission band of S. If the activator, A, is chosen so that its absorption band overlaps the emission band of the sensitizer, the emitted photon may be absorbed and emitted as luminescence characteristic of A. The net process is to degrade the energy of incident photons from the absorption band of S to the emission band of A. In a resonant process of energy transfer the energy is

transferred by a radiationless mechanism. This paper will deal with the resonant process of energy transfer.

Theories of resonance energy transfer are not new. Franck (23) demonstrated the mechanism in gases and a quantum theory was given by Kallmann and London (33).

A theory of resonance transfer in condensed media was first developed by Förster (21, 22) for allowed transitions in organic solutions and crystals. Dexter (15) has extended this theory to include forbidden transitions and applies this theory to inorganic systems. The transfer mechanisms he describes are overlap of the dipole field of the sensitizer with the dipole field of the activator, overlap of the dipole field of the sensitizer with the quadrupole of the activator and exchange effects. In the dipole-dipole (dd) mechanism both the sensitizer and activator have absorption bands in the region of interest. In the dipole-quadrupole (dq) case the sensitizer has an absorption band but the activator does not. In the dq case then an activator with a forbidden transition from the ground state to an excited state can be made to luminesce even though it would not absorb the energy directly.

The physical model used by Dexter to develop the theory is that of an atomic fraction, x_s, of sensitizing impurity atoms and a fraction, x_a, of activating impurity atoms arranged randomly at the appropriate lattice sites of an insulating crystal. A low

concentration of both x_s and x_a is assumed so that the probability of transfer from one sensitizer to another is negligible, so that no new crystalline phases are formed, and so that the effects of cluster formation are unimportant.

The transfer process consists of five stages: (1) absorption of a photon of energy E_o by the sensitizer, (2) relaxation of the lattice around the sensitizer so that the available energy in a transition is now $E_1 < E_0$, (3) transfer of energy E_1 to the activator, (4a) relaxation around the activator so that the available energy in an electronic transition is now $E_2 < E_1$, (4b) relaxation of the lattice around the sensitizer to a state similar to the original unexcited state, (5) emission of energy E_2 from the activator.

It is important to remember that the lattice relaxes around S and A after an electronic transition before another transition occurs. This localizes the excitation on S or A. Steps (2) and (4a) described above occur in about 10^{-13} seconds, the excess energy being dissipated to the lattice as phonons. This process is the one associated with the Stokes' shift (14). Step (5) of course, depends on the forbiddenness of the transition but requires a time of at least 10^{-8} seconds or longer. In general, the Stokes' shifts described above (steps (2) and (4a)) are large enough so that $E_2 < E_0$ and no back transfer from an activator to a sensitizer can occur. Thus, when an excitation appears on A it must stay until either an

emission or a non-radiative process can occur. It should be pointed out that back-transfer can occur if S and A are sufficiently close so that transfer takes place before relaxation (steps (4a) and (4b)) occurs.

The resonance transition may be treated by first-order time-dependent perturbation theory provided: a) the time for transfer is very much longer than the lattice relaxation time; b) the Stokes' shift is sufficiently great so that back-transfer is inefficient; and c) impurity concentrations are sufficiently low so that interactions (i) between sensitizers, (ii) between activators, and (iii) between sensitizers and activators - other than nearest neighbors - are all negligible. Some of these conditions will be discussed later.

Dexter specifies the transition probability as

$$P_{SA} = \left(\frac{2\pi}{\hbar}\right) | \langle H_1 \rangle |^2 \rho_E \ , \qquad (2.9)$$

where $\hbar$ is Planck's constant, ρ_E is the density of states, and $\langle H_1 \rangle$ is the matrix element of the perturbation to the Hamiltonian between the initial and final states of the system. The initial state of the system is the one in which the sensitizer is excited, ψ_s', and the activator is in the ground state ψ_a. The final state is the one in which the sensitizer is now in the ground state, ψ_s and the activator is excited ψ_a'. The primes here indicate excited states. This is simply a description of the process in step (3) above. The

probability then is of the form

$$P_{SA} = \left(\frac{2\pi}{\hbar}\right) \rho_E \left| \int \psi_I H_1 \psi_F d\tau \right|^2, \tag{2.10}$$

where ψ_I and ψ_F refer to the initial and final states, respectively, that have just been described.

Dexter proceeds to normalize the wave functions on an energy scale and absorb the density of states factor, ρ_E, in the normalization. He introduces probability functions $p_s'(w_s')$ and $p_a(w_a)$ to express the probabilities that S is in the particular energy w_s' and A is in the state w_a. Using the Franck-Condon principle, which states that electronic transitions occur in a time short compared with lattice vibrations and there is small probability of loss of electronic excitation energy to the lattice in any transition, Dexter requires that the transition probability, P_{SA}, contain a Dirac delta-function

$$\delta[(w_s' - w_s) - (w_a' - w_a)] .$$

The total probability of energy transfer from S to A is then

$$P_{SA} = \left(\frac{2\pi}{\hbar}\right) \sum_I \sum_F (g_s' g_a)^{-1} \int dw_a' \int dw_s \int dw_a p_a(w_a) \int dw_s' p_s'(w_s')$$

$$\times \left| \langle H_1(w_s', w_a'; w_s, w_a') \rangle_{IF} \right|^2 \delta[(w_s' - w_s) - (w_a' - w_a)] , \tag{2.11}$$

and the indices I and F on the energy parameter have been omitted for brevity. The factor g_s' indicates the degeneracy of the excited level of the S atom or ion, similarly for g_a. Carrying out the integration over w_s by means of the delta-function and substituting

$$E = w_s' - w_s = w_a' - w_a,$$

Dexter obtains

$$P_{SA} = \left(\frac{2\pi}{\hbar}\right) \sum_I \sum_F (g_s' g_a)^{-1} \int dE \int dw_a\, p_a(w_a) \int dw_s'\, p_s'(w_s')$$

$$X \left| < H_1(w_s', w_a; w_s' - E, w_a + E) > _{IF} \right|^2. \qquad (2.12)$$

In order to calculate the transfer probability, an expression for the perturbation, H_1, must be determined. This interaction may be expressed as the sum of all the Coulomb interactions between the outer electrons and core of A with those of S reduced by the dielectric constant, K, of the medium. Expanding the sum in a Taylor series about the vector $\overline{R}$, the internuclear separation distance of S and A, the interaction energy is

$$H_1(R) = \left(\frac{e^2}{KR^3}\right)\{\vec{r}_s \cdot \vec{r}_a - 3(\vec{r}_s \cdot \vec{R})(\vec{r}_a \cdot \vec{R})/R^2\}$$

$$+ \left(\frac{3e^2}{2KR^4}\right)\{\sum_{i=1}^{3}(R_i/R)r_{ai}^2 r_{si}(-3 + 5R_i^2/R^2)$$

$$+ 10(XYZ/R^3)(x_a y_a z_s + x_a z_a y_s + y_a z_a x_s)$$

$$+ \sum_{i \neq j}^{3}\sum^{3}[(R_j/R) - 5R_i^2 R_j/R^3][-r_{ai}^2 r_{sj} - 2r_{ai} r_{aj} r_{si}]\}$$

$$+ \ldots \qquad (2.13)$$

This is the interaction giving rise to Van der Waal's forces.

$$r_s = \sum_m \vec{r}_{s,m}$$

indicates vectors to all the electrons on S measured from the nucleus of S and similarly for

$$r_a = \sum \vec{r}_{a,n}.$$

The first curly brackets give the energy for a dipole-dipole interaction and the second the dipole-quadrupole interaction.

Dexter goes on to determine P_{SA} for dipole-dipole and dipole-quadrupole interactions. Since experimentally the dq process is important in this case, Dexter's development for dq transfer will be sketched. The development for dd and indeed dq transfer would

differ only in the assignment of a value for H_1.

To determine the transfer probability for dq transfer the absolute square of the matrix element is calculated from the second curly bracket of equation (2.13). Before insertion $< |< H_1 > |^2 >_{AV}$ is calculated by averaging over all orientations of $\vec{R}$. The quadrupole transition probabilities are expressed as the double dot product of the dyadic

$$|< N >|^2 = |< x^2 >|^2 + |< y^2 >|^2 + |< z^2 >|^2 + 2|< xy >|^2$$

$$+ 2|< yz >|^2 + 2|< xz >|^2. \qquad (2.14)$$

Summing over

$$|< H_1 >|^2_{AV} \text{ and } |< N_a >|^2$$

Dexter obtains

$$< |< H_1 > |^2 >_{AV} = \frac{9e^4 a}{4R^8 K^2} |< \vec{r}_s >|^2 |< N_a >|^2, \qquad (2.15)$$

where $a = 1.266$. The transfer probability is then

$$P_{SA}(dq) = \frac{9e^4 \pi a}{2\hbar K^2 R^8 g'_s g_a} \sum_I \sum_F \int dE \left\{ \int dw'_s p'_s(w'_s) |< \vec{r}_s(w'_s, w'_s - E) >|^2 \right\}$$

$$X \left\{ \int dw_a p_a(w_a) |< N_a(w_a, w_a + E) >|^2 \right\} \qquad (2.16)$$

The quantity in the first curly bracket relates to the sensitizer and can refer to either absorption or emission data. The second curly bracket refers to the quadrupole activator. There is little hope of expressing the quadrupole matrix elements in terms of absorption curves since a quadrupole transition is so much weaker than an electric dipole transition--about a factor of 10^{-6} (19, p. 646). Dexter says that it is sometimes possible to guess at the shape of the absorption band through a knowledge of the emission band.

Further manipulation allows the statement of transition probability in terms of the absorption and emission curves, giving

$$P_{SA}(dq) = \frac{135\pi\alpha\hbar^9 c^8}{4n^6 R^8 \tau_s \tau_a} \frac{g_a'}{g_a} \left(\frac{\xi}{K^{1/2}\xi_c}\right)^4 \int \frac{f_s(E)F_a(E)}{E^8}\, dE . \qquad (2.17)$$

In the above equation τ_s is the lifetime of S in the excited state, τ_a is the lifetime of A in the excited state, ξ/ξ_c is the ratio of the electric field at an isolated atom to that within the crystal, $f_s(E)$ represents the observed shape of the sensitizer emission band and $F_a(E)$ represents the guessed at shape of the activator absorption band. $f_s(E)$ and $F_a(E)$ are normalized to unity. Note the dependence on R^{-8}.

In order to relate the transition probability to experimentally determinable parameters, Dexter defines the dependence of

$P_{SA}(dq)$ on concentration. Defining a convenient paramter, γ, through the relation

$$P_{SA}(dq) = \gamma^{8/3}/v^{8/3}\tau_s \tag{2.18}$$

and

$$y = \gamma C^{+} x_a \tag{2.19}$$

the quantum efficiency as a function of concentration is found as

$$\bar{\eta}_q(dq) = y\int_o^{\infty} \frac{e^{-yt}}{1 + t^{8/3}}\, dt\,. \tag{2.20}$$

This relation is plotted in Figure (2. 2).

In equation (2. 18) v is defined as $v = (4/3)\pi R^3$, where R is the distance between S and A. In equation (2. 20) C^{+} is the number density of lattice sites that can accomodate the impurity A. For NaCl $C^{+} = 2.23 \times 10^{22} cm^{-3}$ and for KCl $C^{+} = 1.6 \times 10^{22} cm^{-3}$.

In order to relate quantum efficiency, $\bar{\eta}_q$, directly to concentration of the activator, x_a, some assignment must be made for the values in equation (2. 17) in order to calculate $P_{SA}(dq)$. Dexter states the criterion for appreciable transfer as $\bar{\eta}_q = 1/2$. From Figure(2. 2) this corresponds to $y = 0.65$ as a critical concentraion, $(x_a)_c = 0.65/\gamma C^{+}$. In order to calculate γ and thus $(x_a)_c$, he assigns values to the quantities in equation (2. 17) as $(\xi/K^{1/2}\xi_c)=1$, E = 5 e. v., $n^6 = 13$, $\tau_a = 0.1$ sec., $g_a'/g_a = 5$,

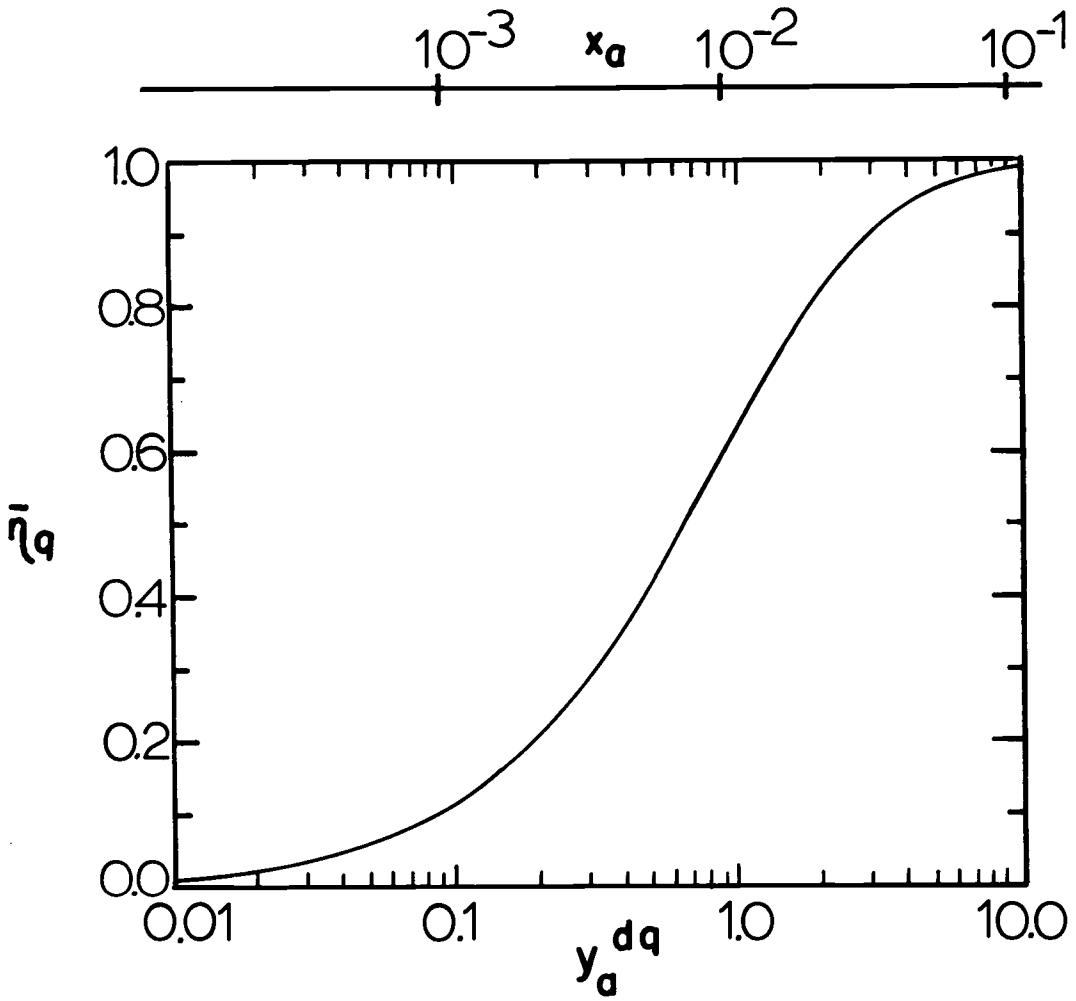

Figure 2.2 Quantum efficiency as a function of reduced activator concentration for dq transfer. The values of mole fraction of activator, x_a, are those estimated by Dexter.

$\int f_s(E)F_a(E)dE = 1/3$ e. v., and $C^+ = 2.25 \times 10^{22}$ cm^{-3}. γ now becomes 3×10^{-21} cm^3 and $(x_a)_c = 0.96 \times 10^{-2}$. These assignments are reasonable for a NaCl crystal. This then is the basis for assignment of values for x_a shown in Figure (2. 2). Choosing different values than those assigned here would result in a new value for γ, hence a new value for $(x_a)_c$ and a new assignment of values for x_a. Thus studying the quantum efficiency as a function of x_a and noting the value of x_a for which the quantum efficiency begins to change will not differentiate between dd, dq, qd, or qq. See Figure (2. 3) which illustrates $\overline{\eta}_q$ vs. y for dd and for qq transfer. Note how similar the two curves are and the curve for dq comes between these two. In order to differentiate between the various types of transfer <u>experimentally</u> one would have to measure the rate of change of the quantum efficiency as a function of y accurately enough to distinguish between the slopes of the various curves. With quantum efficiency measurements this is extremely difficult if not impossible.

This study will concentrate on phosphors that exhibit dipole--quadrupole transfer and will see what information may be deduced upon the application of Dexter's theory. The systems chosen for study were KCl:Pb:Mn and NaCl:Pb:Mn. These two phosphors were chosen for several reasons: 1) they had been demonstrated to luminesce, 2) pure starting materials were available, and 3) techniques for measurement of concentration in these halides had been

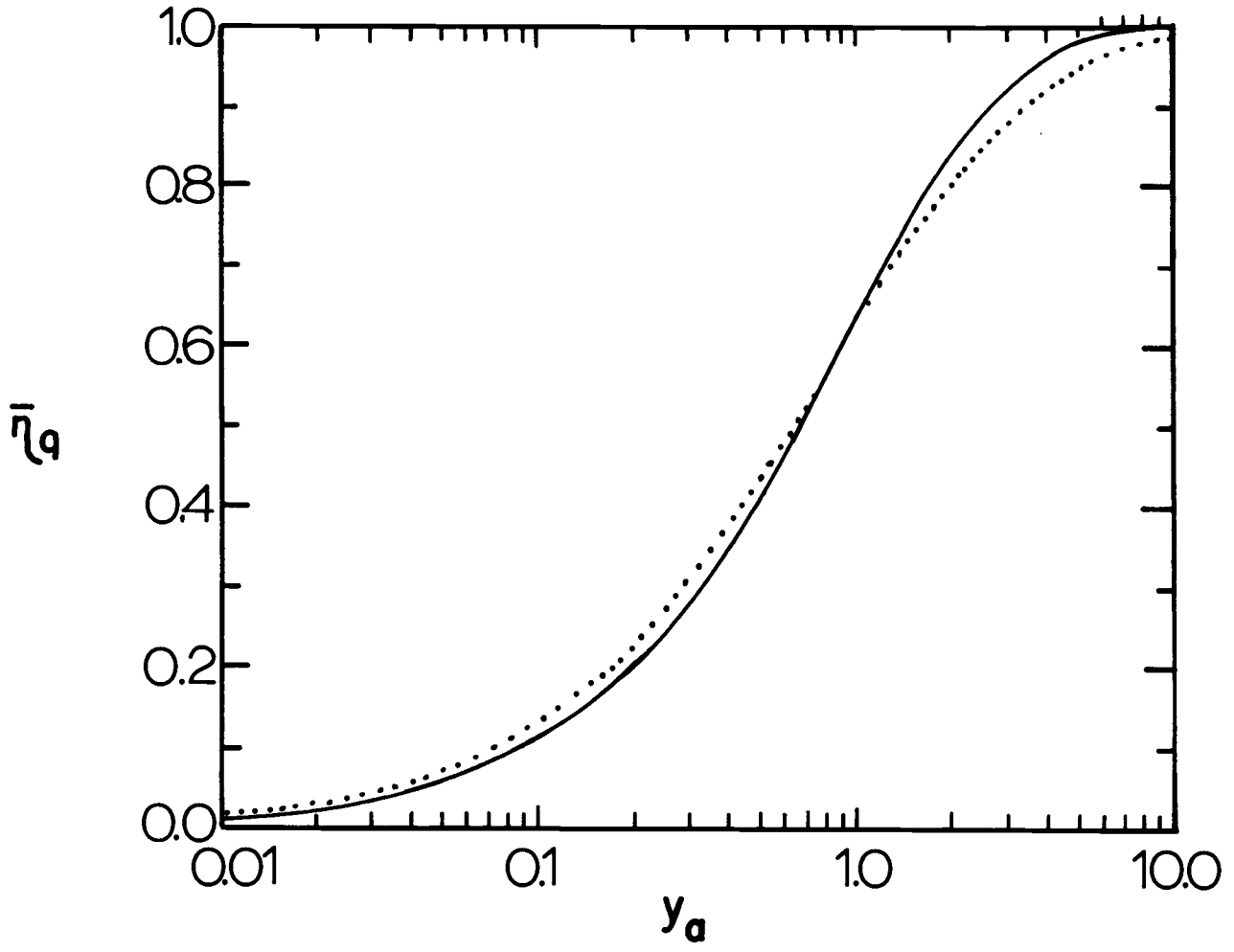

Figure 2. 3. Quantum efficiency as a function of reduced activator concentration for dd transfer (dotted line) and for qq transfer (solid line).

set up at this laboratory. The last condition is probably the most important since it seemed apparent that a knowledge of the quantum efficiency as a function of concentration of the sensitizer and activator in the crystal would be absolutely necessary.

Recently Dow (17) has considered resonance energy transfer by means of localized excitons, i. e., semi-bound excited states of the base lattice. An introduction to exciton theory is given by Dexter and Knox (16). Dow objects to Dexter's theory because he believes that the medium could alter the interaction, i. e. that both impurities are coupled to the host exciton bands as a result of interaction with neighbors. Physically we might expect that indirect coupling of impurities to each other is small for a large impurity separation or for excited impurity states lying far below the host exciton bands. Accordingly Dow indicates that the case of long-range transfer reduces to Dexter's theory with a two atom interaction and the medium effects included in a dielectric response function.

Generally the transition rates may be written

$$P_{SA} = \frac{2}{h} |\Delta_{eff}|^2 \rho_F \qquad (2.21)$$

where Δ_{eff} is the effective electronic factor in the transition matrix element (for Dexter's theory $\Delta_{eff} = \Delta/K$, Δ being the bare electronic matrix element and K is the dielectric constant of the medium) and

ρ_F is the vibrational overlap of the normalized activator absorption spectrum. Thus the electronic states determine the bare interaction strength, polarization effects reduce this interaction and the lattice vibrations merely provide an effective density-of-final-states factor in the transition rate. Dow calculates Δ_{eff} considering the host exciton states' effect on the bare interaction matrix element. Such virtual exciton migration is strong coupling in the sense that S and A are strongly coupled to a nearest neighbor host atom and each host is strongly coupled to another; but it is weak coupling in the sense that the effective indirect interaction between S and A is small. The mathematical technique used is the method of classical Green's functions for the treatment of localized perturbations. Impurities are considered in a three-dimensional crystal allowing for a direct interaction between impurities and including the contributions to virtual exciton migration from all orders of perturbation theory. To get a qualitative feeling for the effects of virtual exciton migration Dow specializes to the case of a one-dimensional crystal for which the Green's function is known. He emphasizes that this treatment could be applied to real crystals for which there were perfect crystal Green's functions calculated.

After specialization to a one-dimensional crystal, Dow writes Δ_{eff} as a sum of long-ranged and short-ranged parts

$$\Delta_{eff} = \Delta_{l.\,r.} + \Delta_{s.\,r.} = (\Delta/K) + \Delta_{s.\,r.} \qquad (2.22)$$

For large impurity separations the matrix element entering equation (2.21) is Δ/K which is the same as Dexter's theory predicts, but for smaller values of R, the short-ranged term can seriously modify the effective interaction. Then Dexter's resonance transfer theory in its usual form is valid for distances so large that

$$\Gamma = |\Delta_{s.\,r.}/\Delta_{l.\,r.}| << 1 \qquad (2.23)$$

This is essentially a statement of an assertion in the Dexter theory that the impurities are assumed to be far enough apart so that their wave-functions are uncorrelated. Dow (18, p. 197-198) estimates gamma for a dq process. Using $n = R/a_L$, where a_L is the lattice spacing, he obtains

$$\frac{\Delta_{s.\,r.}}{(\Delta/K)} = n^4 (10\,\delta a)^{1-n} (ev)^{n-1} \qquad (2.24)$$

δa is the energy separation in ev of the excited state of the impurity and the lowest host exciton band. Using $\delta a = 1$ ev Dow obtains for the ratio: 1.6 for $n = 2$, 0.8 for $n = 3$, 0.25 for $n = 4$ and 0.06 for $n = 5$ indicating that virtual excitons contribute significantly to transfers over distances shorter than four lattice spacings or about 16A. Dexter estimates that for dq transfer S may be expected to sensitize about 100 sites. For a site density of

$C^{+} = 2.23 \times 10^{22}\ cm^{-3}$ as in NaCl this corresponds to a cube with a side of 16A. Thus Dow asserts that the dq transfer should be dominated by virtual exciton transfer. This account of virtual exciton transfer has been restricted to one dimension, but Dow asserts that generalization to three dimensions does not give significantly different results. The sole threat to the virtual exciton mechanism is exciton-phonon interaction which would destroy the coherence of the intermediate states. Dow believes that the exciton-phonon interactions brought in by generalization to three dimensions are compensated by the increased number of paths for the migration; thus he believes his estimates of the strength of the indirect interaction to be about right for a real crystal.

In conclusion Dow states that two conditions must be satisfied in order that the Dexter theory be applicable. Virtual excitons must not offer an efficient pathway for transfer, $\Gamma << 1$, and it must be impossible, on the average, for two S's or two A's to be near enough to each other that one could provide coherently coupled intermediate state influencing the energy migration rate. These requirements limit the domain of validity of the Dexter theory to very low impurity concentrations. For dd and dq processes, for instance, the maximum impurity concentrations are 10^{-5} and 10^{-3} mole fraction respectively.

While these two papers provide the theoretical basis for a

discussion of sensitized luminescence, the purely phenomenlogical will not be neglected. The absorption, excitation and luminescence spectra will be examined and compared with what data there is available.

III. EXPERIMENTAL

Diffusion

Materials

Care was taken to obtain chemicals of high purity. The sodium and potassium chlorides used to grow single crystals were purified by passage of reagent grade salt supplied by Merck and Company through ion exchange columns. This procedure is particularly effective in removing polyvalent cation impurities. After passage through the columns the concentrated salt solution is evaporated to dryness. This technique was developed by Fredericks, Rostoczy and Hatchett (24) and perfected by Fredericks, Schuerman and Lewis (25).

The manganese chloride used in the experiment was B and A reagent grade, minimum purity 99.0 percent as $MnCl_2 \cdot 4H_2O$. The salt was dried under HCl in order to remove all water, including the waters of hydration (53, p. 348). The dried material was then stored in a weighing bottle in a dessicator. Carrier solutions of $MnCl_2$ were made up by weighing a convenient amount of dried $MnCl_2$, correction of the weight by the degree of purity, dissolving the salt and dilution to 100 ml in a volumetric flask with approximately 6N HCl. The strong acid was found to retard deterioration of the solutions. The strengths of these solutions were approximately 1.4 mg/ml. A new

carrier solution was made up about every six months to minimize the effects of decomposition.

The radioactive tracer was obtained as carrier free $Mn^{54}Cl_2$ in HCl solution from New England Nuclear, Boston, Mass. The tracer was diluted to a convenient volume with 6N HCl. Standard aliquots of 25 μl were taken for calibration of radioactive counting.

Crystal Growth

In order to perform the diffusion experiments, single crystals of sodium and potassium chloride were required. The Kyropoulos technique (43) was used to grow these crystals. Approximately 150 grams of dry purified salt was weighed out and placed in a quartz crucible. The crucible was placed inside a large quartz tube and sealed. The tube was evacuated and heated at a temperature of about 150° C while pumping until no more water was given off. The temperature was increased slowly while still under a vacuum to about 300° C. At this point about one-half atmosphere dry HCl was added and the salt was heated in steps to 500° C, changing the HCl at each step and pumping out all water. At about 600° C one atmosphere of chlorine gas was added to oxidize any organics from the resins and polyethylene containers remaining in the salt. Usually, although not always, the salt was melted under the chlorine atmosphere and chlorine dissolved in the melt. This helped to insure that all

organics were oxidized by the chlorine. When the salt was dry and clean, the temperature was lowered to room temperature; the crucible was removed from the quartz tube and transferred to the growth furnace. The growth furnace is a quartz tube having a zone heated by a graphite element surrounding the tube. The crucible was placed in this zone and heated under dry argon. The argon was changed periodically while heating to the melting point in order to flush out any water vapor. The salt was then melted under an atmosphere of argon. In order to accomplish the actual growth a single crystal called a seed crystal was attached to a cold finger rotating about its longitudinal axis. The crucible was rotated in the opposite direction to the seed crystal; the seed was dipped into the melt and withdrawn slowly. Salt will crystallize out of the melt onto the single crystal as it is withdrawn producing a large crystal of salt, called a boule. The growth from the melt and also the treatment with chlorine described previously can be considered to be purification steps.

Smaller single crystals of convenient size for diffusion experiments were cleaved from the boules. Cleaving is generally done with razor blades by exerting pressure along a 100 crystal direction.

The crystals produced as described were of a high degree of purity although probably not quite as pure as those described in (25). The only impurity detected by optical absorption measurements was

a small amount of hydroxide. The hydroxide concentration in sodium or potassium chloride may be calculated from ultraviolet absorption measurements using a relation reported by Gie and Klein (28). They found that the ratio, $\alpha(cm^{-1})/c(ppm)$, was equal to 0.9 cm^{-1}/ppm for NaCl and 0.4 cm^{-1}/ppm for KCl, where α is the u.v. absorbance of a sample divided by its thickness and c is the concentration in parts per million. In sodium chloride hydroxide was found at a concentration of 2 ppm, while the hydroxide concentration in potassium chloride was 0.65 ppm. The hydroxide absorption band was found at 185 nm in sodium chloride and at 204 nm in potassium chloride.

Diffusion Procedure

The impurity, manganese chloride, is introduced into the single crystals of sodium or potassium chloride by a technique known as vapor phase diffusion. That is, the crystal and solid manganese chloride are heated so that there is an appreciable vapor pressure of manganese chloride over the faces of the crystal.

A piece of single crystal sodium or potassium chloride is cleaved from the boules described above. The piece is usually about 1.5 cm by 1.5 cm by 0.6 cm. After cleaving it is annealed in two-thirds atmosphere HCl starting at 650°C and dropping to 200°C in two and one-fourth days. This has the effect of reducing the

hydroxide ion concentration to a level of less than 2 ppb in potassium chloride and 0. 5 ppm in sodium chloride. Since hydroxide ion diffuses out of the crystal there will be a concentration gradient from the center to the faces. The diffusion of hydroxide ion in potassium chloride has been discussed by C. A. Allen (1).

The method used for vapor phase diffusion is quite similar to that described by Keneshea and Fredericks (35). A tube of about 19 mm pyrex or vycor is sealed off and flattened at the bottom. Pyrex tubes are used if the diffusion anneal is to take place at a temperature less than about 550° C and vycor tubes are used for higher temperatures. Radioactive and carrier manganese chloride in a known ratio are delivered into and evaporated on the bottom of the tube. The last small amount of water is driven off by heating under HCl with a heat gun. When dry a pyrex pedestal about one and one-fourth inches high is placed on top of the evaporated material in order to physically separate the salt crystal from the diffusing material. The tube is then evacuated, about one-third atmosphere HCl is added and the tube is sealed off. This diffusion tube, as it is called, is then ready to be placed in a furnace at a definite temperature for a known time. The furnaces used for this diffusion anneal are Marshall high temperature testing furnaces with a Wheelco Model 407 controller. The temperature of the furnace is sensed by a chromal-alumel thermocouple and the temperature is maintained

to within 1°C.

Before the diffusion tubes are introduced into the furnace, the furnace is preheated to the temperature of the diffusion anneal. The diffusion tube is attached to a platinum-platinum 13 percent rhodium thermocouple so that the bead is positioned outside the tube about halfway up the face of the single crystal. The temperature determined this way is within 4°C of the temperature of the crystal (35). The diffusion tube is placed into the annealing furnace at a known temperature for a known time. During the diffusion anneal the temperature is checked at least twice, depending on the time of anneal. Temperatures of anneal ranged from about 450°C to 650°C for both sodium and potassium chlorides. The times ranged from 10 days to 18 hours for the lowest and highest temperatures respectively.

When a diffusion tube is placed in a furnace, the outside heats somewhat faster than the crystal inside. It is possible that the dopant may be transported from the bottom of the tube to the cooler crystal. This would result in diffusion with mixed boundary conditions of surface and vapor phase diffusion. To test this possibility, a water-cooled coil was placed around the bottom of the tube to give the crystal inside time to warm up. Then the coil was removed and the diffusion anneal begun. No difference in the diffusion profiles between cooled and not-cooled tube bottoms was noted.

Slicing Procedure

After the diffusion anneal the diffusion tube was taken from the furnace and allowed to cool in the air by convection. The tube and crystal cool quite quickly this way and it may be considered quenching. Within five minutes the tubes are cool enough to hold and are broken open. About 3 mm are cleaved from the sides of the crystal so that only diffusion into the large flat faces of the crystal is considered. The crystal is then cleaved lengthwise through the thickness dimension in order to give two large-faced samples. These samples are mounted to brass pedestals with epoxy cement and allowed to set. When firmly attached the pedestals are placed in an American Optical Company Model 960 microtome and a razor blade is placed in the moving arm. The blade and top of the crystal are backlighted and aligned by eye and the razor blade is pulled across the crystal face in approximately 20 micron increments. The powder obtained by this sectioning technique is collected in a vial that has been previously cleaned and weighed. The powder is dried in an oven, cooled, and weighed on a Mettler microgram balance. From a knowledge of the weight of powder, the crystal face area and the density of the salt, the distance into the crystal may be calculated. Usually 14 samples are taken in this manner although more can be

taken if needed.

Radioactive Counting

In order to determine the concentration of manganese in the slices the radioactivity of each slice is measured. Manganese -54 undergoes a nuclear reaction to chromium-54 by electron capture with a half-life of 280 days (26, p. 538). In the process a gamma ray is emitted of energy 0.835 MeV. The activity is measured on a Packard Model 410A Auto-Gamma Spectrometer using a potassium iodide scintillation detector. Calibration samples of 25 μl of tracer are used to calculate the concentration of manganese. The mole fraction of manganese is found by

$$c\ (\text{mole fraction}) = K\ c(\text{counts/min/micron})$$

where

$$K = \frac{Vc'M_1}{M_2V^*\rho Ar} \quad . \tag{3.1}$$

In the above equation V is the volume of carrier solution of concentration, c', V^* is the volume of radioactive tracer solution, ρ is the density of the sodium or potassium chloride and is equal to 2.165 gm/cm^3 for NaCl and 1.987 gm/cm^3 for KCl (9, p. 627 and 653), A is the area of the crystal face, M_1 is the molecular weight of the sodium or potassium chloride, M_2 is the molecular weight of

manganese chloride and r is the counting rate of the standard in counts/min/μ liter. The units of K are mole fraction of Mn^{+2} per counts/min/micron. The raw data for the concentration, i. e., counts/min/micron, is obtained for each sample by simply dividing its counting rate by its thickness.

Calculation

When the raw data has been collected and reduced to mole fraction of Mn^{+2} and thickness of the samples, it is plotted on a large piece of graph paper. A typical curve of mole fraction Mn^{+2} vs. penetration distance is shown in Figure (3. 1). As can be seen in the Figure, a smooth curve is drawn through the experimental points and extrapolated back to give a value of concentration, c_o, and the surface, $x = 0$.

The equation to be solved for one dimensional diffusion into a semi-infinite medium is (13, p. 148-9)

$$\frac{\partial c}{\partial t} = \frac{\partial}{\partial x}\left(D(c)\frac{\partial c}{\partial x}\right), \qquad (3.2)$$

where the diffusion coefficient, D, is explicitly a function of concentration, c. Boltzmann showed that for certain boundary conditions, provided D is a function of c only, c may be expressed in terms of a single variable, $x/2t^{1/2}$, and equation (3. 2) may be reduced to

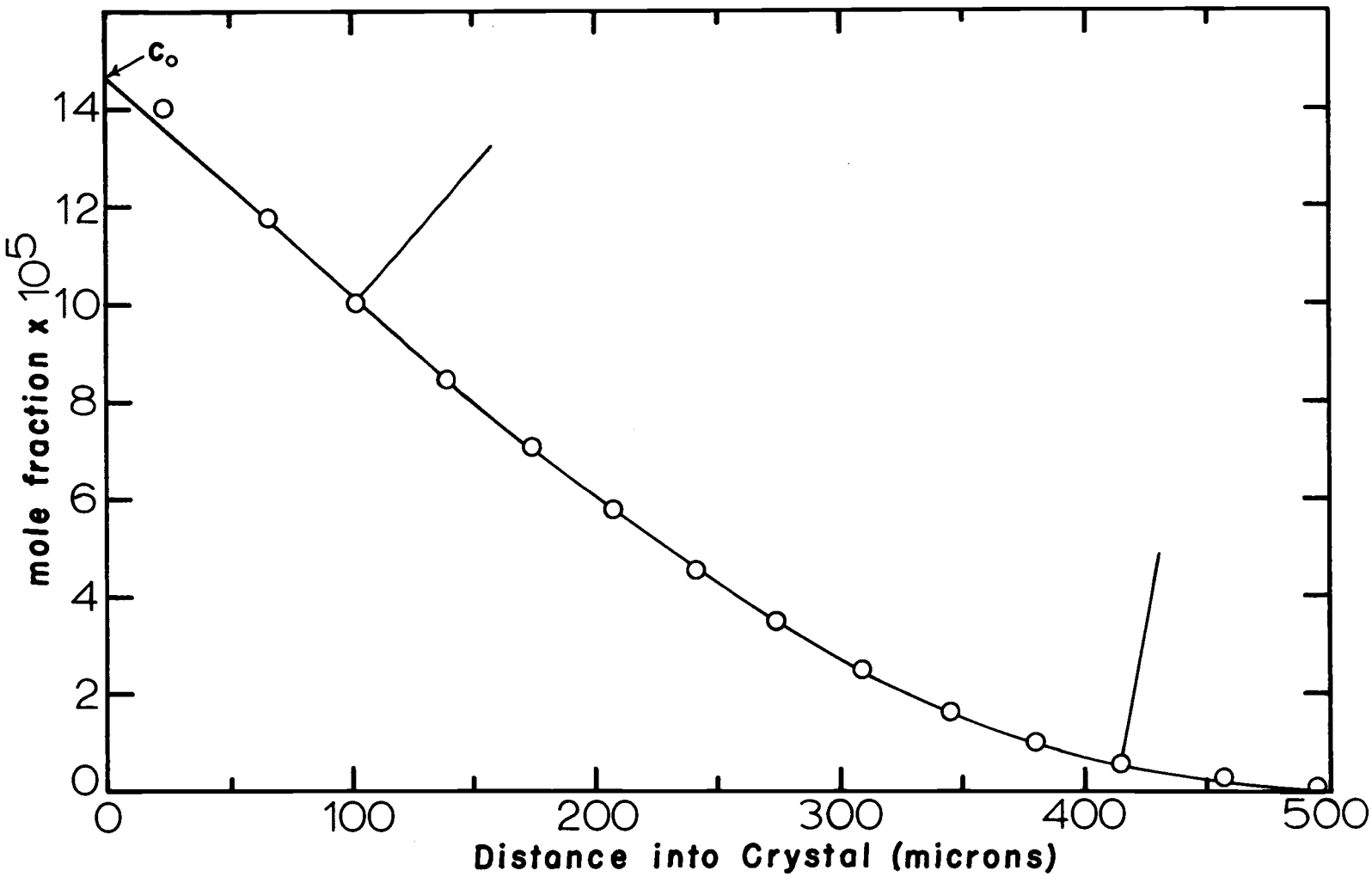

Figure 3. 1. Concentration of manganese as a function of distance into the crystal for a typical diffusion in sodium chloride. The lines at points 3 and 12 are perpendicular to the curve at that point and allow a measure of dc/dx.

an ordinary differential equation by the introduction of a new variable, y, where

$$y = x/2t^{1/2} \quad . \tag{3.3}$$

Then

$$\frac{\partial c}{\partial t} = \frac{dc}{dy}\frac{dy}{dt} = -\left(\frac{x}{4t^{3/2}}\right)\frac{dc}{dy}, \tag{3.4}$$

and

$$\frac{\partial c}{\partial x} = \frac{dc}{dy}\frac{dy}{dx} = \left(\frac{1}{2t^{1/2}}\right)\frac{dc}{dy} \quad , \tag{3.5}$$

also

$$\frac{\partial}{\partial x}\left[\, D(c)\frac{\partial c}{\partial x}\right] = \frac{\partial}{\partial x}\left[\frac{D}{2t^{1/2}}\,\frac{\partial c}{\partial y}\right] = \frac{1}{4t}\,\frac{d}{dy}\left[\, D\frac{dc}{dy}\right] \quad , \tag{3.6}$$

so finally (3.2) becomes

$$-2y\frac{dc}{dy} = \frac{d}{dy}\left[D\frac{dc}{dy}\right] . \tag{3.7}$$

The boundary conditions associated with this experiment are

$$\begin{aligned} c &= c_o \qquad x = 0 \qquad t > 0 \\ c &= 0 \qquad x > 0 \qquad t = 0 \end{aligned} \tag{3.8}$$

Upon transformation they become

$$\begin{aligned} c &= c_o \qquad y = 0 \\ c &= 0 \qquad y = \infty \end{aligned} \tag{3.9}$$

Integration of (3. 7) gives

$$2\int_{c}^{c_o} ydc = \int_{c_o}^{c} d[D\frac{dc}{dy}]. \qquad (3.10)$$

In these experiments t = constant so using (3. 3) equation (3. 10) becomes

$$\frac{1}{2t}\int_{c}^{c_o} xdc = \int_{c_o}^{c} d[D\frac{dc}{dx}]. \qquad (3.11)$$

This equation is more convenient to use since the data is obtained in terms of x and c. Integrating the right hand side of the equation, we get,

$$\frac{1}{2t}\int_{c}^{c_o} xdc = D(c)(\frac{dc}{dx})_c - D(c_o)(\frac{dc}{dx})_{c_o}. \qquad (3.12)$$

From the experimental values of c vs x plotted in rectangular coordinates the slope, $(dc/dx)_c$, at the point (c, x) and the slope $(dc/dx)_{c_o}$ at (c_o, x = 0) may be determined. The left hand side of (3. 12) is obtained by graphical integration between c and c_o. Thus all quantities except D(c) and $D(c_o)$ are known.

In order to evaluate $D(c_o)$ consider that as $c \to 0$

$$(\frac{dc}{dx})_{c \to o} << (\frac{dc}{dx})_{c_o}$$

while $D(c)$ is of the same order of magnitude as $D(c_o)$. Hence

$$D(c)\left(\frac{dc}{dx}\right)_{c \to 0} << D(c_o)\left(\frac{dc}{dx}\right)_{c_o}$$

and may be disregarded for $c \to 0$. $D(c_o)$ is then given as

$$-D(c_o)\left(\frac{dc}{dx}\right)_{c_o} = \frac{1}{2t} \int_{c \to 0}^{c_o} x\,dc \qquad (3.13)$$

By graphically integrating from some very small value of c to c_o one can obtain $D(c_o)(dc/dx)_{c_o}$ which is a constant. Once this is found $D(c)$ can easily be evaluated from (3.12) at various values of c. This method of analysis was first used by Mantano (51) and is described by Crank (13, p. 232-3) and Keneshea and Fredericks (35). $D(c)$ is plotted as a function of c for several temperatures in Figure (3.2).

Consider now equation (2.6) for Lidiard's development which relates $D(c)$ and c. From experimental plots of $D(c)$ vs. c an average value of $-\Delta G$ may be found. A smooth curve is fitted to the experimental points and from the curve smoothed data are taken: $D_i(c)$ at c_i and $D_j(c)$ at c_j. A ratio between $D_i(c)$ and $D_j(c)$ is calculated from the experimental values and then $D_i(c)$ and $D_j(c)$ are calculated from their respective values of c using (2.6) and guessing at $-\Delta G$. Equation (3.14) shows the ratio to be calculated.

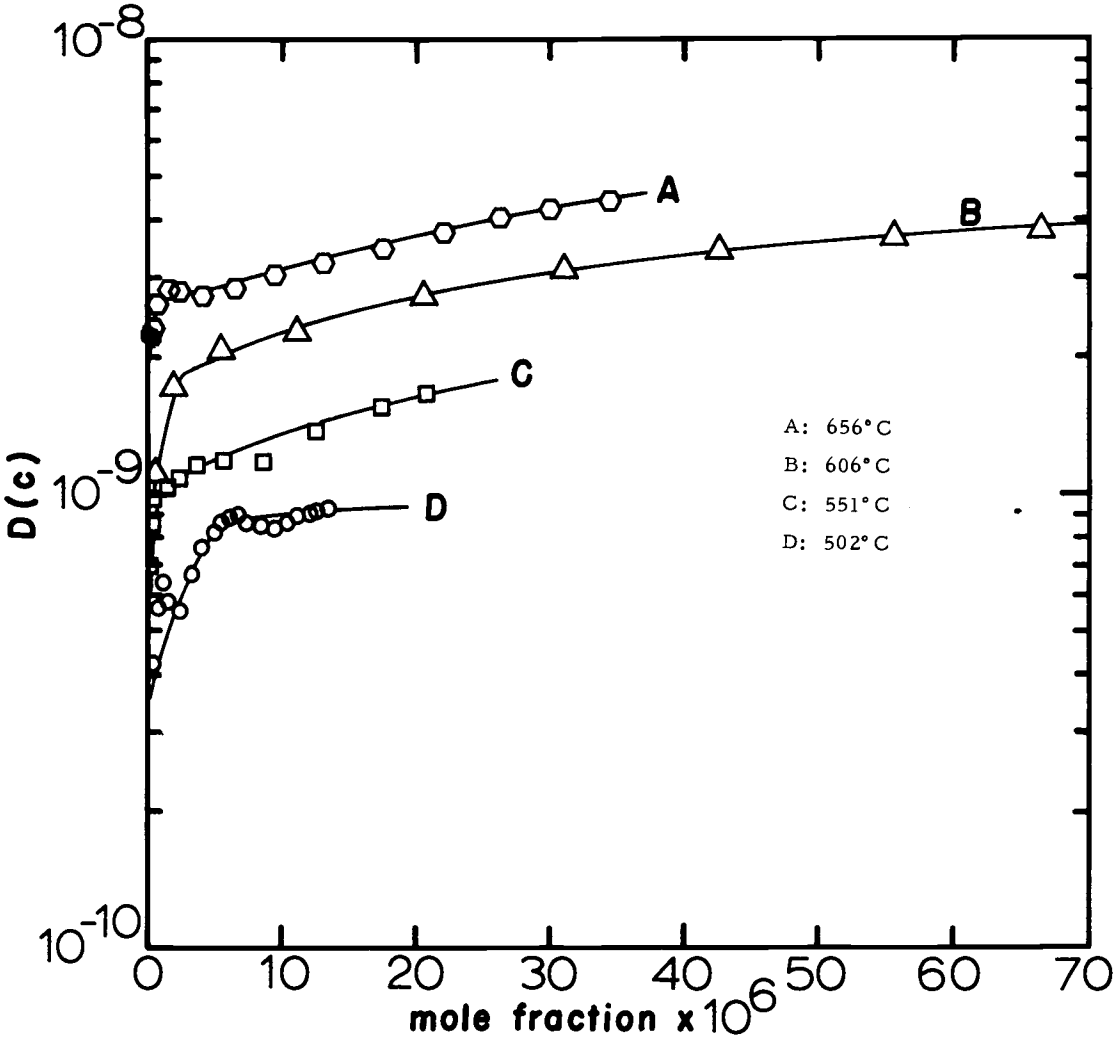

Figure 3. 2. D(c) as a function of concentration of manganese in NaCl for four experiments at different temperatures.

$$\frac{D_i(c)}{D_j(c)} = \frac{1-(1+48c_i\, e^{-\frac{\Delta G}{kT}})^{-1/2}}{1-(1+48c_j\, e^{-\frac{\Delta G}{kT}})^{-1/2}} \qquad (3.14$$

The value of $-\Delta G$ used is the value for which

$$[D_i(c)/D_j(c)]_{expt} = [D_i(c)/D_j(c)]_{calc} .$$

For any one experiment this process is repeated several times and an average value of $-\Delta G$ is calculated. If this value of $-\Delta G$ is substituted back into (2.6) a value of D_s may be calculated for each experimental point, $(D_i(c), c_i)$. In this way average values of D_s and $-\Delta G$ may be obtained at any particular temperature.

In order to get a "best" value of $-\Delta G$ and D_s a least squares program is run on the experimental points to minimize the sum of the deviations of the experimental points from a smooth curve. The smooth curve thus obtained corresponds to a "best" value of $-\Delta G$ and this yields a "best" value of D_s. The computer used was a CDC 3300 at the Oregon State University Computer Center.

The program used to find "best" values of $-\Delta G$ and D_s requires starting values of these quantities which can be provided by the procedure described above. This is a rather tedious calculation that could be eliminated. Instead of making the calculation for each experiment an "educated guess" was made for values of $-\Delta G$ and

D_s on the basis of earlier completed experiments and these were used as starting values in the program described above. "Best values" of $-\Delta G$ and D_s for that experiment were then calculated by the computer. In order to check that the "best values" actually corresponded to a true minimum in the sum of the deviations and not just a saddle point, the "best values" were calculated using starting values of $-\Delta G$ and D_s both greater and less than the expected "best values". The calculated "best values" of $-\Delta G$ and D_s were the same within the allowed deviation. This check was performed for several experiments at different temperatures.

Care must be taken to assure that the data used actually satisfies the model postulated. One basic assumption in Lidiard's calculation of $D(c)$ is that the concentration of positive ion vacancies is equal to the concentration of divalent cation impurity, i. e. thermal vacancies are not significant. Manganese II ion is more soluble in NaCl than in KCl and generally the assumption holds in NaCl; not so in KCl where at times the concentration of thermal vacancies calculated on a Schottky model became an appreciable fraction of the impurity introduced vacancies. If c_b is the concentration of the impurity introduced cation vacancies and c_v is that of the thermal vacancies, then when $c_v \approx c_b$ the assumption is violated. To insure that these sources of error would not be a problem, all calculated $D(c)$'s were rejected which corresponded to the condition

that $c_b \leq 10c_v$.

Another source of error which can affect the values of D(c) and hence $-\Delta G$ is illustrated in Figure (3. 1). In order to calculate D(c) from equation (3. 12), $(dc/dx)_c$ must be known. As can be seen from Figure (3. 1) $(dc/dx)_c$ is less well known at low c and hence D(c) at low c is less accurately known. To minimize this problem all points were rejected for which $c \leq 0.05\, c_o$.

Luminescence

Sample Preparation

In order to prepare luminescent samples, divalent lead and manganese ions must be introduced into a sodium or potassium chloride lattice. Three techniques were used to accomplish this: simultaneous vapor phase or surface diffusion of the impurities and growth from the melt of doped single crystals.

Vapor Phase Diffusion. The vapor phase diffusion technique has been described already for the diffusion of manganese. For the luminescence measurements radioactive tracer and carrier for both lead and manganese were evaporated onto the bottom of the tube. For the luminescence work crystals with quite a bit larger faces were used. Where the average surface for diffusion was about 1 cm^2, the average surface for luminescence was about 3 cm^2.

Large faces were used so that when slices were taken there would be enough powder to thoroughly cover the excitation beam in the luminescence phase of measurement. These large-faced crystals were placed on a pedestal over the evaporated dopants, the top of the diffusion tube closed off, the tube evacuated, one-third atmosphere of HCl introduced and then sealed off. The diffusion anneal was carried out the same way as described for manganese. After the anneal the crystal was cooled, cleaved, mounted and sliced in the same way as detailed for manganese diffusion.

The slices obtained from the sectioning of a luminescent crystal were contained in small clean vials as for manganese diffusion. The salt was not dried before weighing on the microbalance as it was noticed on early samples that heating at about 100° C for about five hours caused discoloration of the salt. This could possibly be due to oxidation of the Mn^{+2} to higher oxidation states by heating in air. The undried salt was allowed to come to equilibrium in the weighing room and weighed. The concentration of manganese in the slices was determined as before (equation (3. 1)) and the concentration of the lead was determined in a similar way. Lead-210 decays by β^- emission to Bismuth-210 with a half-life of 22 years (26, p. 561). In the process a gamma ray is emitted of energy 0. 046 MeV which is measured on the Packard Auto-Gamma Spectrometer Model 410A described before. The Lead-210 was obtained from New

England Nuclear, Boston, Mass. as carrier free lead chloride and was diluted as described for the manganese tracer.

Although the lead-210 gamma did not interfere in the manganese counting, the manganese-54 gamma did interfere slightly in the counting for lead. This interference was subtracted out before any calculations of concentrations were made.

The calculation of manganese concentrations were made as described before through the use of equation (3. 1). The concentration of lead in the slices was calculated using (3. 1) but with the value for M_2 now representing the molecular weight of lead chloride. The units of K then became mole fraction of Pb^{+2} per counts/min/micron.

The data may now be plotted as a diffusion profile for lead and manganese into the same crystal.

Surface Diffusion. In order to increase the concentrations of the impurities in the crystal, surface diffusion experiments were used. Instead of evaporating the dopant onto the bottom of the tube it is evaporated to dryness, taken up in alkali halide-saturated ethyl alcohol and evaporated onto the faces of the crystals; these faces are then placed together and annealed. After the anneal these crystals were treated in exactly the same way as described above.

Doped Crystal Growth. Another method used to obtain luminescent alkali chloride crystals was to grow a doped boule from the

melt by the Kyropoulos technique. This technique has already been described for growth of pure crystals. Two sodium chloride and one potassium chloride crystals were grown doped with lead and manganese. The first sodium chloride crystal grown was doped with 0.7 mole percent lead and 0.8 mole percent manganese (42). The boule produced was so heavily doped that it was opaque. This indicated precipitation of the impurities. The second sodium chloride crystal grown had 8.9×10^{-4} mole fraction manganese chloride and 3.4×10^{-4} mole fraction lead chloride in the melt. The boule produced was clear in visible light. The potassium chloride crystal had 9.6×10^{-4} mole fraction manganese chloride and 3.4×10^{-4} mole fraction lead chloride in the melt. This crystal boule too was clear.

As indicated before these crystals were grown by the Kyropoulos method described for pure crystals. The only difference was that while the salt was melting and the boule being pulled a mixture of about half and half argon-hydrogen chloride gas was passed over the salt to reduce possibility of inclusion of hydroxide ion in the crystals. All of the crystals described above, the two sodium chloride and one potassium chloride, showed luminescence.

These crystals cooled rather slowly after being grown and were effectively annealed after growth. As indicated in the results section annealed crystals show a side band and annealing tends to favor precipitation and coagulation of impurities. In order to

minimize this all samples were heated in platinum foil for about one hour at 600°C and quenched to about room temperature in liquid nitrogen. This should insure a random distribution of impurities.

As noted before manganese doped samples have a tendency to discolor if heated in air. The single crystals heated in platinum did turn very slightly dark, although not nearly as much as powders due to the relatively small amount of surface area of a single crystal. In order to solve the discoloring problem, the quenched single crystals were cleaved and powder samples were obtained by mounting on a microtome and shaving the inside face. Since the samples were taken from the inside of the crystal, it was assumed that very little oxide or hydroxide was included in the samples used for luminescence measurements.

The concentration of manganese in the doped crystals was measured by standard polarographic techniques. Manganese II ion has a half-wave potential at -1.51 volts in 0.1 M KCl (9, p. 1726). A series of standards of known concentration of Mn^{+2} in 0.1 M NaCl was made up and used to calibrate for the diffusion current, i_d, vs. concentration of manganese. It was only necessary then to measure i_d experimentally and obtain concentration. The instrument used for the polarographic measurements was a Heath Company Model EUW - 401 polarography system with a Heath D.M.E. apparatus Model EUA - 19 - 6 referenced against a saturated calomel electrode.

Optical Equipment

All absorbance measurements were made on a Perkin-Elmer Model 450 Spectrophotometer. This instrument has a useable range from 0.165 to 2.7 microns. The far U.V., U.V. and visible ranges (up to 750 nm) use a matched pair of photomultipliers for detection and either a deuterium or tungsten source for energy. The infrared region uses the tungsten source for energy and a pair of lead sulfide cells for detectors (59, p. 1-12).

The luminescence work was performed through use of a spectral-fluorescence attachment to the Perkin-Elmer 450 Sepctrophotometer (60). Excitation of the luminescence was achieved by light from a 150 watt Xenon arc lamp or a deuterium source, passing through a Corning glass filter with a band pass of 250 to 400 mμ, diffracting off a grating and illuminating the sample with a band of light. The luminescence that results is directed by a series of lenses and mirrors into the main monochromator of the Perkin-Elmer 450 itself. The luminescence is separated into its components and directed onto the photomultiplier in the sample compartment. The signal thus obtained is displayed on a recorder as relative deflection as a function of wavelength. The signal obtained in this way must be corrected for response of the photomultiplier as a function of energy and for attenuation of the light passing through the monochromator. The

relative energy, E, incident on the photomultiplier is given as (59, p. 65)

$$E = T \times F \tag{3.15}$$

in which T is the recorder deflection and F is a calibration factor. F is given as

$$F = \frac{1}{S\, T_q\, D^{-1} R^n} \tag{3.16}$$

where S is the detector sensitivity as a function of wavelength, T_q is the transmittance of the optics in the monochromator, D^{-1} is the reciprocal linear dispersion of the prisms, R is the reflectance of the aluminized mirrors and n is the number of reflections. Typical values of T_q, D^{-1} and R are given in the Perkin-Elmer Manual (59, p. 66-69) and these quantities were used as given. The detector sensitivity was measured by measuring the light intensity at the sample chamber using a Hilgar-Schwarz thermopile Model FT 16.1/521. The light was then attenuated a known amount by use of calibrated reference screens supplied with the Perkin-Elmer 450 Spectrophotometer and allowed to fall on the photomultiplier tube giving a pen deflection. The absorbances of the reference screens were measured directly and are listed in the Appendix. The pen deflection per incident energy as a function of wavelength was calculated and used for a measure of relative detector sensitivity. Thus

it was possible to calculate a relative F value as a function of wavelength. The curve calculated for F may be found in the Appendix along with the experimentally determined values for S.

Low Temperature Measurements

In order to cool the samples to make low temperature measurements a cold cell was used. The cell is constructed so that the cooled sample can be held close to the exciting source and the luminescence can be easily measured. The temperature of the sample can be measured by a copper-constatan thermocouple on the cold finger near the sample. It was found to be accurate within ±3° C. The spectral-fluorescence attachment is made so that the irradiating light strikes a sample on the bottom at a 90° angle to the plane of the sample. The luminescent light is taken from the bottom also but off at about a 60° angle. The cold cell holds the sample closely enough to the window so that very little luminescence is lost.

Quantum efficiency measurements are among the most useful of luminescence measurements. Quantum efficiency measurements were made at room temperature and at 90° K on powder samples obtained from the sectioning process described before. In order to measure the amount of light absorbed a powdered sample of pure material, either sodium or potassium chloride, was placed in the holder on top of a mirror and the sample irradiated with the usual

exciting light. Since the pure material would absorb none of the exciting light it would all be scattered. A fraction of it would be scattered into the lens system leading to the monochromator and the intensity of this fraction could be measured. If now a doped sample is placed in the holder, without the mirror, and is irradiated, some irradiating light is reflected and/or scattered off. A fraction, equal to the fraction discussed before, is scattered and/or reflected into the monochromator again and can be measured. The difference in the intensity of the reflected light from the doped sample and pure sample is a measure of the energy absorbed at any wavelength.

It is understood that samples having an absorbance band will reflect light in that absorbance band better than a pure sample; therefore, comparing the reflectance of pure and doped samples may not be valid. This problem was recognized, hence the reason for the mirror in the pure sample. Light getting past the first layers of pure salt will be reflected by the mirror and will scatter back out off the salt layers. In this way it is hoped that none of the light penetrating into the body of the salt is lost and the value measured as the total reflectance actually is an accurate value. This process gives a value for total reflectance that is reproducable to within five percent. In order to get an idea of the effect of the mirror, the reflectance of a pure sample without a mirror was obtained and found to be about 50 percent of that with a mirror. It is not true that the effect

of an inaccuracy here will be to shift all the quantum efficiencies by an equal amount because each sample has a different reflectance spectra to be subtracted from the total reflectance. It is true that an error of about 25 percent in the determination of total reflectance would be necessary before a significant change in the relative values of the quantum efficiencies would be noted.

The luminescence of the doped sample is measured directly. In order to relate luminescence measurements taken at different times to each other it was necessary to use a "reference luminescence sample". This sample was simply a powdered lead and manganese doped sodium chloride crystal that was physcially placed in the same place in the beam every time. The luminescence at the various instrument settings was read and all the different readings were related to one particular reading by calculation of a factor.

Calculation

When all the luminescence measurements had been corrected for instrument response and normalized, the relative deflection as a function of wavelength in nanometers was plotted.

Two kinds of efficiency may be considered here: energy efficiency, $\overline{\eta}_e$, and quantum efficiency, $\overline{\eta}_q$ (44, p. 306-307). Energy efficiency is the ratio of energy emitted to energy absorbed and is given by the formula

$$\bar{\eta}_e = \frac{\int E_{em}\, d\lambda}{\int E_{abs}\, d\lambda} \quad . \tag{3.17}$$

Quantum efficiency is the ratio of quanta emitted to quanta absorbed and is given by

$$\bar{\eta}_q = \frac{\int E_{em}\, \lambda\, d\lambda}{\int E_{abs}\, \lambda\, d\lambda} \quad . \tag{3.18}$$

The relationship between $\bar{\eta}_q$ and $\bar{\eta}_e$ is given as

$$\bar{\eta}_q = \eta_e \frac{\lambda_{em}}{\lambda_{abs}} \, , \tag{3.19}$$

where λ_{em} and λ_{abs} are the values of the maximum of the emission and absorption bands respectively. The average value of the emission maximum was 650 nm and the average value of the absorption maximum was 290 nm for the sodium chloride matrix.

In order to find the quantum efficiency, the energy efficiency, $\bar{\eta}_e$, was found by measuring the area under the relative deflection vs. wavelength curve for emission (Figure (3.3)) and dividing by the relative size of the absorption band. The size of the absorption band was found by subtracting the area under the reflection spectrum of the doped sample from the area under the reflection spectrum of the pure sample and assuming that the amount not reflected was

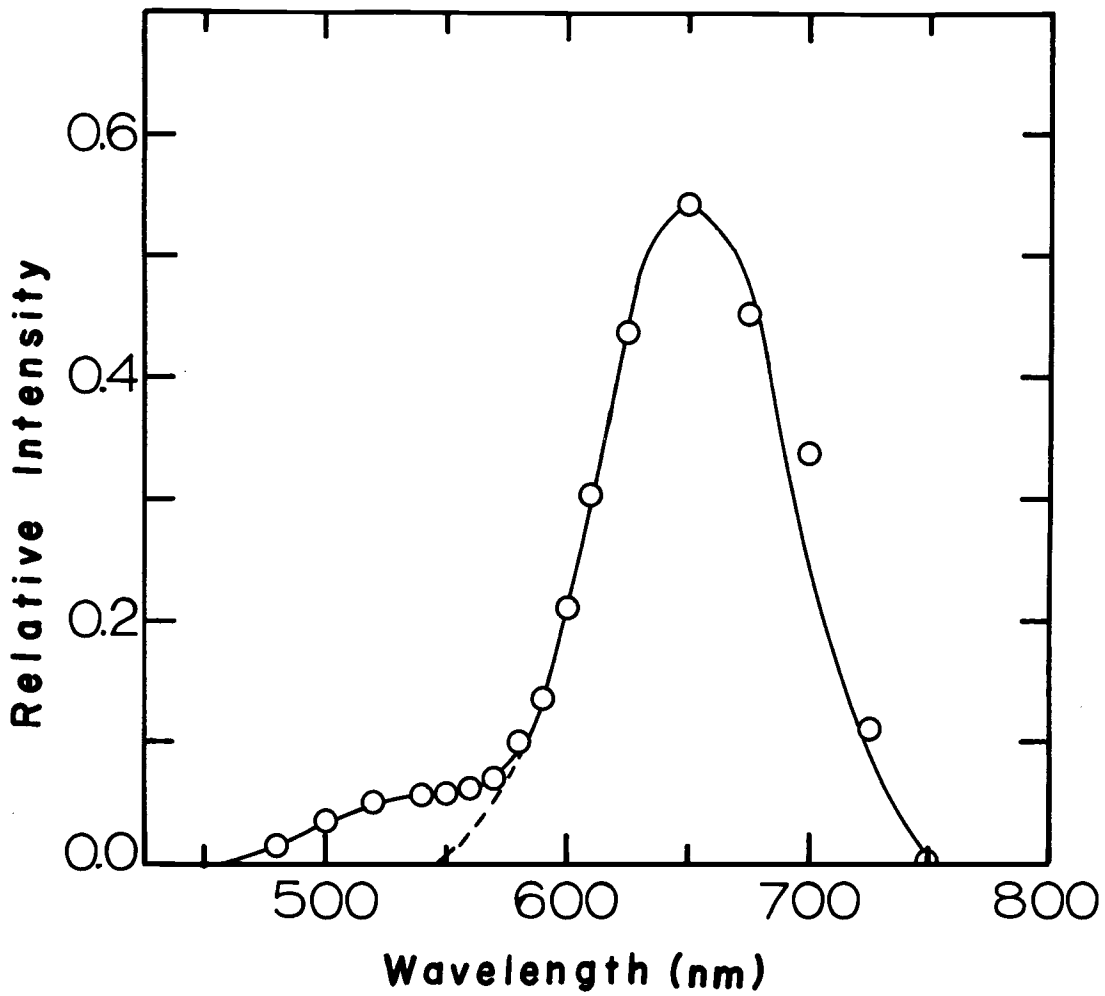

Figure 3. 3. Relative emission intensity as a function of wavelength. The area to the low wavelength side of the dotted line near 550 nm was omitted when measuring the area under the emission band. The area under the emission band is the area used in the numerator of equation (3. 17).

absorbed (See Figure (3. 4)). The energy efficiency was then multiplied by $\lambda_{em}/\lambda_{abs}$ to give quantum efficiency. All quantum efficiency determinations were on samples at low temperatures (90° K). The raw data for all the quantum efficiency determinations is collected in the Appendices.

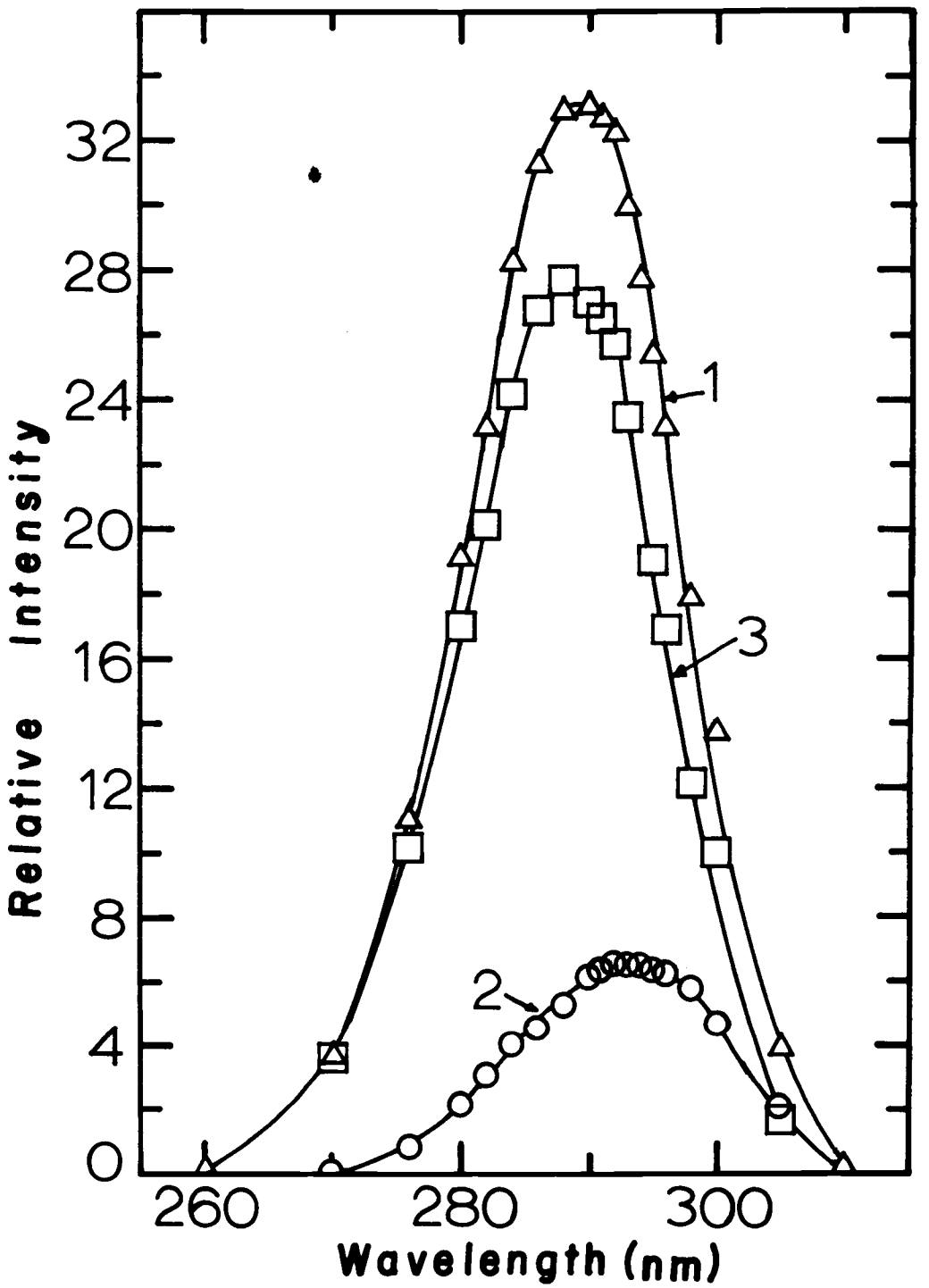

Figure 3.4. Relative intensity of reflected light as a function of wavelength. (1) reflection spectrum of "pure" NaCl; (2) reflection spectrum of doped NaCl, and (3) difference between 1 and 2. The area under 3 is the value for the denominator of equation (3.17).

IV. RESULTS AND DISCUSSION

Diffusion

Manganese in Sodium Chloride

Figures (4. 1) and (4. 2) show the concentration of manganese as a function of distance into a single crystal of sodium chloride for different temperatures. Table (4. 1) shows the average values for $-\Delta G$ and D_s at each temperature. The values given are averages of two crystals at the temperature specified with the spread locating the actual value for each crystal.

Table 4. 1. Average values of D_s and $-\Delta G$ for diffusion of Mn^{+2} into NaCl.

Temp (°C)	$D_s(cm^2/sec)$	$-\Delta G$ (ev)
449	$3.29 \pm .48 \times 10^{-10}$	0.72 ± 0.01
502	$1.19 \pm .07 \times 10^{-9}$	0.72 ± 0.00
537 (a)	$1.48 \pm .09 \times 10^{-9}$	0.68 ± 0.01
551	$1.82 \pm .22 \times 10^{-9}$	0.70 ± 0.00
601	$4.57 \pm .79 \times 10^{-9}$	0.62 ± 0.04
606 (a)	$5.38 \pm .12 \times 10^{-9}$	0.62 ± 0.01
656	$7.79 \pm 1.31 \times 10^{-9}$	0.65 ± 0.03

[a]Only one crystal available at this temperature. Limits given are standard errors for least square fits.

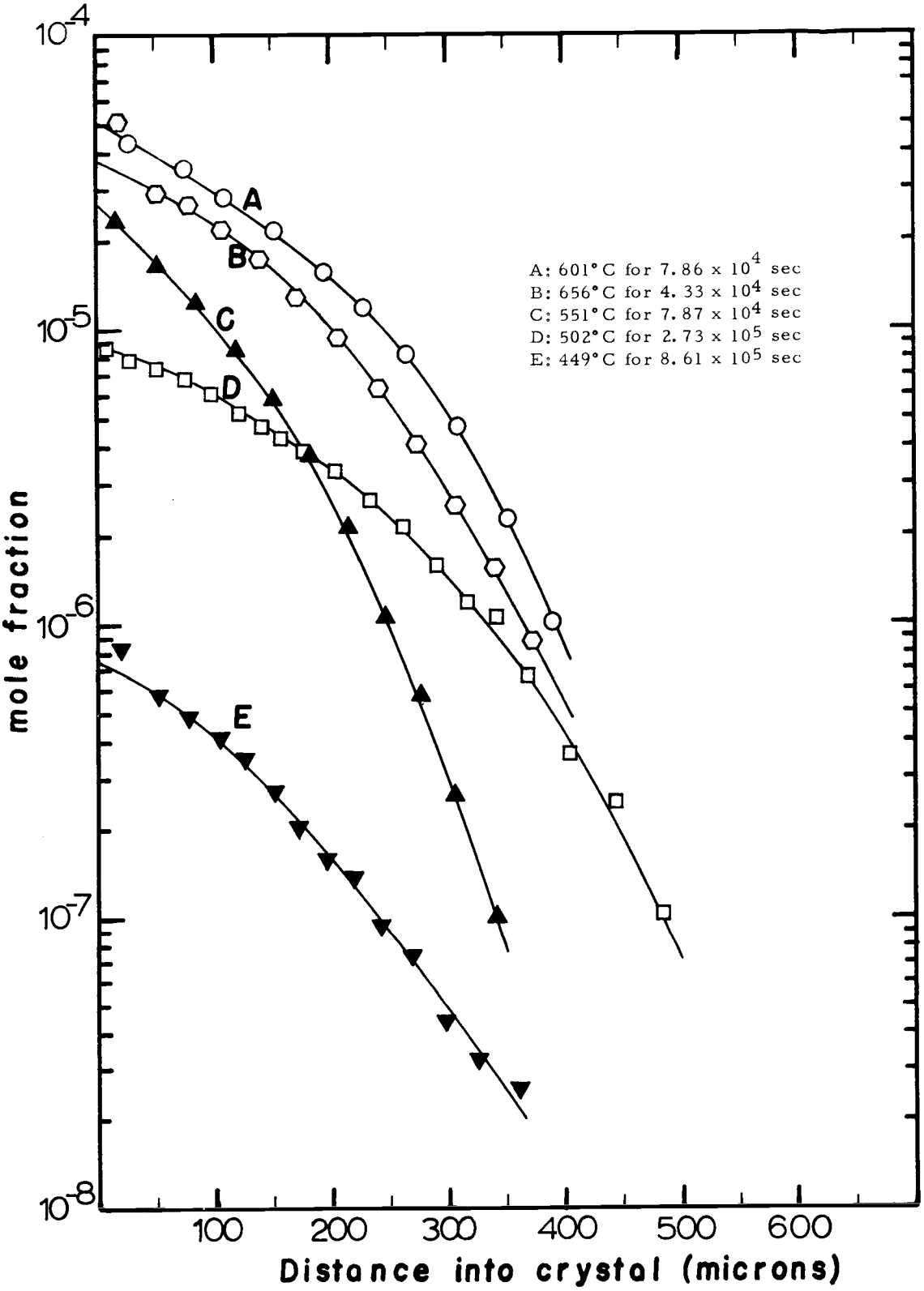

Figure 4.1. Mole fraction of manganese as a function of distance into sodium chloride crystals for various times and temperature.

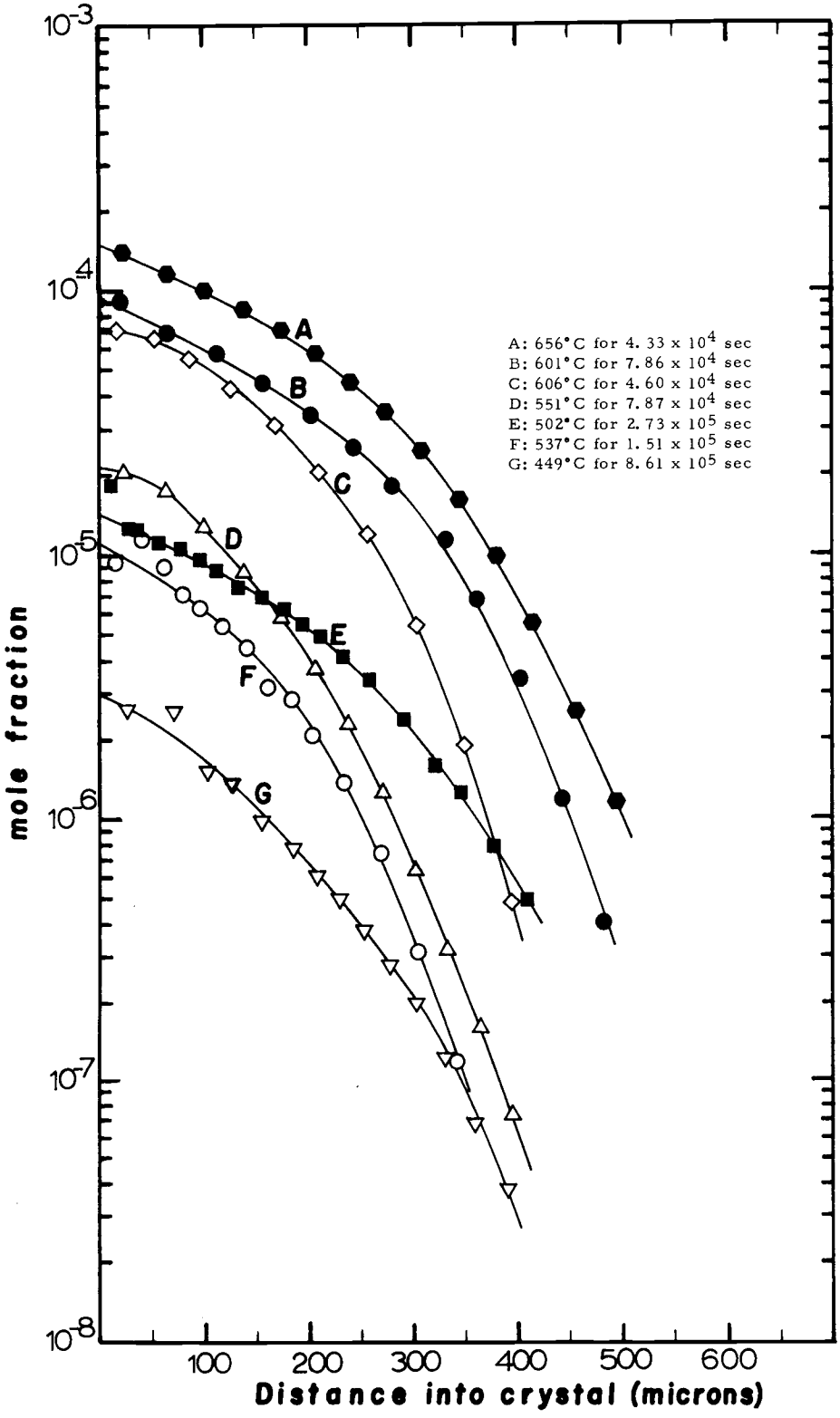

Figure 4. 2. Mole fraction of manganese as a function of distance into sodium chloride crystal for various times and temperatures.

D_s is plotted vs. $1/T$ ($^\circ K^{-1}$) in Figure (4. 3). The straight line through the experimental points was obtained by a least squares fit of the data to a straight line. As noted previously, from equation (2. 7), the slope of this straight line will lead to a value for U_o, the activation energy for exchange of positions between a divalent cation and its associated vacancy. U_o from Figure (4. 3) is $0.889 \pm .073$ ev. The limits were estimated from the difference of the slopes of D_s vs. $1/T$ calculated for the lower values of D_s at each particular temperature and for the higher values of D_s at each temperature. All the lower data gave a line with a slope leading to $U_o = 0.883$ ev and all the higher data gave a line with a slope leading to 0. 896 ev. The average U_o is given above. Hence the saturation diffusion coefficient is

$$D_s = 5.87 \times 10^{-4} \text{ cm}^2/\text{sec } e^{-20,500 \text{ cal}/RT}$$

Note the other lines on Figure (4. 3). The dashed line is that obtained by Lure, Murin and Brigevich (47) using radiotracers to study vapor phase diffusion. With techniques much the same as used in this determination they obtained $U_o = 0.66$ ev, which is quite a bit lower than that obtained here, but they note that the NaCl used contained Ag and Al impurities to the extent of 10^{-3} mole percent. Lure et al. also express the free energy of association as

$$\Delta G(\text{ev}) = 0.7 - 1.9 \times 10^{-4} T$$

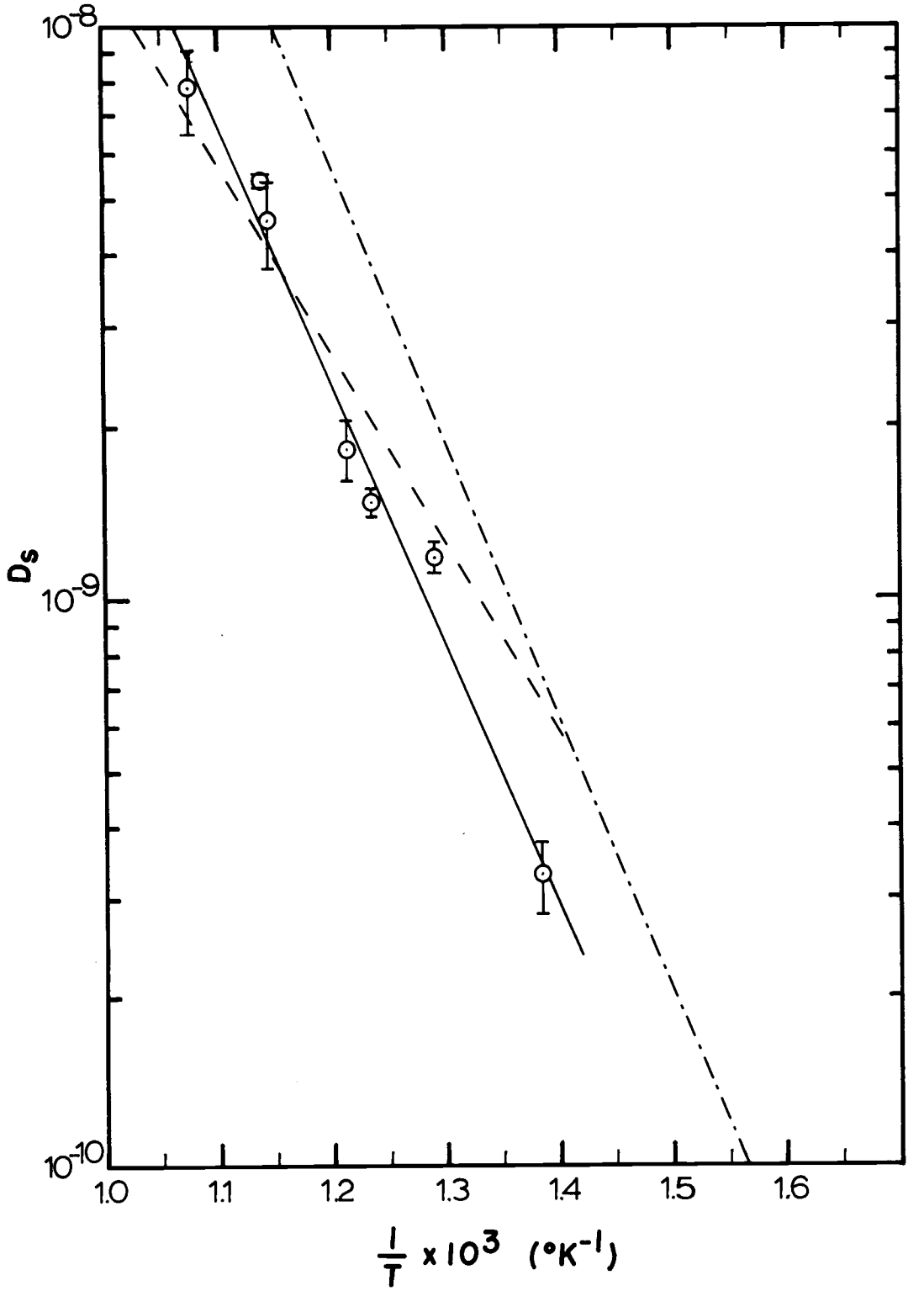

Figure 4. 3. Saturation diffusion coefficient for diffusion of manganese into sodium chloride as a function of reciprocal temperature (°K^{-1}). Solid line is from least squares fit to the data of this work, dashed line is that reported by Lure et al. and the dotted and dashed line is that reported by Stewart and Reed.

The dotted and dashed line in Figure (4. 3) shows the data obtained by Stewart and Reed (70) using surface diffusion techniques and electron para-magnetic resonance to measure relative concentrations of manganese. They note that their crystals contained a trace of iron as found by optical and X-ray spectrographic analyses. Stewart and Reed report that

$$D_s = D_o \exp(-\phi/kT)$$

is applicable with $D_o = 3.48 \times 10^{-3}$ cm^2/sec and $\phi = 0.954 \pm .037$ ev. Note that Stewart and Reed's results are not included in the limits of error of this work.

No estimate of the free energy of association could be made by them since they measured only relative concentrations of manganese II. Measurements of relative concentration by ESR is generally accurate to plus or minus one to two percent but for measurement of absolute concentration errors of the order of 30 percent are common. Both Stewart and Reed and Lure et al. report impurities in the sodium chloride. No estimate is made by Stewart and Reed of the amount of iron present, while Lure et al. estimate 10^{-3} mole percent impurity concentration.

Iron and aluminum impurities in alkali chlorides are rather uncommon compared to the alkaline earths; calcium, magnesium and strontium. Fredericks and Schuerman (25, p. 38) have reported

finding alkaline earths present to about 9 ppm (molar) in Merck reagent grade KCl as measured by an EDTA titration. Unintentional aliovalent impurities will increase the vacancy concentration and increase the degree of association. Impurities having the same valence as the host cation will not affect the diffusion since they will not bring in vacancies with them. Stewart and Reed introduced the manganese into the crystal by surface diffusion. They note that they used polished crystals and measured the concentration to an average depth of 150 microns. In the vapor phase work performed here concentrations were measured about 600 microns into the crystal to be sure of observing bulk effects and to minimize surface effects. In some crystals anomalous behavior which we attribute to surface effects are observed as far as 50 microns into the crystal.

The free energy of association, $-\Delta G$, is shown in Figure (4. 4). as a function of temperature in degrees Kelvin. From this curve the free energy of association may be expressed as

$$-\Delta G(ev) = -1.090 + 5.0 \times 10^{-4} T$$

The difference in the signs of the equation for ΔG reported by Lure et al. and reported here is due to the definition of ΔG. Lure et al. define the free energy of association as ΔG while we define it as $-\Delta G$.

The values of $-\Delta G$ shown in Figure (4. 4) are quite a bit higher than the usual values for the free energy of association; lead, for

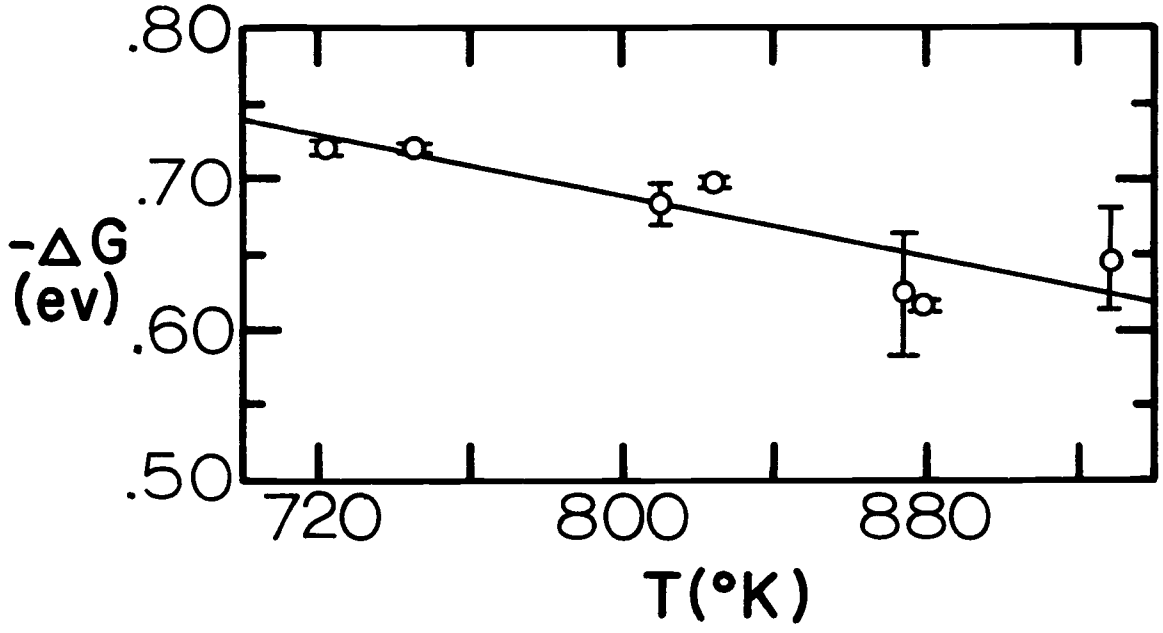

Figure 4.4. Free energy of association as a function of temperature for manganese in sodium chloride. The straight line is a least squares fit to the data points. The entropy of association is found from the slope of the straight line, i.e. $\Delta S = \partial(-\Delta G)/\partial(T)$.

instance, has $-\Delta G = 0.37$ at 500° C. Manganese being much smaller has a much higher charge density than lead and one would expect a higher free energy of association. With a free energy of this magnitude, next nearest neighbor association can be expected, however no value of $-\Delta G$ has been obtained here for that. Watkins (73) in studying the ESR spectra of Mn^{+2} in alkali chlorides assigned one spectrum to Mn^{+2} with an associated vacancy in the next nearest neighbor position. Using the ratio of intensities of the spectra and assuming that the vibrational frequencies for the two different vacancies are the same, he finds that $E_1 - E_2 = +0.034$ ev, where E_1 is the binding energy (not free energy of association) of the nearest neighbor complex and E_2 is the binding energy of the next nearest neighbor vacancy complex. E_1 has been estimated by Watkins as 0.39 ev. He states that the estimate must be considered tentative for two reasons: 1) calcium ions in about the same concentration as manganese were found as an impurity, and 2) he could not guarantee that there was not a precipitated phase acting as a source for manganese as the temperature was raised.

E_1 can be estimated from this work. If the PV work can be considered small then $H_1 \approx E_1$; this work has found $H_1 = 1.09$ ev.

In Table (4.2) is collected the activation energy, U_o, for several ions in sodium chloride and their radii.

Table 4. 2 . Activation energies of some impurities in NaCl.

Impurity	Radius (A)[a]	U_o(ev)	Source
Ni^{+2}	0. 74	1. 3	(32)
Co^{+2}	0. 74	1. 1	(32)
Zn^{+2}	0. 74	1. 02	(61)
Mn^{+2}	0. 80	0. 889 $\pm$. 006	(This work)
		0. 66	(47)
		0. 954 $\pm$. 037	(71)
Cd^{+2}	0. 97	0. 92	(2)
Ca^{+2}	0. 99	0. 90	(56)
Pb^{+2}	1. 20	0. 99	(3, 50)
Na^{+}	0. 95		

[a]Ionic radii from Pauling (57, p. 514 and 518)

The activation energies are only meaningful when estimated from the slope of D_s vs $1/T$ where D_s is the saturation diffusion coefficient, i. e., the diffusion coefficient of the impurity when $p = 1$ at each particular temperature. D_s was the quantity used to determine the activation energy for the impurities Pb, Cd, Ca, Mn (this work), and Zn. The references for Ni, Co and Mn (71) do not explicitly specify that D_s has been used. These last three experiments were performed by surface diffusion techniques and the concentrations of impurities may be large enough so that $D = D_s$.

Referring to Table (4. 2), note that the largest activation energies are for the smallest ions. Since U_o is the energy necessary to push a divalent cation between two chloride ions into a vacancy in the nearest neighbor position, one might expect that the smaller the ion the less the amount of energy needed. Nickel, with a d^8 configuration, and cobalt, with a d^7 configuration, have ground states which interact with an octahedral field (12, p. 724 and 577), so there is an extra energy of activation needed to overcome the stabilization energy. On a qualitative basis this might explain the higher activation energies for Ni^{+2} and Co^{+2}. McClure (49, p. 426) gives a value of 10Dq = 6000 cm^{-1} for Ni^{+2} in an octahedral field of 6 Br^-. Since Cl^- is a slightly stronger ligand according to the spectrochemical series, 10Dq $\approx$ 6500 cm^{-1} for 6Cl^-. McClure also gives a value of 10Dq = 8600 cm^{-1} for 6H_2O around Ni^{+2}. Cotton and Wilkinson (12, p. 736) give a value of 9000 cm^{-1} for the $^3A_{2g} \rightarrow {}^3T_{2g}$ absorption in $(Ni(H_2O)_6)^{+2}$. Using this information and the energy level diagram for a d^8 ion (12, p. 577), the stabilization energy of the ground state of Ni^{+2} in an octahedral field of 6 Cl^- ions can be placed at approximately 0. 8 ev. In a similar manner the stabilization energy for Co^{+2} in an octahedral field of 6 Cl^- ions is estimated at 0. 6 ev. Simply subtracting these stabilization energies from U_o would give a value of about 0. 5 ev for the "hard sphere part" of the activation energies for nickel II and cobalt II. Of course, the octahedral field is not completely removed during the movement process, just distorted, and so this estimate

of the "hard sphere" part of U_o is really much too low.

The next two ions listed in Table (4. 2) are Zn^{+2} with a d^{10} electron configuration and Mn^{+2} with d^5. A d^5 configuration ground state is not split in the octahedral field of 6 Cl^- ions and, of course, the d^{10} configuration is a closed shell. Thus Mn^{+2} and Zn^{+2} ought to act as hard spheres. The remaining ions in Table (4. 2), Cd^{+2}, Ca^{+2} and Pb^{+2}, have electron configurations that should exhibit hard sphere characteristics.

In a sodium chloride lattice the chlorides along the $<110>$ directions are separated from each other by an average distance of 0. 3A on a hard sphere approximation, i. e., they do not touch. Substitution of a divalent cation of radius $\sim$ 0. 75A for a Na^+ ion of radius 0. 95A would allow the chloride ions to relax inwardly on the divalent cation until the chlorides touched, particularly the chlorides between the divalent cation and the associated vacancy. The extra positive charge on the divalent cation and the net negative charge on the associated vacancy would aid this relaxation. Therefore, U_o might be higher for this case than for an ion of radius about equal to that of sodium because this directed relaxation of the intervening chlorides would have to be overcome. Ions with radii about equal to sodium's would have little or no relaxation and larger ions such as lead would cause a relaxation outwardly which would be advantageous for the exchange of places. Watkins (74) has used this idea of

directed relaxation to explain the lower activation energy needed for vacancy motion from one associated position to another in NaCl:Mn. Of course, the bigger ions must push the intervening chlorides further apart to move through, but this really isn't as serious an objection as it seems at first. The interstitial positions in NaCl are large enough to accomodate a sphere of radius 0.6A. Instead of moving through the chlorides in a straight line to the vacancy, a divalent impurity could move into the interstitial position and then to the vacancy position; thereby bypassing the necessity of having two chloride ions separate a distance equal to the diameter of the divalent cation. This distance would be considerable in the case of lead particularly. Divalent cations equal to or larger than sodium would have good access to this pathway but, because of directed relaxation, ions smaller than sodium would have a rather poor access, i.e., they would have to overcome the directed relaxation first. The contention here then is that the energy saved by a small ion in moving to the interstitial and thence to the vacancy is smaller than the energy needed to overcome the directed relaxation present for small ions. Rothman et al. (61) refer to a private communication from Tosi which states that relaxation around an ion as small as Zn^{+2} may be very large and if the anions relax inwardly far enough, next nearest neighbor association can become important. The diffusion of Mn^{2+} appears to support the directed

relaxation model.

In order to get an idea of the displacements involved in this mechanism, consider the tetrahedron of chloride ions surrounding an interstitial. An impurity ion passing through a face of the tetrahedron would separate the three chloride ions in the face equally - an equilateral triangle. On this model the equilateral triangle of the chlorides would have a side of length 4. 52A when a manganese ion was passing through and a side of length 5. 20A when a lead ion passed through. This corresponds to a separation distance between chlorides of 0. 90A for manganese and 1. 58A for lead. Compare this with 1. 60A for manganese and 2. 40A for lead for direct movement and the interstitial picture indeed looks attractive. We can note that chloride ions have an average separation of 0. 3A in sodium chloride anyhow, so 0. 9A would correspond to pushing both intervening chlorides back against their neighbors along a < 110> direction.

The Pauling radii used in Table (4. 2) and for the above calculation depend on assumptions that probably are not applicable. Tosi and Fumi (72) have calculated the ionic radii of various alkali halides with the NaCl structure by use of solid state data and application of the Huggins-Mayer form of the Born repulsive energy while allowing the crystal hardness parameter to vary from salt to salt. They found that the disparity between the radii of the cations and anions in the alkali halides is not as great as implied by the Pauling radii.

They found $r_+ = 1.20A$ and $r_- = 1.62A$ for NaCl. Tosi-Fumi radii are consistent with information obtained from X-ray maps of the electronic distribution in sodium chloride. No estimates of corrected radii for the ions in Table (4. 2) have been made by Tosi and Fumi but one might expect that because of the extra positive charge on a divalent cation the relative increase for a divalent cation would not be as great as for the sodium cation and the smaller the divalent cation the less the change. Sodium goes from 0. 95A to 1. 20A by the different estimates; a change of about 25 percent. Estimating a ten percent increase for Mn^{+2} and a 15 percent increase for the more polarizable Pb^{+2} we have 0. 9A for Mn^{+2} and 1. 4A for lead as new values. On this model then the interstitial positions can now accomodate a sphere of radius 0. 8A. Considering movement of an impurity ion through the face of the tetrahedron into the interstitial position as before, the length of the side of the equilateral triangle is 4. 4A for manganese and 5. 2A for lead requiring a separation distance between chlorides of 1. 2A and 2. 0A for manganese and lead respectively. The usual separation between chlorides in sodium chloride is 0. 8A using Tosi and Fumi values. Direct movement through the chlorides would require a chloride separation of 1. 8A and 2. 8A for manganese and lead respectively. Thus, use of the Tosi and Fumi radii makes the interstitial pathway picture even more attractive.

In order to estimate the magnitude of the energy of the directed relaxation we can make use of a paper by Boswarva and Lidiard (5). In calculating the energy of formation of Schottky defects in ionic crystals they calculate the energy of the latice relaxation of the six chlorides around a cation vacancy as 0. 55 ev for sodium chloride. A cation vacancy in NaCl has a net charge of -1. If a divalent cation which has a net charge of +1 is substituted for a host cation in the nearest neighbor position to a vacancy and if that ion is small enough to allow relaxation of the two intervening chlorides toward it, the energy of that directed relaxation can be estimated as 0. 55 ev in NaCl. Of course the polarizibility and compressibility factors would be different in this case but the energy is quite insensitive to changes in these parameters (5, p. 25). To decide if an ion is "small enough" one can refer to Boswarva and Lidiard again (5, p. 40). The lattice displacements of the six chlorides around a vacancy which correspond to 0. 55 ev is 0. 18A for each chloride for NaCl. A divalent cation with a vacancy in the nn position would have the two intervening chlorides move almost exclusively (directed relaxation). Their displacement would be greater than 0. 18A each, perhaps as much as twice that value, i. e. 0. 36A. In order to accomodate this movement in NaCl for instance, the largest possible divalent cation could have a Tosi-Fumi radius of about 1. 0 A--corresponding to a Pauling radius of about 0. 85 A. Divalent cations with a Pauling

radius greater than 0.85 A would have to overcome a fraction of the 0.55 ev directed relaxation energy until the ion was as large as sodium for which no directed relaxation would be expected.

Therefore, in NaCl, ions with a Pauling radius less than 0.85 A should have a directed relaxation energy of about 0.55 ev to overcome for movement. Ions larger than 0.85 A radius should see a reduced directed relaxation until ions of the same size as sodium (in the Tosi-Fumi concept) when little or no directed relaxation energy is present.

Since cadmium will be of interest later, it will be discussed in sodium chloride briefly. It is a divalent cation with a Pauling radius about equal to sodium's so that it should be smaller than sodium when transposed to Tosi-Fumi values; therefore, it should have some relatively small contribution to its activation energy from directed relaxation.

Table (4.3) compares the experimental values of $\Delta S = \frac{\partial(-\Delta G)}{\partial T}$ for various divalent impurity cations.

The configurational entropy of the orientation of the impurity-vacancy complex is accounted for by the factor of 12 in equation (2.2). The term ΔS, tabulated in Table (4.3) includes all other contributions to the entropy that occur as a result of replacing a host cation adjacent to a divalent impurity cation with a vacancy. These contributions include 1) distortion of the charge cloud of the divalent

impurity cation, 2) movement of the intervening anions out of their equilibrium positions, and 3) movement of the impurity cation off of its equilibrium position. There are other more subtle effects but to a good approximation these are the most important. These also are the entropy contributions that would vary most with different divalent cations. One might then hope to explain the variation of ΔS with ions of different radii on this basis, however the data for NaCl are very scattered and not worth such a treatment. This analysis will be applied to impurity cations in KCl for which the data are somewhat better behaved.

Table 4..3. . Entropy of association for some divalent cations in NaCl.

Impurity	Radius A[a]	ΔS (ev/deg)	Source
Mn^{+2}	0.80	5.0×10^{-4}	This work
		1.9×10^{-4}	(47)
Cd^{+2}	0.97	14.6×10^{-4}[b]	(2)
Ca^{+2}	0.99	4.9×10^{-4}	(56)
Pb^{+2}	1.20	2.8×10^{-4}	(3, 50)
Na^{+}	0.95		

[a]Ionic radii from Pauling (57, p. 514 and 518)

[b]Calculated for a straight line through the data at temperatures > 400° C.

Manganese in Potassium Chloride

Figure (4. 5) (4. 6) and (4. 7) show the concentration of manganese as a function of distance into the crystal for diffusion into KCl at various times and temperatures. Table 4. 4 summarizes the results. The numbers shown are averages of two crystals with the errors indicating the spread of that average.

Table 4. 4. D_s and $-\Delta G$ for diffusion of Mn^{+2} into KCl.

Temp. (°C)	$D_s(cm^2/sec)$	$-\Delta G$ (ev)
457	$1.75 \pm .39 \times 10^{-9}$	0.68 ± 0.04
465	$2.79 \pm .23 \times 10^{-9}$	0.70 ± 0.01
474	$4.49 \pm .55 \times 10^{-9}$	0.56 ± 0.01
482	$4.40 \pm .18 \times 10^{-9}$	0.59 ± 0.00
512	$1.94 \pm .02 \times 10^{-9}$	0.76 ± 0.00
533	$2.62 \pm .45 \times 10^{-9}$	0.75 ± 0.03
564	$6.49 \pm .11 \times 10^{-9}$	0.72 ± 0.00
583	$6.93 \pm .12 \times 10^{-9}$	0.70 ± 0.00
616	$1.42 \pm .30 \times 10^{-8}$	0.61 ± 0.03
653	$1.85 \pm .08 \times 10^{-8}$	0.64 ± 0.01

Figure (4. 8) shows the saturation diffusion coefficient, D_s plotted vs. $1/T$ ($°K^{-1}$). The slope of the best straight line through the higher temperature data leads to a value for U_o of $1.053 \pm .017$ ev. The error here is estimated the same way as for Mn^{+2} in NaCl. In the temperature region 512° C to 653° C the saturation diffusion coefficient is given by

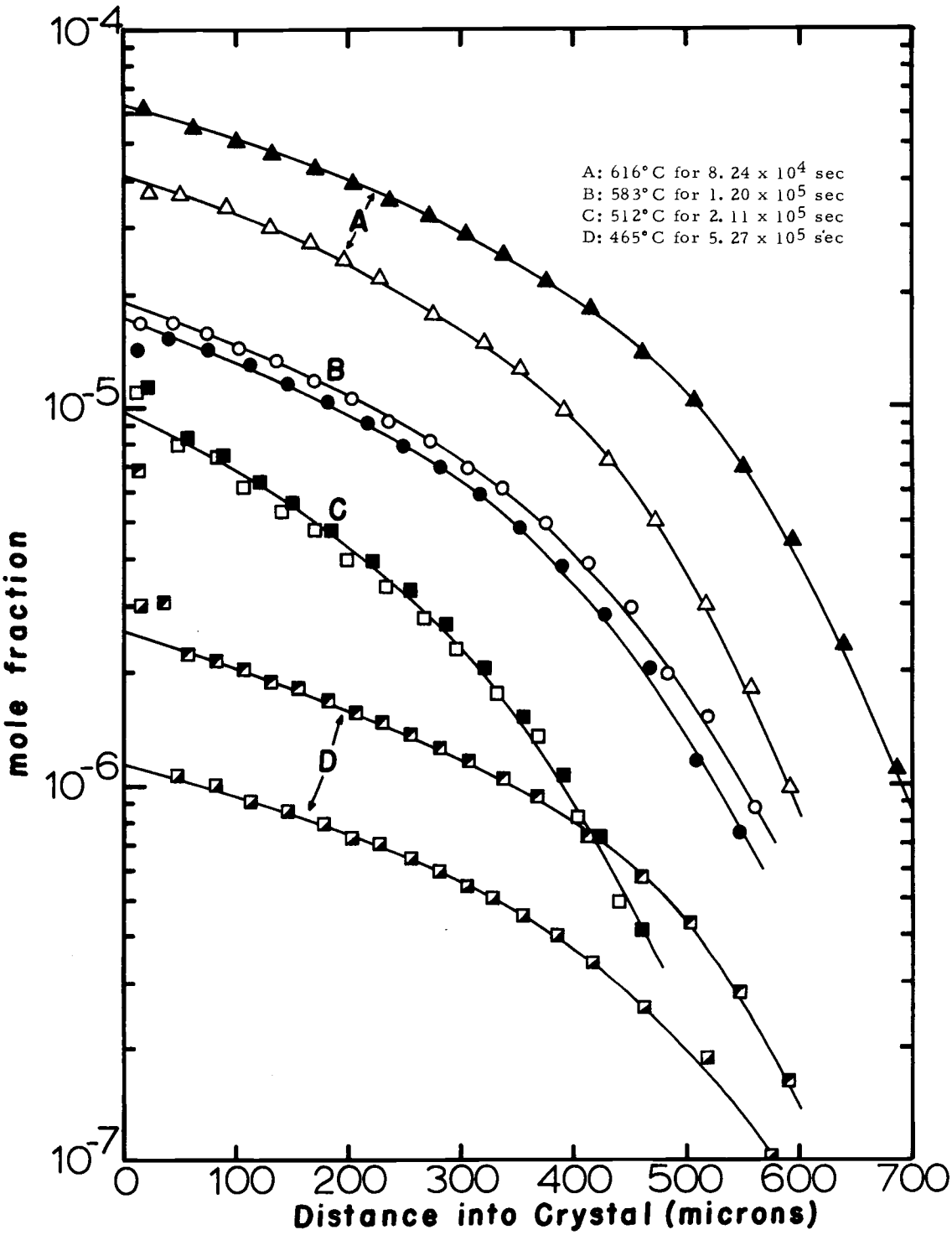

Figure 4.5. Mole fraction of manganese as a function of distance into potassium chloride crystal for various times and temperatures.

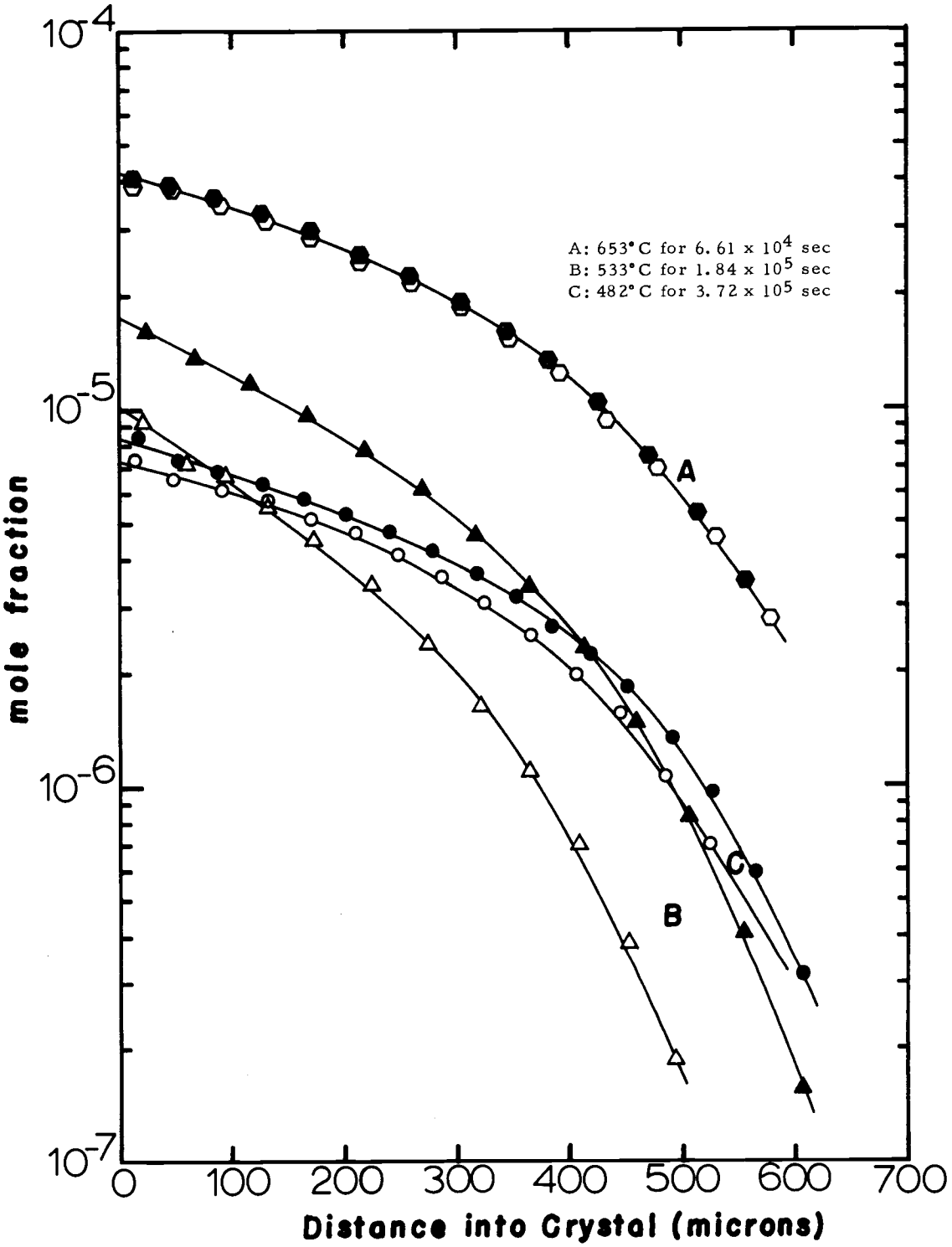

Figure 4.6. Mole fraction of manganese as a function of distance into potassium chloride for various times and temperatures.

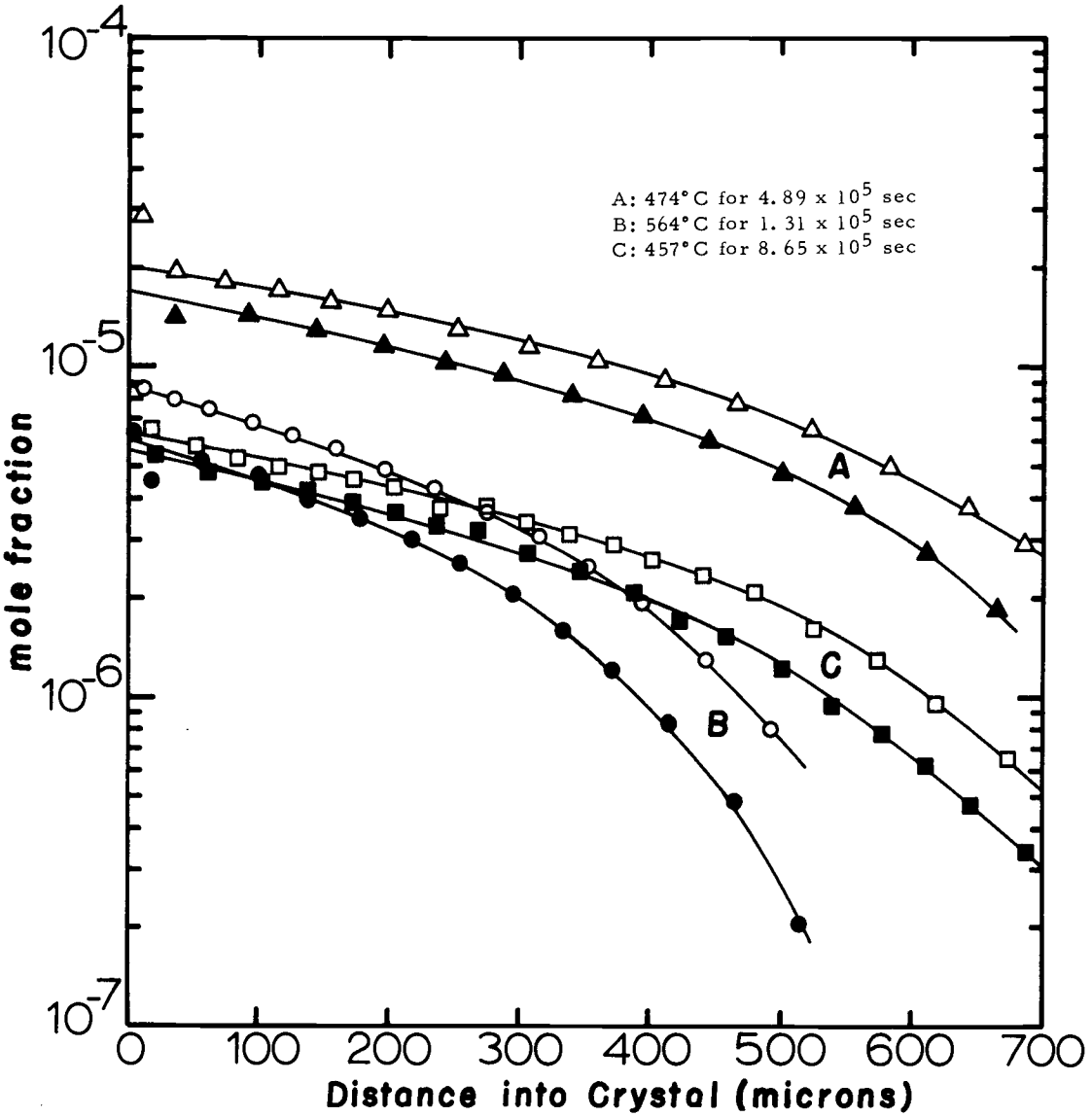

Figure 4.7. Mole fraction of manganese as a function of distance into potassium chloride for various times and temperatures.

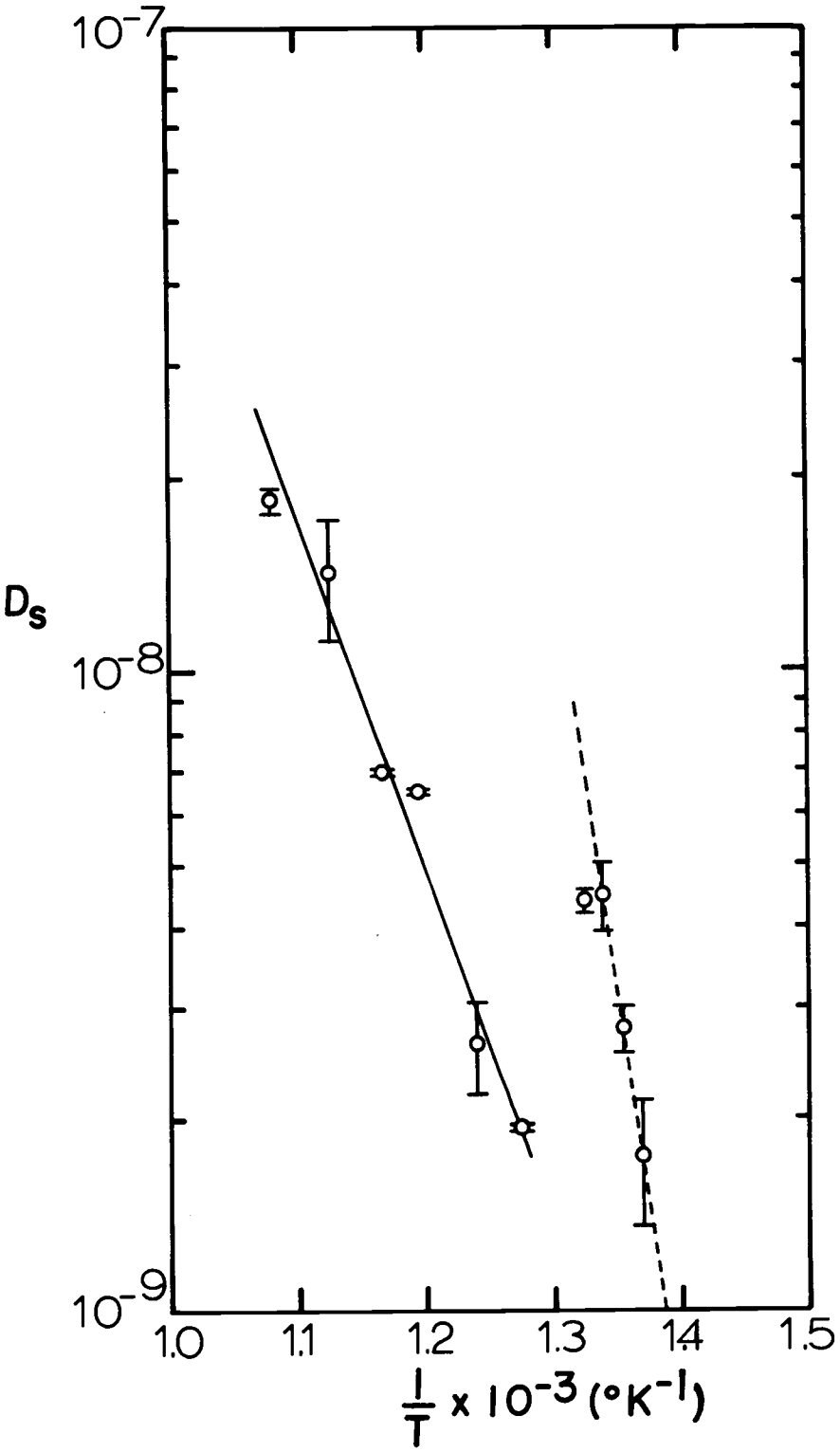

Figure 4.8. Saturation diffusion coefficient for diffusion of manganese into potassium chloride as a function of reciprocal temperature ($°K^{-1}$). Solid line at higher temperature is from least squares fit to the data along that line. Dashed line at lower temperatures is from least squares fit to the 3 points along it.

$$D_s = .0116 \text{ cm}^2/\text{sec } e^{-24,300 \text{ cal}/RT} . \qquad (4.1)$$

Figure (4.8) also contains points that are not on the straight line through the data at higher temperatures. The experimental results suggest a combination of two processes, the higher temperature one described above and another at lower temperatures, joined by a transition region from 482 to 512° C. The narrow temperature range of this transition suggest an attempt at explanation in terms of a "phase change" theory which states that at lower temperatures the lattice surrounding the manganese has relaxed so much that it is no longer interlocking fcc, but has assumed some other symmetry to reduce the strain this small dipositive ion has precipitated. As the temperature is raised a transition temperature is reached at which the lattice around the manganese reverts back to the fcc structure and the diffusion proceeds as described before. This theory does not state that the whole KCl crystal changes phase but only a rather small region around the manganese impurity.

Morlin (54) has measured the d. c. conductivity of CsCl as it passes through its phase transition region around 470° C and has found a discontinuous change in conductivity vs. 1/T. The Nernst-Einstein equation relates conductivity, σ, and diffusion, D, as

$$\frac{\sigma}{D} = \frac{Ne^2}{kT} \qquad (4.2)$$

or

$$\sigma = \text{const. (at constant T) } D \quad . \tag{4.3}$$

The change of conductivity as a function of D at constant temperature is

$$(\partial\sigma)_T = \text{const. } (\partial D)_T \quad . \tag{4.4}$$

So the relative change in σ and D is

$$\frac{(\partial\sigma)_T}{\sigma} = \frac{(\partial D)_T}{D} \quad . \tag{4.5}$$

Morlin (54) shows a change in σ of about 4×10^{-5} ohm^{-1}cm^{-1} at $\sigma = 10^{-5}$ ohm^{-1}cm^{-1}, so that $(\partial\sigma)_T/\sigma = 4$. Figure (4.8) shows a change in D of about 4×10^{-9} cm^2/sec at $D = 2 \times 10^{-9}$ cm^2/sec giving $(\partial D)_T/D = 2$. It might be argued that the change in σ for a phase change is a macroscopic change involving the whole crystal and the change for D is a microscopic one involving only a small portion of the lattice; therefore, this agreement is purely fortuitous. However, as far as the manganese ion is concerned this proposed "phase change" seems to be happening throughout the crystal. Since the manganese ion feels the effect of a "phase change" in the region around it as though it were happening throughout the entire crystal, this agreement between $(\partial\sigma)_T/\sigma$ for CsCl and $(\partial D)_T/D$ for manganese in KCl is a point in favor of the "phase change" theory.

Another point in favor is the fact that the high temperature

phase appears to be fcc because of the more reasonable value for the activation energy at higher temperatures. The D_s values used to calculate the activation energy are found from the D(c) values at each temperature by postulating fcc symmetry (see equation (2. 6)).

In the luminescence section it is shown that the emission of manganese in KCl is quite similar to its emission in NaCl indicating that at room and low temperatures the manganese ion is in a similar environment in both lattices. This might be construed as an indication that the Mn^{+2} in KCl at room temperature is in a lattice of fcc symmetry since Mn^{+2} in NaCl is thought to be in a lattice of fcc symmetry at room temperature (perhaps Mn^{+2} in NaCl goes through a phase change at a lower temperature than KCl:Mn^{+2} ?). In this connection it ought to be noted that the energy level diagram for a d^5 ion is the same in a tetrahedral and an octahedral field, i. e. it is rather insensitive to any distortions in the surroundings. Therefore, no deductions from the data on luminescence can be made as to the similarity or non-similarity of the manganese surroundings in NaCl and KCl.

Morlin (54) observed the conductivity of CsCl upon the addition of small amounts of $SrCl_2$ (up to a concentration of 3.8×10^{-6} mole fraction) and found no effect on the conductivity previously observed through the phase transition in pure CsCl. If manganese will cause a localized "phase change" in KCl, one might expect an effect on

the conductivity in the phase transition region of CsCl for additions of $SrCl_2$ ($r_{Sr^{+2}} / r_{Cs^+} \approx r_{Mn^{+2}}/r_{K^+}$). None is seen but this may be due to the rather low (compared to diffusion experiments) level of impurities introduced; an order of magnitude increase in the $SrCl_2$ might bring on an effect in the conductivity in the phase transition region of CsCl.

A possible "phase change" around the manganese in KCl might be that the dominant form of divalent cation-vacancy association at lower temperatures is next nearest neighbor (nnn) and at higher temperatures is nearest neighbor (nn) with a transition region having a combination of both associations. The diffusion of the impurity-vacancy complex with nn association can be represented by an equation

$$D_{s_1} = D_o e^{-U_o/RT} \tag{4.6}$$

where the subscripts 1 refer to nn association. The subscripts 2 will be used to refer to nnn association.

For the movement of a manganese ion in the case of nnn association, the difference in free energy $\Delta G_1 - \Delta G_2$ between nn and nnn association at a particular temperature must be supplied plus the energy of activation $E^* = U_o$ for movement of the manganese ion. The quantity $\Delta G_1 - \Delta G_2$ can be identified experimentally as the free energy of association for nn association, i. e. $\Delta G_1 - \Delta G_2 = \Delta G_1 = \Delta G_a$.

This statement says that ΔG_2, the free energy of association for nnn association, is zero. This may seem unrealistic, however, closer examination of the experimental quantity ΔG_a will explain this. The theory considers that there are no interactions between divalent cations and vacancies further away than nearest neighbor and so assigns $\Delta G_{n\neq 1} = 0$. The experimental quantity that is called ΔG_a or ΔG_1 and is shown in Figure (4.9) is actually the difference between ΔG for nn associations and ΔG for any other kind of association particularly nnn association since in actuality nnn association must occur before nn association can occur. Thus the experimental quantity corresponding to $\Delta G_1 - \Delta G_2$ is ΔG_a.

When the predominant associated form is nnn D_s can be written as

$$D_{s_2} = D_o e^{-U_o/RT} e^{-\Delta G_1/RT}$$

$$D_{s_2} = D_o e^{\Delta S_1/R} e^{-(\Delta H_1 + U_o)/RT}. \qquad (4.7)$$

From equation (4.7) the slope of D_{s_2} vs. $1/T$ ought to yield $\Delta H_1 + U_o$ and the pre-exponential term ought to be a factor of $e^{\Delta S_1/R}$ greater than D_o. From equation (4.12) ΔH_1 is 1.598 ev; U_o is 1.053 ev from equation (4.1) and the sum is 2.651 ev as an estimate of $\Delta H_1 + U_o$. The change in entropy on going from nnn to nn association is not quite given by ΔS_a. In the

development of the theory the configurational entropy of nn association was not included in ΔG_1 (see equation (2. 2)). To correct this the entropy of configuration must be calculated.

The configurational entropy is related to the degeneracy by

$$S_s = R \ln 1/s \quad , \tag{4.8}$$

where s = the degeneracy. There are six nnn positions and 12 nn positions so

$$\Delta S_s = S_{nn} - S_{nnn} = R \ln s_2/s_1$$

$$\Delta S_s = -R \ln 2 \quad . \tag{4.9}$$

Therefore the value for ΔS_1 to be used is ΔS_a plus the configurational entropy, ΔS_s. ΔS_a is given in equation (4. 12) as 1.06×10^{-3} ev/deg, so

$$\Delta S_1 = \Delta S_a + \Delta S_s = R(12.3 - 0.70) \tag{4.10}$$

$$\Delta S_1/R = 11.6 \text{ and } e^{11.6} = 1.1 \times 10^5.$$

So the pre-exponential for impurity diffusion with nnn association ought to be a factor of 1.1×10^5 greater than that for nn association.

The dashed line through the lower temperature data of

Figure (4. 8) can be represented by

$$D_s = 1.3 \times 10^{10} \text{ cm}^2/\text{sec } e^{-63,000 \text{ cal}/RT}. \qquad (4.11)$$

Note that no weight is given to the point at $1/T = 1.325 \times 10^{-3}$. It was felt that this was the beginning of the transition region and should not be included. Comparison of equations (4. 1) and (4. 11) shows that the pre-exponential in (4. 11) is greater than that in (4. 1) by a factor 1.1×10^{12} which is 10^7 times the estimated value. Possibly the assertion in equations (4. 6) and (4. 7) that D_o is identical for nn and nnn association is in error, but it would be difficult to justify a factor of 10^7 change in D_o in terms of its physical significance.

The experimental activation energy is 2. 73 ev which is very close to the calculated value, however, until more data is collected below 450° C this agreement must be considered preliminary.

Watkins (73) has reported that in a study of the ESR spectra of manganese II in KCl he has concluded that the nnn site is the more stable at room temperature.

An attempt to explain the transition region of Figure (4. 8) in terms of a combination of higher and lower temperature processes might be made but such an attempt would be rather pointless until experimental points are obtained in the transition region between

482 and 512° C. It is this narrow range of temperatures in which a transition occurs that suggests an explanation in terms of "phase change" ideas.

The rather high value of the activation energy for movement of the manganese ion, 1.053 ev, may be noted. Table (4. 5) lists some values of U_o for various divalent cation impurity diffusion in KCl.

Table 4. 5. Activation energies for various impurities in KCl.

Impurity	Radius (A)[a]	U_o (ev)	Source
Mn^{+2}	0. 80	1. 053	This Work
Cd^{+2}	0. 97	0. 54	(34)
Hg^{+2}	1. 10	0. 57	(1, p. 117)
Pb^{+2}	1. 20	1. 18	(36, 37)
K^{+}	1. 33		

[a]Radii from Pauling (57, p. 514 and 518)

Not considering Mn^{+2}, the activation energy increases with the radius. The explanation for the high value of U_o for manganese would be quite similar to that proposed for the sodium chloride host, i. e., directed relaxation of the chlorides in toward the manganese cation because of its relatively small size. Using Tosi and Fumi radii (72) as discussed before we can calculate some of the relavent sizes. For potassium chloride they report $r_+ = 1.51$ A and $r_- = 1.63$ A. The Tosi and Fumi radii for manganese and lead were

estimated previously as 0.9 A and 1.4 A respectively. The chlorides are separated from each other in the undistorted lattice by an average distance of 1.2 A. As mentioned in the discussion for NaCl a separation of 1.2 A is necessary for movement of a Mn^{+2} ion through a face of the tetrahedron of Cl^- ions and into the interstitial position; a separation of 2.0 A is needed for the same movement of Pb^{+2} ions. It seems then that almost no energy will be required to separate chlorides in the case of manganese, since the equilibrium separation is already 1.2 A.

From the paper by Boswarva and Lidiard (5) we can estimate the energy of the directed relaxation in KCl. The relaxation energy of the six chlorides surrounding a cation vacancy is calculated to be 0.60 ev (5, p. 40) in KCl. By the same reasoning as used for NaCl the energy of the directed relaxation can be estimated as 0.6 ev for a small enough ion in KCl. The lattice displacement of the six chlorides around a vacancy which corresponds to 0.60 ev is 0.21 A for each chloride in KCl (5, p. 40). A divalent cation with a vacancy in the nn position would have the two intervening chlorides move almost exclusively (directed relaxation). Their displacement would be greater than 0.21 A, perhaps 0.40 A. The largest possible divalent cation could have a Tosi-Fumi radius of about 1.3 A--or a Pauling radius of about 1.0 A.

In KCl then, ions with a Pauling radius less than 1.0 A should

have a directed relaxation energy of about 0. 60 ev to overcome for movement. Ions larger than 1. 0 A radius should see a reduced directed relaxation until ions of the same size as potassium (Tosi-Fumi radii) when little or no directed relaxation energy is present.

Manganese is undersized in both lattices so it should have the full directed relaxation of each lattice to overcome for movement into an associated vacancy. $U_o(KCl) > U_o(NaCl)$ experimentally is reasonable from the point of view of directed relaxation but it appears that the energy to separate chlorides ought to be higher in NaCl. $U_o(KCl)$ is almost 0. 20 ev greater than $U_o(NaCl)$ but the energy due to directed relaxation is only about 0. 1 ev greater in KCl.

Comparison of U_o for lead in KCl and NaCl (Tables (4. 2) and (4. 5)) shows that $U_o(KCl) > U_o(NaCl)$. To explain this consider the relative sizes of the Tosi and Fumi radii: 1. 20 A for Na^+, 1. 51 A for K^+ and about 1. 4 A for Pb^{+2} (estimated). Pb^{+2} substituted for a sodium ion causes the chloride ions to relax outwardly--a favorable position for movement. Pb^{+2} substituted for a potassium ion allows the chloride ions to relax inwardly--an unfavorable position. Again we must say that the energy required to overcome directed relaxation in the KCl lattice is greater than that saved by the energetically easier route to the interstitial in KCl. Thus, $U_o(KCl) > U_o(NaCl)$ for lead is reasonable.

The only other ion appearing in both Tables (4. 2) and (4. 5) is

Cd^{+2} for which $U_o(KCl) < U_o(NaCl)$. The Pauling radius of Cd^{+2} is less than the 1.0 A maximum for KCl and one would expect that the directed relaxation energy would be greater than in NaCl where it has been estimated to have only a small contribution to its activation energy from directed relaxation. The more widely separated chlorides in KCl will not have to separate as much to allow a cadmium ion to pass so this part of the activation energy will be lower in KCl than in NaCl. This type of treatment may be qualitatively accurate but it is very difficult to explain the difference between $U_o(KCl)$ and $U_o(NaCl)$ of almost 0.4 ev on this model.

Allen (1, p. 117) found a value of 0.57 for U_o in the KCl:Hg^{+2} system. He calculated D_s from equation (2.6) knowing both D(c) and c, however he notes that he used a value of $-\Delta G$ that was much too high especially at the higher temperatures (1, p. 116 and 130) to calculate D_s. Increasing ΔG in equation (2.6) will cause D_s to decrease. Thus D_s perhaps should be higher at the higher temperatures increasing the slope of D_s vs. $1/T(°K)^{-1}$ and U_o. $U_o = 0.57$ ev is a low estimate for Hg^{+2} and possibly $U_o = 0.54$ ev is too low for KCl:Cd^{+2}, although no specific criticism of the experiment of Keneshea and Fredericks (34) can be made.

Figure (4.9) indicates $-\Delta G$ vs. T for KCl:Mn^{+2}. The meaning of ΔG has been discussed before and an explanation for the anomalous effects at the lower temperatures has already been presented. The

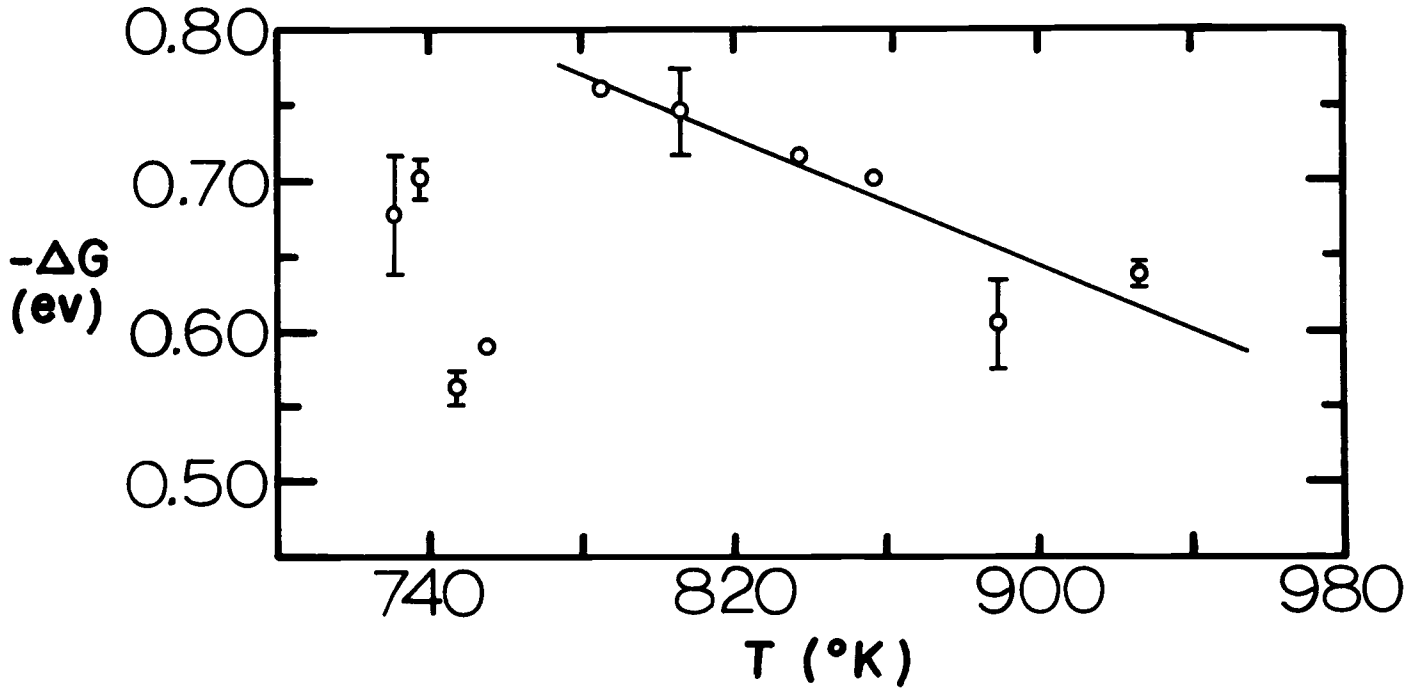

Figure 4.9. Free energy of association as a function of temperature for manganese in potassium chloride. The straight line is a least squares fit to the data along that line. Those points that have no error limits signify experiments that showed identical -ΔG's for both crystals at that temperature.

free energy of association at the higher temperatures can be expressed as

$$-\Delta G(ev) = -1.598 + 1.06 \times 10^{-3} T \qquad (4.12)$$

for 785°K < T < 930°K.

Table (4.6) lists the entropy of association for several impurities in KCl.

Table 4.6. ΔS for some impurities in KCl.

Impurity	Radius (A)[a]	$\Delta S(ev/°K)$	Source
Mn^{+2}	0.80	1.06×10^{-3}	This work
Cd^{+2}	0.97	0.08×10^{-3}	(34)
Ca^{+2}	0.99	0.02×10^{-3}	(4)
Hg^{+2}	1.10	0.46×10^{-3}	(1, p. 81)
Pb^{+2}	1.20	1.27×10^{-3}	(36, 37)

[a]Radii from Pauling (57, p. 514 and 518)

Generally the trend is to increasing ΔS with increasing radius, except for the obvious exception of manganese. As mentioned before for sodium chloride, the entropy of association has three main contributions: 1) movement of the intervening anions out of their equilibrium positions, 2) distortion of the charge cloud of the divalent impurity ion and 3) movement of the impurity cation off of its equilibrium position. For ions as large as Ca^{+2} and larger, types

1 and 3 will be of minimal importance, i. e., there is relatively little directed relaxation. However, the polarizability of an ion increases with its size so that the charge cloud of a larger ion will be more distorted than that of a smaller ion. For spherical molecules or ions the polarizability, α, is equal to the radius of the species cubed, i. e., $\alpha = r^3$ (67, p. 103). Using this formula the polarization for the ions in Table (4. 6) are given in Table (4. 7)

Table 4. 7. Polarizations of some ions.

Ion	Radius (A)[a]	$\alpha = r^3$ (cm^3)
Mn^{+2}	0. 80	0.51×10^{-24}
Cd^{+2}	0. 97	0.92×10^{-24}
Ca^{+2}	0. 99	0.97×10^{-24}
Hg^{+2}	1. 10	1.33×10^{-24}
Pb^{+2}	1. 20	1.73×10^{-24}

[a]Radii from Pauling (57, p. 514 and 518)

While the formula for calculation of α from r is probably not accurate for large variations in r, this does serve to point up the fact that lead is much (more than three times here) more polarizable than manganese and we will expect significantly more distortion of the charge cloud of lead when a vacancy moves into an adjacent position. This would be the major factor leading to the increase of entropy from calcium to lead. For cadmium and manganese the

contribution from charge cloud distortion will be rather small, but here we see the onset of the contribution from movement of the intervening anions out of their equilibrium positions. This, of course, is due to directed relaxation. Finally we would not expect manganese particularly to remain in the equilibrium position it occupies with host cations in all the nearest neighbor positions when we replace one of those hosts with a vacancy. The chloride ions collapsing in on it would tend to force the manganese off of its old equilibrium position more than would be expected for a larger ion.

Thus we can see that manganese exhibits entropy contributions of kinds 1 and 3 while the entropy of association for lead comes predominantly from charge cloud distortion, type 2.

Luminescence

The absorption, excitation and luminescence spectra of the NaCl:Pb:Mn and KCl:Pb:Mn phosphors are shown in Figures (4. 10) and (4. 11). It should be noted that manganese shows no absorption spectrum in these phosphors and that the absorption spectrum for lead and manganese doped halides exactly follows that for lead doped halides. The absorption spectra for lead are also similar to those obtained by Burstein et al. (8). The excitation curves should be taken to indicate the points of maximum excitation rather than a detailed outline of the excitation curve because the bandwidth of the

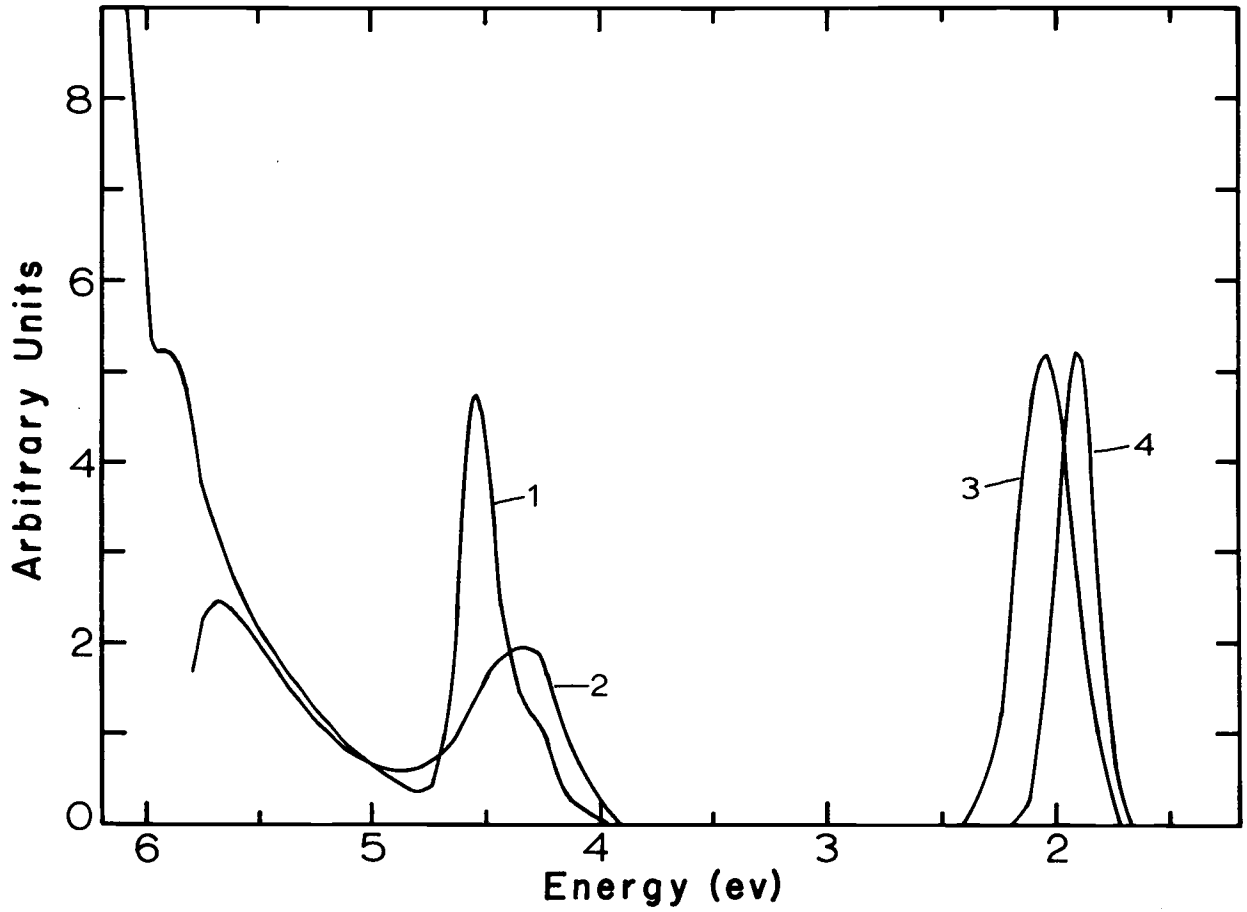

Figure 4. 10. Absorption, excitation and emission spectra for lead and manganese impurities in NaCl. Lines (1) absorption spectrum for NaCl:Pb and NaCl:Pb:Mn: (2) excitation spectrum for manganese emission in NaCl:Pb:Mn phosphor; (3) room temperature manganese emission spectrum of NaCl:Pb:Mn and (4) low temperature manganese emission spectrum of NaCl:Pb:Mn phosphor. All spectra are at room temperature unless otherwise noted. Low temperature is 90 ± 3°K. All spectra taken are on quenched samples.

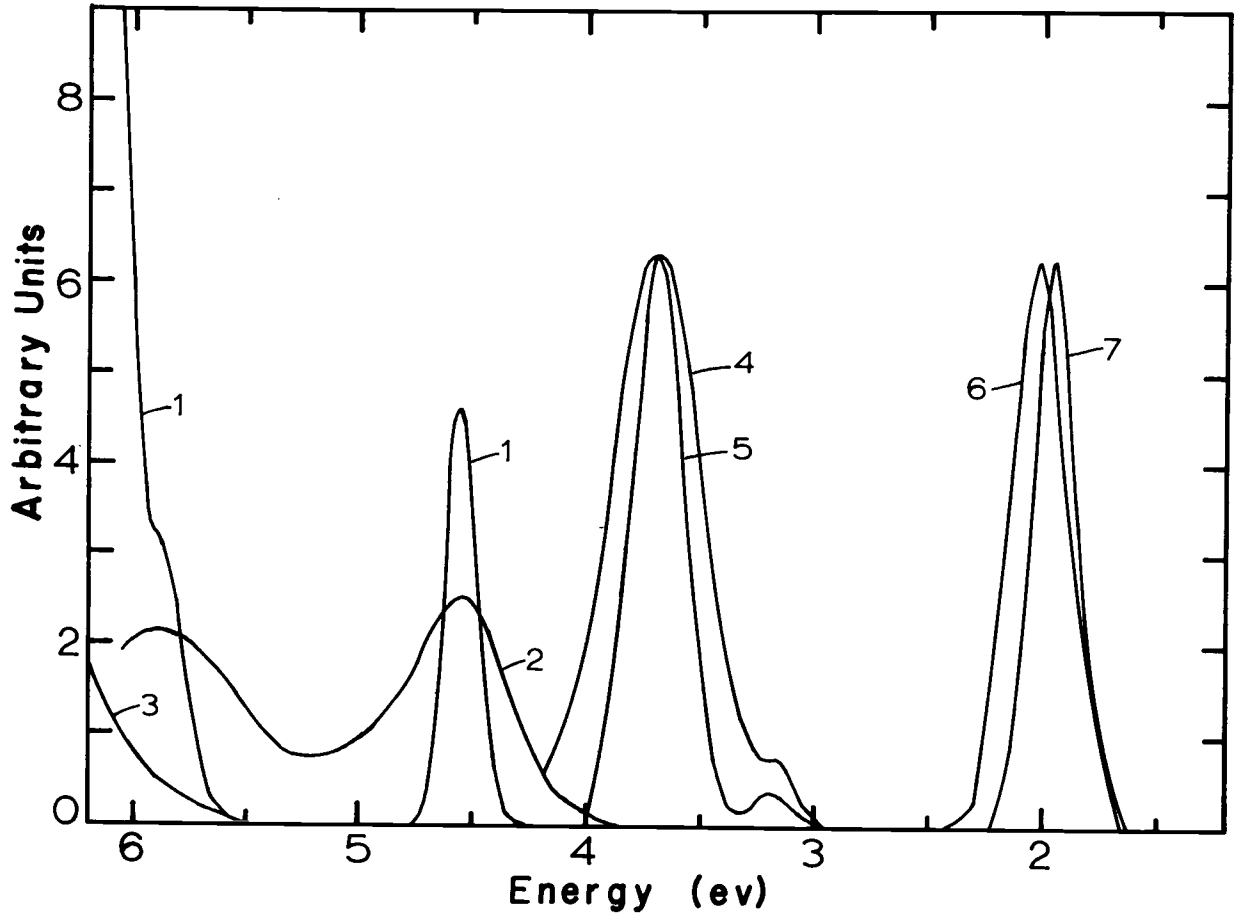

Figure 4.11. Absorption, excitation and emission spectra for lead and manganese impurities in KCl. Lines (1) absorption spectrum for KCl:Pb and KCl:Pb:Mn; (2) excitation spectrum for manganese emission in KCl:Pb:Mn phosphor; (3) absorption spectrum of KCl:Mn; (4) room temperature lead emission spectrum of KCl:Pb:Mn; (5) low temperature lead emission of KCl:Pb:Mn phosphor; (6) room temperature manganese emission spectrum of KCl:Pb:Mn and (7) low temperature manganese emission spectrum of KCl:Pb:Mn. All spectra at room temperature unless otherwise noted. Low temperature is 90 ± 3° K and all samples have been quenched.

exciting light was rather wide. The excitation curves do show maxima at the peaks of the lead absorption, indicating that these are the absorption centers. Note that the excitation maximum for the KCl phosphor occurs just at the absorption peak at 4. 55 ev, while the excitation peak for the NaCl phosphor occurs at the peak of the 4. 28 ev absorption of lead in NaCl. Burstein et al. (8) in considering the absorption of lead in NaCl made a tentative assignment of the 4. 28 ev band to lead-lead pairs in the crystal, while the 4. 55 ev band was assigned to single lead centers, lead-vacancy pairs and lead chloride precipitated phase. He made these assessments on the basis of the change in the absorption spectrum as the sample was heat treated.

For easy reference most of the data to be presented on the next pages are summarized in Table (4. 8).

Schulman, Ginther and Klick (64) in studying the luminescence of NaCl:Pb found luminescence at 3. 88 ev when exciting in the 4. 55 ev band and at 2. 76 ev when exciting in the 4. 28 ev band. They also found that the asymmetrical shape of the absorption curve remained about the same for a wide range of concentrations indicating that the ratio of 4. 28 ev absorbers to 4. 55 ev absorbers is about equal for those concentrations. Using this information they assigned the 4. 55 ev band to transitions in singlet Pb^{+2} ions and the 4. 28 ev band to a transition to an excited state of the singlet Pb^{+2} ion different

Table 4.8. Summary of absorption and emission data.

Sample[a]	Position of Absorption Peaks (ev)	Position of Emission Peaks (ev)[b]	Reference
NaCl:Pb (annealed)	4.77, 4.55, 4.28		(8)
NaCl:Pb (quenched)	4.55		(8)
NaCl:Pb		3.88 (4.55), 2.76 (4.28)	(64)
NaCl:Pb:Mn		3.94 (4.69), 3.45 (4.51) 2.82 (4.51), 2.18 (4.51)	(38)
NaCl:Pb:Mn (annealed)	4.69, 4.55, 4.28	2.26 (4.28), 2.05 (4.28)	This work
NaCl:Pb:Mn (quenched)	4.55, 4.28	2.05 (4.28)	This work
KCl:Pb (annealed and quenched)	4.55		(8)
KCl:Pb:Mn		3.63 (4.69, 4.51) 1.94 (4.61, 4.51)	(38)
KCl:Pb:Mn	4.55	3.61 (4.55), 1.85 (4.55)	(68)
KCl:Pb:Mn (quenched)	4.55	3.70 (4.55), 2.02 (4.55)	This work

[a] All samples at room temperature.

[b] Numbers in parentheses indicate maximum of exciting light.

from the one leading to the 3.88 ev emission. This explanation does not account for the change in absorption band on quenching observed in this work and by Burstein et al. (8). Certainly an electronic transition in a singlet ion should not be affected by thermal history unless it is admitted that the ion's surroundings change. If the surroundings change then the shift in absorption is due to the surroundings and not to a transition to a different excited state. For this reason Burstein et al.'s assessment of the situation is preferred.

KCl:Pb shows no change on heat treatment and has no 4.28 ev absorption band. The reason for the difference in lead doped sodium and potassium chloride is due to the size of the Pb^{+2} ion. The lead ion is about the same size as the potassium ion but quite a bit bigger than the sodium ion, introducing strain in the NaCl lattice and decreasing the solubility. Quenching experiments were also performed on crystals produced in this lab and the results may be seen in Figures (4.12)and (4.13). These samples were quenched by heating in platinum foil in air for 15 minutes at about 630°C and cooling to liquid nitrogen temperature quickly. The time of heating was purposely kept short to minimize the number of oxygen or oxygen-containing centers that might diffuse into the crystal. Reference to Figure (4.13) for KCl shows no change in the absorption spectrum between quenched and annealed samples and little change in the excitation spectrum around 4.55 ev. However, the quenched sample

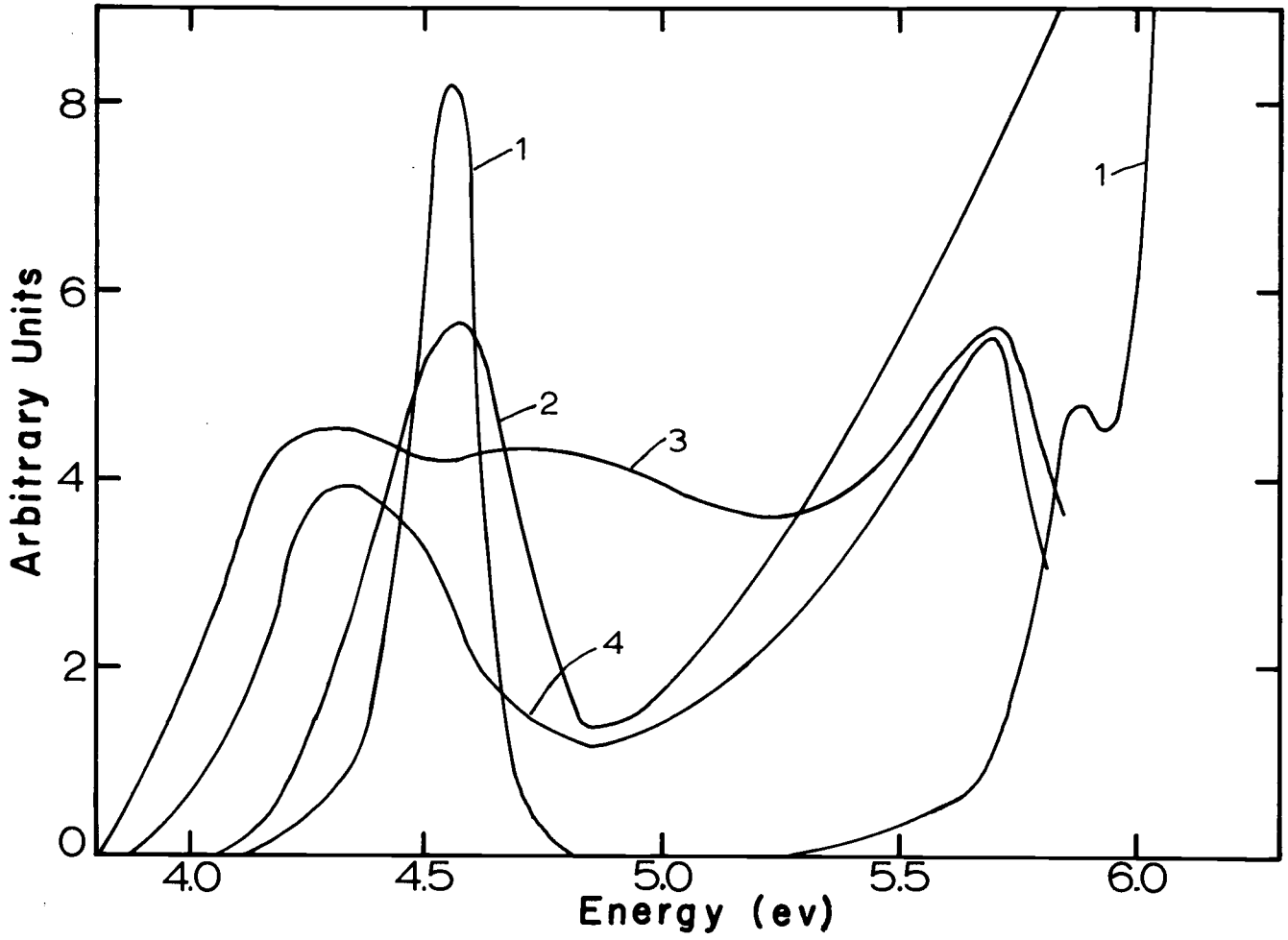

Figure 4.12. Absorption and excitation spectra for quenched and annealed samples of NaCl:Pb:Mn. Lines (1) absorption spectrum of quenched NaCl:Pb:Mn; (2) absorption spectrum of annealed NaCl:Pb:Mn; (3) excitation spectrum for emission of manganese for annealed NaCl:Pb:Mn and (4) excitation spectrum for manganese emission for quenched NaCl:Pb:Mn. All spectra at room temperature.

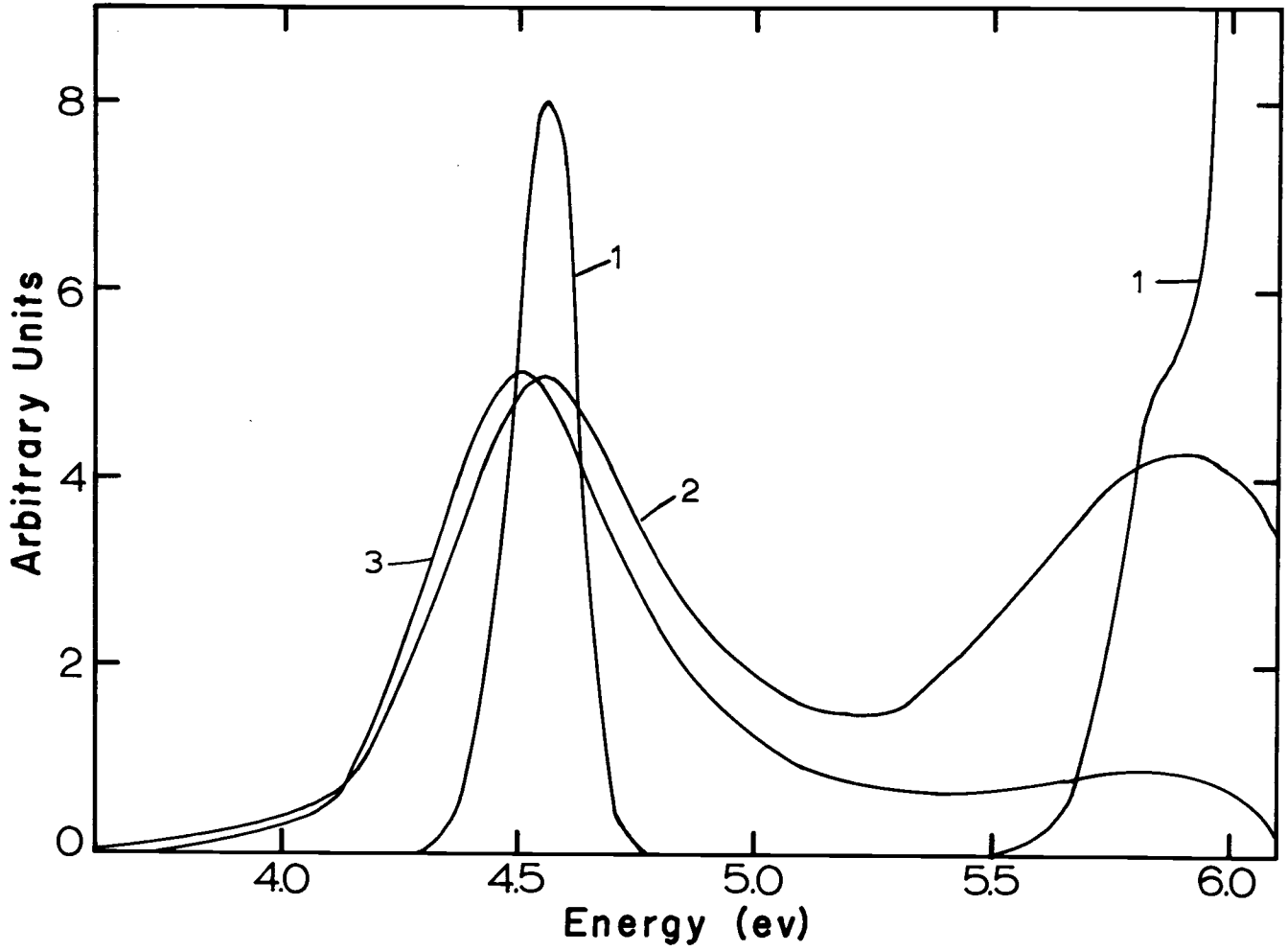

Figure 4.13. Absorption and emission spectra for quenched and annealed KCl:Pb:Mn. Lines (1) absorption spectra of quenched and annealed KCl:Pb:Mn; (2) excitation spectrum for manganese emission for quenched KCl:Pb:Mn and (3) excitation spectrum for manganese emission for annealed KCl:Pb:Mn phosphor. All spectra at room temperature.

does seem to have a better excitation peak at about 5.91 ev than the annealed sample. Figure (4.12) shows the excitation and absorption spectra for quenched and annealed NaCl:Pb:Mn. Quenching cleans up the absorption spectrum considerably and heightens the 4.55 ev absorption band. The maxima of the quenched excitation bands are at 4.34 ev and 5.70 ev. The annealed phosphor shows maxima at 4.28 ev, 4.70 ev and 5.70 ev. Of course, the maximum in the absorption spectra for both quenched and annealed samples is at 4.55 ev, but quenching eliminates the band around 4.77 ev completely and much of the band at 4.28 ev. Burstein et al. (8) made a tentative assignment of the 4.77 ev band to Pb-impurity or Pb-vacancy cluster centers, which they define as the situation where one lead ion is associated with two or more vacancies. The degree of purity of this salt would seem to rule out the possibility of Pb-impurity formation. A comparison of Figures (4.10, 4.11, 4.12 and 4.13) and Burstein et al.'s assignments indicates that the absorbing center in the KCl phosphor is single Pb^{+2} ions or Pb^{+2}-single vacancy pairs, while the absorbing center in the NaCl phosphor may be a variety of species in the annealed sample or in the quenched case, single lead centers, lead-vacancy pairs, lead-lead pairs or precipitated phase lead chloride. The lead concentration was kept below 10^{-3} mole fraction and usually below 10^{-4} mole fraction to minimize the formation of a precipitated phase or lead-lead pairs. In any case the samples

used for quantum efficiency as a function of concentration were all quenched. It might be asked whether the manganese ions would complex with the lead ions in the phosphor to form the luminescent species. To answer this it can be noted that there is no difference in the absorption spectrum, either quenched or annealed, for lead or lead and manganese doped NaCl. The formation of a lead-manganese pair would probably result in a new band or a rather large increase in an existing band. Also, the excitation band for manganese luminescence shows absorption of radiation in existing bands of lead, i. e. 4. 28 ev and 4. 55 ev, and not into new bands. The absorption band of lead corresponds to the $^1S_0 \rightarrow {}^3P_1$ transition and is a dipole transition (69). Manganese ion has a very weak absorption spectrum in sodium and potassium chloride (68). All transitions from the ground state are parity and spin-forbidden and the absorption proceeds by a quadrupole transition. Thus any transfer of energy from a lead to a manganese center is a dipole-quadrupole transfer.

Referring again to Figures (4. 10) and (4. 11), a look at the luminescence bands seems appropriate at this point. In the sodium chloride phosphor the only luminescence observed is that of manganese; none for lead is seen. Schulman, Ginther and Klick (64) have investigated the luminescence of lead doped sodium chloride and found emission peaks at 2. 76 ev, and 3. 88 ev. Khalilov et al. (38)

found lead luminescence in NaCl:Pb:Mn at 3.94, 3.45 and 2.82 ev depending somewhat on the excitation energy. The manganese emission band is very nearly gaussian for both the room temperature and low temperature, 90°K, luminescence. The low energy side of the peak is rather difficult to resolve due to the fact that the sensitivity of the photomultiplier decreases rapidly around 1.77 ev. However, by use of a narrow slit this effect may be minimized and a reasonably gaussian curve is observed. The maximum at room temperature is observed at 2.05 ev with a band width at half-maximum of 0.28 ev. This value conflicts with the data of Khalilov et al. (38) who give the maximum at 2.18 ev with a band width of 0.28 ev. The value reported by this work is believed to be correct, i.e., 2.05 ev is the maximum because the degree of purity of this salt precludes interference due to unknown ions. Lowering the temperature to 90°K causes the maximum to shift to 1.91 ev and the bandwidth also narrows to 0.20 ev. Both the room and low temperature emission bands are very close to a gaussian shape. Notice the large shift in energy from the absorption peak at 4.55 ev to the emission band at room temperature at 2.05 ev.

The KCl phosphor shows very strong luminescence of lead along with the manganese emission. As can be seen from Figure (4.11) the lead luminescent is almost perfectly gaussian at both room and low temperatures. In all cases the designation "low temperature"

refers to 90 ± 3° K. The lead emission spectra narrows with temperature from a half width of 0. 46 ev at room temperature to 0. 27 ev at low temperature. The maximum does not shift however, staying at 3. 70 ev. The energy response of the photomultiplier changes relatively more slowly in this energy range than near 1. 77 ev and the waveform of the emission may be corrected to equal photomultiplier response more readily.

The manganese emission in KCl is much the same as that in NaCl. The room temperature maximum is at 2. 02 ev with a band width of half-maximum of 0. 29 ev. Khalilov et al. (38) find a lead emission in KCl:Pb:Mn at 3. 63 ev and a manganese emission at 1. 94 ev. Shvarts and Vale (68) find lead emission for the same phosphor at 3. 61 ev and manganese emission at 1. 85 ev with band widths at room temperature of 0. 58 ev and 0. 36 ev respectively.

At low temperatures the manganese emission in KCl also shifts to lower energy and narrows. The maximum is at 1. 95 ev with a half-width of 0. 22 ev.

Note the similarities in the emission spectrum of manganese in NaCl and KCl: 1) the room and low temperature emission peaks occur at almost the same wavelengths, 2) the low temperature maximum shifts to longer wavelengths in both matrices, and 3) the band widths at half-maximum are almost the same in each matrix for both room and low temperature conditions. This data is summarized

in Table 4. 9.

Table 4. 9. Manganese emission spectrum.

Phosphor	Manganese Emission Peak (ev)		Half Widths (ev)	
	R. T.[c]	L. T.	R. T.	L. T.
NaCl:Pb:Mn	2. 05	1. 91	0. 28	0. 20
	2. 18[a]	--	0. 28[a]	--
KCl:Pb:Mn	2. 02	1. 95	0. 29	0. 22
	1. 94	--	--	--
	1. 85[b]	--	0. 36[b]	--

[a] From reference (38)

[b] From reference (68)

[c] R. T. refers to room temperature and L. T. refers to low temperature, i. e., $90 \pm 3°$ K.

The manganese II ion in sodium or potassium chloride is surrounded by six chlorine ions with octahedral symmetry (the symmetry is disturbed in these hosts when a vacancy is in a nearest neighbor position). The ground state of the d^5 system in a weak octahedral field has one electron in each d orbital all with spins parallel. This is the same ground state as the free ion, ^6S, and it is not split by the ligand field. All excited states of the d^5 system have different spin multiplicity and transitions to them are spin forbidden. Because of weak spin-orbit interactions, however, these

transitions are not totally absent and very weak absorption bands are seen. Figure (4.14) shows a simplified energy level diagram for the manganese II ion in an octahedral field showing the ^6S ground state and only the quartet states. If the emission transition takes place between the ^4G excited state and the ^6S ground state as seems reasonable, then a value of Dq = 1200 cm^{-1} would be obtained from this curve as shown from the solid vertical line in the figure. McClure (49, p. 426) gives a value of Dq = 750 cm^{-1} for $6H_2O$ octahedrally positioned about a divalent manganese and Cotton and Wilkinson (12, p. 702) find Dq = 860 cm^{-1} for the $(Mn(H_2O)_6)^{+2}$ ion. Of course, if the emission is about 2.04 ev for manganese then the absorption should be at a higher energy to take account of the Stokes' shift. Hence Dq = 1200 cm^{-1} is certainly an upper limit to the strength of the ligand interaction. The spectrochemical series predicts a stronger ligand interaction for H_2O than for Cl^- and Dq ought to be less for Cl^- than for H_2O. More will be said about this at the end of this section.

Inspection of Figure (4. 14) will show that for sufficiently high value of 10 Dq the ground state will cease to be ^6S. Cotton and Wilkinson (12, p. 705) note that the ground state will become a doublet state (not shown) in which only one electron is unpaired. The pairing energy is quite high however and only a few of the strongest ligands can increase 10 Dq enough to cause spin pairing. Transitions from this new ground state would not be spin forbidden so the transitions would be allowed and hence would be dipole. No

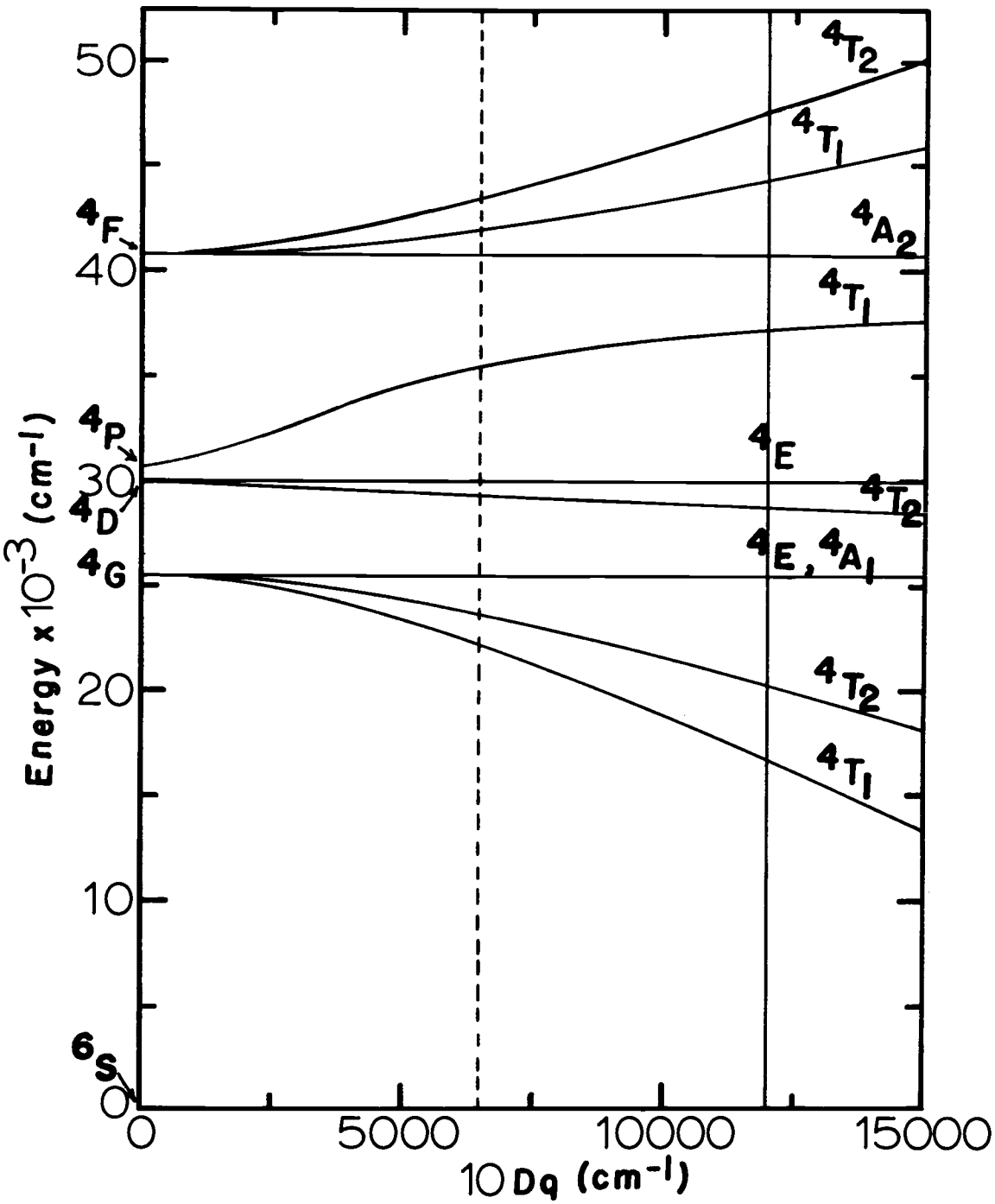

Figure 4.14. Partial energy level diagram showing only the quartet states for a d^5 ion in an octahedral (and/or tetrahedral) field. From Cotton and Wilkinson (12, p. 702). The vertical solid line is at 10 Dq = 12,000 cm^{-1} - the upper limit to the strength of the ligand interaction as determined from the emission of manganese. The dashed vertical line is at 10 Dq = 6500 cm^{-1} - the value of the ligand field interaction found from postulating Mn^{+2} absorption at 2.76 ev.

allowed transitions are noted in the absorption spectrum of manganese in either sodium or potassium chloride so the ground state is still ^6S. Since the symmetry about the manganese II ion is very nearly the same in both sodium and potassium chloride, it is not surprising that the emission peaks are so similar.

It is possible to distort the octahedral field around a manganese ion in several ways: 1) a vacancy in the nearest neighbor position, i. e., associated vacancy, 2) another manganese in the nearest neighbor position, or 3) a lead ion in the nearest neighbor position. One of the more important assumptions in Dexter's theory is that effects depending on pairs or clusters of activators are unimportant and, for the dipole quadrupole case, that the sensitizer and activator are sufficiently separate so that spin exchange effects are not important.

In order to study the effects of distortion on the ligand field a heavily doped sodium chloride crystal was used. "Heavily doped" was a concentration of about 2.6×10^{-3} mole fraction Mn (by polarography) and 2×10^{-4} mole fraction Pb (by optical absorption). It was concentrated enough that the annealed sample was opaque, indicating considerable precipitation of impurity. The low temperature spectrum of this salt was studied as an annealed sample and as a quenched one. When quenched the sample was clear to visible light and the ultraviolet absorption spectrum cleared up considerably.

The low temperature spectra of the annealed and quenched sample are shown in Figure (4. 15). The quenched sample has a maximum at 1.95 ev and a half-width of 0. 26 ev. The shape of the curve is also very nearly gaussian. The quenched emission band also has a small side band at about 2. 32 ev. The annealed sample has a maximum at 1. 92 ev and a half-width of 0. 28 ev. There is also a side band making a rather strong appearance at 2. 26 ev with a half-width of 0. 38 ev.

Except for the small side band, the spectrum of the quenched sample looks quite a bit like the other spectra of quenched phosphors in which the concentration was perhaps a factor of 50 less. In quenching of course, the temperature is dropped very quickly and the ions are frozen in the positions occupied at the elevated temperature. It seems reasonable to assume that the ions are dispersed randomly throughout the crystal at high temperatures, the precipitated phase would dissolve since the solubility increases with temperature, and any preferential formation of Pb-Mn or Mn-Mn pairs would be at a minimum. That the precipitated phase disappears at high temperatures is obvious because opaque samples become clear when heated and quenched. Watkins (73) in studying manganese II in alkali chlorides by electron spin resonance observed the changes in the ESR. spectrum with temperature. He concluded that above about 450°C manganese II ions exist only as

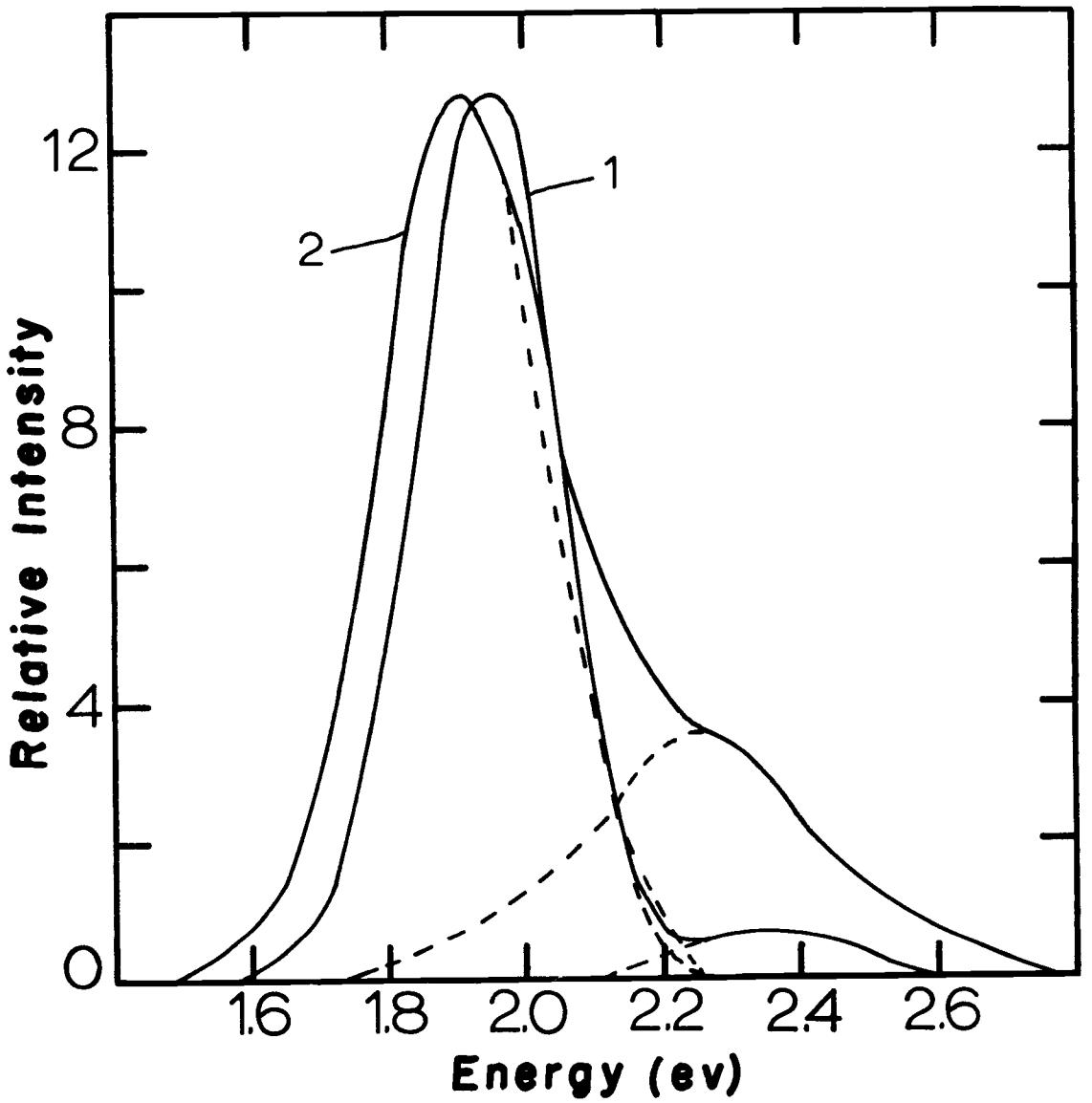

Figure 4. 15. Growth of side band as a function of heat treatment for NaCl:Pb:Mn. Spectrum 1 is the sample quenched in liquid nitrogen after heating at 600° C for 15 minutes. Spectrum 2 is the same sample annealed to room temperature. Both curves normalized to the same main peak heights. Both curves obtained at 90 ± 3°K.

isolated Mn^{+2} ions, Mn^{+2} with a positive ion vacancy in the nearest cation neighbor position, or Mn^{+2} with a positive ion vacancy in the next-nearest neighbor position. Thus the large main band in the quenched sample is due to isolated Mn^{+2}, Mn^{+2} - nn vacancy or Mn^{+2} - nnn vacancy complexes. The side band at 2. 26 ev can be attributed to manganese in a precipitated phase, Mn^{+2} - Mn^{+2} pairs, or Mn^{+2} - Pb^{+2} pairs. The possibility of the Mn^{+2} - Pb^{+2} pairs can be investigated by comparing the excitation spectra for the 2. 26 ev and 1. 92 ev emissions in the annealed sample. The Mn^{+2} ion may cause a large enough perturbation on the absorption spectrum of Pb^{+2}, if it is in an adjacent position, to show a new absorption band. The excitation spectra are shown in Figure (4. 16).

The maximum of the excitation peak for the 2. 26 ev emission is at 4. 28 ev and that for the 1. 92 ev emission is at 4. 35 ev. From the shapes of the excitation curves it looks as though the 2. 26 ev emission comes almost exclusively from absorption in the 4. 55 ev band of lead. Comparison of these curves with the quenched and annealed excitation spectra in Figure (4. 12) shows that the excitation curve for 1. 92 ev emission follows closely the line for the quenched sample while the excitation curve for 2. 26 ev emission follows the annealed spectrum around 4. 28 ev. Since the 4. 28 ev absorption band in lead has been tentatively assigned to lead-lead pairs, it seems possible that the 2. 26 ev emission band is due to manganese

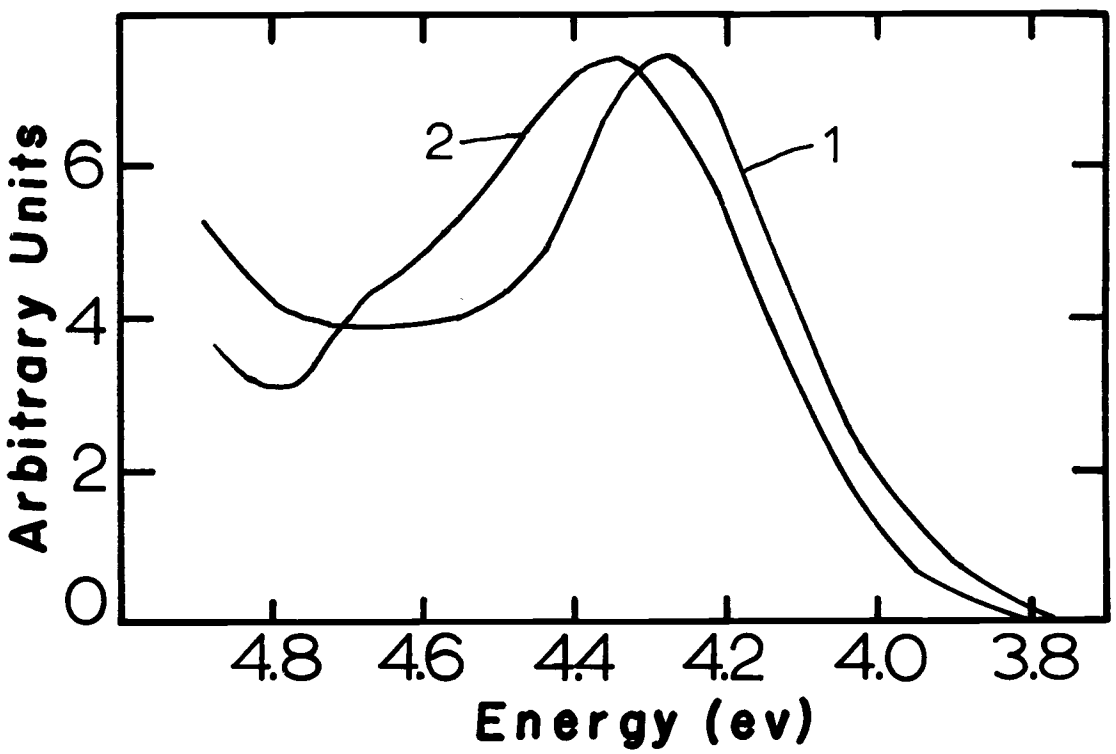

Figure 4.16. Excitation spectra for an annealed sample of NaCl:Pb;Mn. Spectrum 1 is the excitation curve for 2.26 ev emission. Spectrum 2 is the excitation curve for 1.92 ev emission. Both curves obtained at 90 ± 3°K.

ions associated with these lead-lead pairs. Of course, the magnitude of the difference in the excitation spectra, while certainly greater than experimental error, is not great enough to justify a definite assignment. This analysis has not ruled out the formation of precipated manganese chloride or of Mn^{+2} - Mn^{+2} pairs.

KCl:Pb:Mn phosphors show a substantially smaller side band for similar concentrations of impurities than the NaCl case. Quenching experiments discussed before for lead-doped KCl show that lead has little tendency to form aggregates or precipitate out even when annealed. The relative absence of a side band for annealed KCl:Pb:Mn suggests that there are no lead-lead pairs with which the manganese ions can combine. The diffusion studies reported in another section also indicate that manganese is more soluble in sodium chloride than potassium chloride. Hence if Mn^{+2} - Mn^{+2} pairs or manganese chloride-precipitated phase were to form, one would expect them to form somewhat more readily in KCl. If the side band were due to Mn^{+2} - Mn^{+2} pairs or manganese chloride-precipitated phase formation, it should be at least as noticeable in KCl as in NaCl. It is much smaller in KCl, so this suggests that the side band at approximately 2.26 ev is due to manganese associated with lead-lead pairs or perhaps with a precipitated phase of lead chloride.

The 2.26 ev peak is somewhat closer to the value for the

maximum of manganese emission in NaCl:Pb:Mn reported by Khalilov et al. (38) that was mentioned earlier. The phosphor single crystals that were used by these authors were grown by Kyropoulos technique from melts with activator concentrations of 0.01 and one mole percent. The crystal used for our heavily doped experiment was grown from a melt with concentrations of 0.8 mole percent manganese and 0.7 mole percent lead. With the higher concentration of impurities in the melt the manganese in the crystal may have been present almost entirely in a separate phase or precipitated with lead chloride. However, the band width at half-maximum reported at room temperature for the 2.26 ev emission is quite a bit narrower than that reported here for 90°K, i.e., 0.28 ev (38) versus 0.38 ev (this work).

This treatment of the absorption, excitation, and emission spectra of KCl:Pb:Mn and NaCl:Pb:Mn phosphors has indicated the method in which energy is transferred from a sensitizer atom (lead) to an activator atom (manganese). The absorption and excitation spectra show that energy is absorbed only in the lead by a dipole mechanism and somehow is transferred to the manganese from whence luminescence occurs. Manganese has only a very weak absorption spectrum indicating a quadrupole mechanism. Transfer of energy from lead to manganese can occur in this system only by a dipole-quadrupole interaction. This supposes that enough care has

been taken to insure that the impurities are actually distributed throughout the lattice randomly and not in small pockets of precipitated phases throughout the crystal. The experiments mentioned previously indicate that quenching provides such insurance. The mechanism of the energy transfer giving luminescence in the side band where the manganese and lead ions are associated may be by means of localized excitons as discussed by Dow (17) or by electron spin exchange as discussed by Dexter (15).

It would be of interest to consider these phosphors which exhibit dipole-quadrupole transfer in terms of Dexter's theory of transfer of energy outlined previously. Dow (17, p. 1-10) in reviewing Dexter's theory states equation (2.17) as

$$P_{SA}(dq) = \frac{1}{\tau_s} \frac{R_{dq}^8}{R^8} \tag{4.13}$$

where R_{dq}^8 may be expressed in terms of the absorption and emission spectra for the single impurities S and A. He expresses the quantum efficiency as

$$\bar{\eta}_q(dq) = \frac{P_{SA}(dq)\tau_s}{P_{SA}(dq)\tau_s + 1} = \frac{R_{dq}^8}{R_{dq}^8 + R^8} \tag{4.14}$$

then

$$\bar{\bar{\eta}}_q(dq) = \frac{\pi^2 R_{dq}^3 x_a C^+}{2 \sin(3\pi/8)} + Q(x_a^2) \tag{4.15}$$

$Q(x_a^2)$ represents terms non-linear in x_a. Dow then states that the non-linear terms arising in equation (4. 15) result from the invalid assumption that energy is transferred to the nearest neighbor only. This assumption of course, is invalid at high concentrations of the activator, x_a. In the region in which the two atom model of Dexter is valid the average quantum yield for transfer from S is linear in the activator concentration as seen by equation (4. 15). Hence in order for Dexter's theory to be valid the quantum yield must be linear in the activator concentration. These quantities have been plotted in Figure (4. 17).

The slope of the straight portion of the line in Figure (4. 17) is equal to 1. 08 or approximately 1. Therefore, the quantum yield is proportional to the first power of the concentration of the activator in that region as predicted by equation (4. 15). Sodium chloride was the base material used in all five phosphors illustrated in Figure (4. 17) so the value for C^+ is the same for each sample. When the activator concentration increases above 1.5×10^{-4} mole fraction of manganese the experimental curve starts to fall off from the theoretical due to the failure of the assumption that energy is transferred to nearest neighbors only. The limit of applicability of Dexter's theory for the NaCl:Pb:Mn phosphor can be set at approximately 10^{-4} mole fraction as compared to Dow's estimate of 10^{-3} mole fraction for the dq case. All phosphors discussed here have

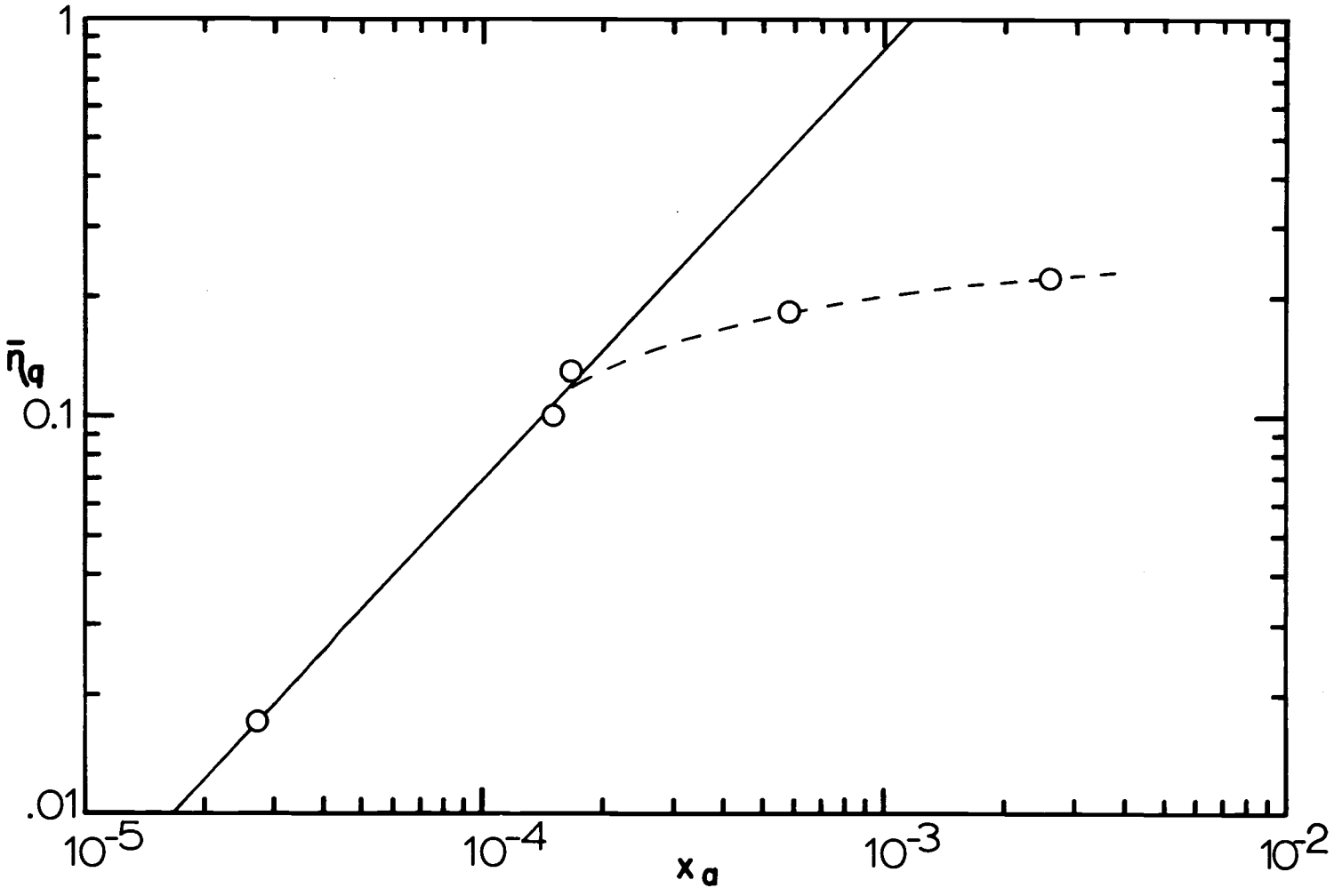

Figure 4. 17. Average quantum efficiency, $\bar{\eta}_q$, as a function of x_a for the NaCl:Pb:Mn phosphor. The slope of the solid line is approximately one indicating linear dependence of the quantum efficiency on mole fraction of manganese in this region. Dashed line indicates the deviation from linearity as the concentration of manganese is increased. All quantum efficiency measurements made at 90 ± 3° K.

been heated for one hour and quenched by immersion in liquid nitrogen. They all exhibit little or no side band.

Dexter's theory relates the quantum yield to activator concentration indirectly through y as shown in Figure (2. 2). Equations (2. 18) and (2. 19) relate x_a to the reduced concentration, y. If we can assume that Dexter's theory applies for $x_a = 1.5 \times 10^{-4}$ and fails for x_a larger than this as displayed in Figure (4. 17), then $\overline{\eta}_q = 0.1$ corresponds to $y = 0.08$. This gives a value of $y = 0.08$ for $x_a = 1.5 \times 10^{-4}$ and aligns x_a and y_a for <u>this</u> case of dq transfer. Figure (4. 18) shows the quantum efficiency as a function of y_a with the experimental points from Figure (4. 17) included. The x_a values shown above the figure have been set by $x_a = 1.5 \times 10^{-4}$ and $\overline{\eta}_q = 0.1$. y_a is found from the figure to be 0. 08. Now γ may be estimated. Equation (2. 19) rearranged gives

$$\gamma = \frac{y}{C^+ x_a} = \frac{0.08}{(2.23 \times 10^{22}\ \mathrm{cm}^{-3})(1.5 \times 10^{-4})}$$

$$\gamma = 23.9 \times 10^{-21}\ \mathrm{cm}^3$$

where $C^+ = 2.23 \times 10^{22}\ \mathrm{cm}^{-3}$ for NaCl. Solving equations (2. 17) and (2. 18) for γ we have

$$\gamma^{8/3} = \frac{1540\pi a \hbar^9 c^8}{n^6 \tau_a} \frac{g_a'}{g_a} \left(\frac{\xi}{K^{1/2}\xi_c}\right)^4 \int \frac{f_s(E)F_a(E)}{E^8}\, dE. \quad (4.16)$$

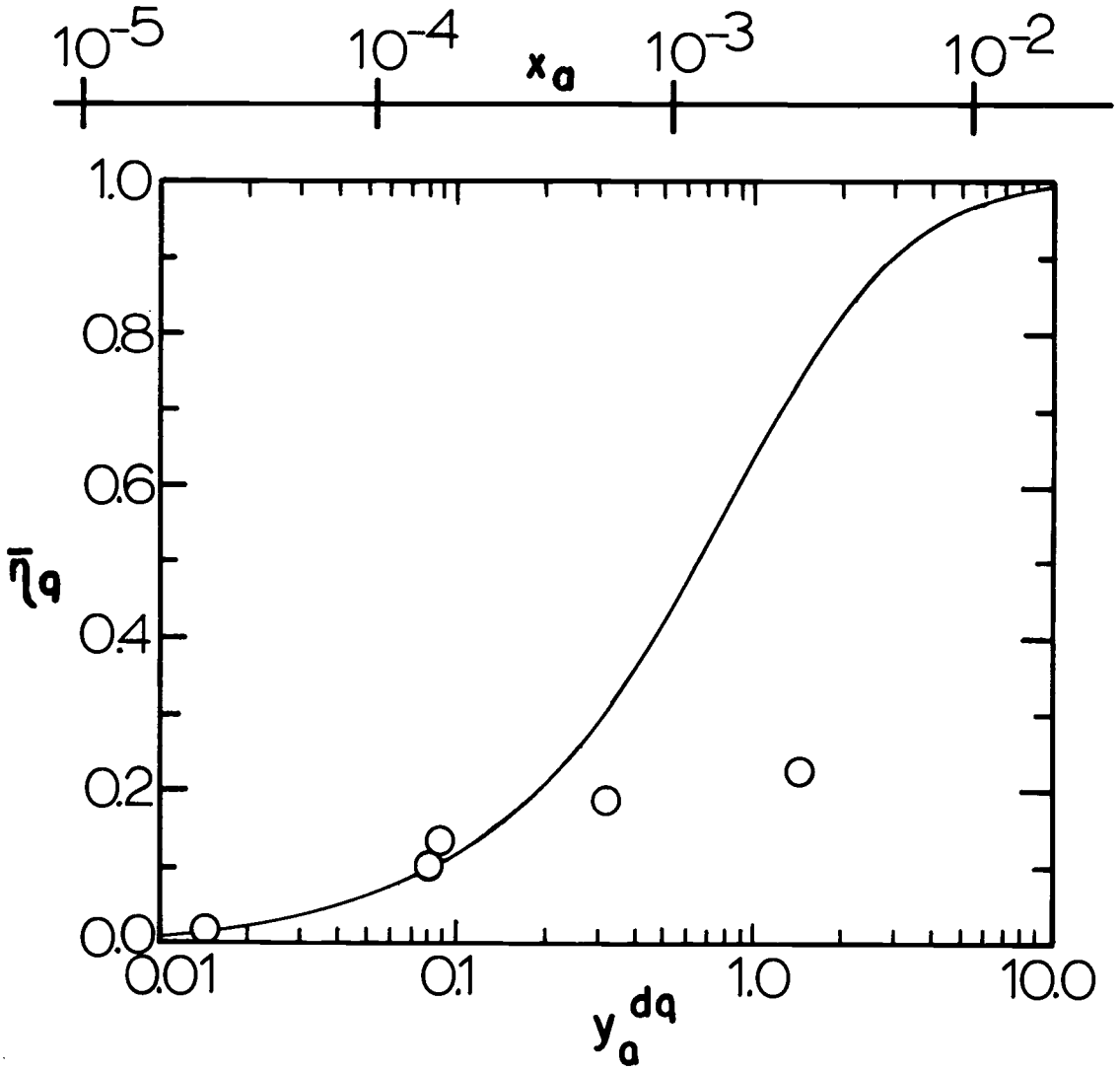

Figure 4. 18. The variation of quantum efficiency with reduced activator concentration, y_a^{dq}, for dq transfer. The experimental points are those from Figure (4. 17) and they are placed on this figure by requiring that the experimental point for $x_a = 1.5 \times 10^{-4}$ and $\bar{\eta}_q = 0.1$ be on the theoretical curve. This fixes the values of x_a above the graph. It also establishes a correspondence between $x_a = 1.5 \times 10^{-4}$ and $y_a^{dq} = 0.08$ and in this way fixes gamma. All quantum efficiency measurements at 90 ± 3° K.

Having determined a value for γ we are now in a position to make some deductions about the overlap of the lead and manganese impurities in NaCl and also about which lead band overlaps with the manganese band. As reported by Schulman, Ginther and Klick (64), NaCl:Pb shows luminescence at 3.88 ev and 2.76 ev. Some estimates must be made for the quantities in equation (4.16): n is the index of refraction and has a value of 1.544 for NaCl at 2.10 ev (9), $\bar{n}$ is expressed in units of ev-sec, c is expressed as cm/sec, τ_a is the lifetime of the manganese in the excited state and Dexter assigns a value of 0.1 sec. Since the average field strength in the medium is reduced by the ratio $1/K = (\xi_c/\xi)^2$ the quantity $(\xi/K^{1/2}\xi_c)^4$ is set equal to unity, α is given as 1.266 by Dexter, and g_a'/g_a is the ratio of the degeneracies of the manganese in the excited and ground states. The ground state of manganese is the case where all the spins are parallel and is non-degenerate, i.e., $g_a = 1$. The first excited state is the case where four spins are aligned and one is inverted and the degeneracy is five. g_a'/g_a for manganese is 5. Substituting these values into equation (4.16) and rearranging we get

$$\int \frac{f_s(E)\, F_a(E)}{E^8}\, dE = 1.41 \times 10^{-4}\ ev^{-9}$$

for $\gamma = 23.9 \times 10^{-21}$. E is defined as $(w_s' - w_s)$ or $(w_a' - w_a)$, i.e. it is the energy exchanged from sensitizer to activator. It is the

energy of emission of lead and of absorption of manganese. The assumptions inherent in this theory require that the sensitizer not be disturbed by the activator so it is assumed that lead will still have emission bands at 3.88 ev and 2.76 ev. Consider $E = 3.88$ ev then

$$\int f_s(E)\, F_a(E)\, dE = 7.2\ (ev)^{-1}$$

For $E = 2.76$ ev we get

$$\int f_s(E)\, F_a(E)\, dE = 0.48\ (ev)^{-1}$$

The integral $\int f_s(E)\, F_a(E)\, dE$ measures the degree of overlap of the emission band of the sensitizer with the absorption band of the activator. Perfect overlap would be $1/1\ (ev)^{-1}$ and rather poor overlap would be $1/10\ (ev)^{-1}$ where ten percent of the areas of the two curves would be in common. The units of $(ev)^{-1}$ come from the normalization requirement that $\int f_s(E)\, dE = 1$ and $\int F_a(E)\, dE = 1$. Then the range of values to be expected for $\int f_s(E)\, F_a(E)\, dE$ is 1 to 0. The value $7.2\ (ev)^{-1}$ calculated for $E = 3.88$ ev is unacceptably large while the value of $0.48\ (ev)^{-1}$ for $E = 2.76$ ev is within the acceptable range.

The value for

$$\int \frac{f_s(E)\, F_a(E)}{E^8}\, dE$$

is a rather strong function of concentration varying as the 8/3 power of $1/x_a$. In order to obtain a reasonable value of the overlap integral, say $1/2(ev)^{-1}$, for E = 3.88 ev the concentration would be about $x_a = 4 \times 10^{-4}$ at which $\overline{\eta}_q = 0.1$. As can be seen from the dotted line in Figure (4.17) a concentration of 4×10^{-4} would have a value of about 0.17 for $\overline{\eta}_q$--not really very much variation for quantum efficiency measurements. The measurements of concentration were done polarigraphically and are accurate to within plus or minus ten percent. The accuracy of the quantum efficiency measurements cannot be placed at better than plus or minus ten and probably is around plus or minus 20 percent.

Is the assignment of E = 2.76 ev reasonable? Consider again the energy level diagram of Figure (4.14). If the absorbance of manganese occurs at 2.76 ev, or 22,200 cm^{-1}, and is a ^6S to ^4G transition then Dq is about 650 cm^{-1}. This is shown in Figure (4.14) by the dashed line. As mentioned before the ligand interaction ought to be less for Cl^- than for H_2O and Dq = 650 cm^{-1} is less than that reported for $(Mn(H_2O)_6)^{+2}$ by Cotton and Wilkinson (12, p. 702) or McClure (49, p. 426).

Assignment of E = 3.88 ev to the transition would require a ^6S to ^4P assignment at Dq = 100 cm^{-1}. One would certainly expect more of a ligand field interaction from Cl^- ions in an octahedral configuration than 100 cm^{-1}.

Therefore, the mechanism of energy transfer from lead to manganese in sodium chloride is a quantum of energy of about 2.8 ev is transferred to manganese with an overlap integral of about $1/2\ (ev)^{-1}$. Since energy is absorbed in Pb^{+2} at about 4.3 ev and transferred at about 2.8 ev, and for manganese is emitted at about 2.0 ev, the Stokes shift for lead is 1.5 ev and for manganese is 0.8 ev.

The foregoing treatment has been based on the assertion that the predominant transfer path is dipole-quadrupole interaction. As discussed previously Dow believes that much supposed dipole-quadrupole transfer is actually transfer via virtual excitons. He uses equation (2.24) to estimate that virtual excitons contribute significantly to dq transfer over shorter than four lattice spacings. This is based on using a value for δa of 1 ev, δa is the energy separation in ev of the excited state of the impurity and the lowest host exciton band. Lead impurity in NaCl absorbs at about 4.5 ev and the band edge is around 8.5 ev. The difference is 4 ev. Substitution of 4 ev for δa in equation (2.24) gives for the ratio Δ s. r. $/(\Delta/K)$: 0.4 for $n = 2$, 0.05 for $n = 3$, and 0.004 for $n = 4$. Hence virtual exciton transfer is not important in NaCl due primarily to its large energy gap. This is also true of KCl since its band edge is at about the same energy.

Dow (17, p. 31) expresses Γ in a somewhat different

manner as

$$\Gamma \approx \frac{(\beta + \delta\beta_o)(\beta + \delta\beta_p)}{\beta\Delta} \left(\frac{\beta}{\delta a}\right)^{R/a_L} \qquad (4.17)$$

where β is the host-nearest neighbor coupling $(\beta + \delta\beta_o)$ and $(\beta + \delta\beta_p)$ is the coupling of sensitizer and activator respectively to the nearest host atom, a_L is the lattice constant and δa, Δ, and R have been defined before. From this equation he notes that the virtual exciton mechanism can be identified by monitering luminescence intensity at fixed impurity concentrations as a function of δa. Variation of δa may be accomplished by substitution of an isotope for the absorber or by pressure modulation. For lead not much variation of the first excited state transition in lead may be expected for various isotopes. It is implied (17, p. 21-22) that variation of δa by means of pressure can be accomplished by distorting the crystal symmetry. Pressures needed to distort the crystal symmetry of NaCl or KCl would be considerable and outside the capabilities of this laboratory.

However, from a consideration of equation (2. 24), the virtual exciton process may be ruled out as a competing mechanism for energy transfer in the NaCl:Pb:Mn and KCl:Pb:Mn phosphors and the transfer mechanism specified as dipole-quadrupole resonance.

V. SUMMARY AND CONCLUSIONS

The diffusion of manganese ion in sodium and potassium chloride was studied. The NaCl:Mn^{+2} diffusion can be represented by

$$D_s = 5.87 \times 10^{-4} \text{ cm}^2/\text{sec } e^{-20,500 \text{ cal/RT}} \qquad (5.1)$$

between the temperatures of 449 and 656°C. The free energy of association of the manganese-vacancy complex is

$$-\Delta G(ev) = -1.090 + 5.0 \times 10^{-4} \text{ T}. \qquad (5.2)$$

The KCl:Mn^{+2} diffusion proved to be more complicated than NaCl:Mn^{+2}. Between the temperatures of 457 and 482°C the impurity-vacancy diffusion coefficient can be represented by

$$D_s = 1.3 \times 10^{10} \text{ cm}^2/\text{sec } e^{-63,000 \text{ cal/RT}}. \qquad (5.3)$$

From 512 to 653°C D_s is given by

$$D_s = 1.16 \times 10^{-2} \text{ cm}^2/\text{sec } e^{-24,300 \text{ cal/RT}}, \qquad (5.4)$$

and in this temperature range the free energy of association is

$$-\Delta G(ev) = -1.598 + 1.06 \times 10^{-3} \text{T}. \qquad (5.5)$$

A "phase change" theory has been postulated to account for the abrupt change in D_s vs. $1/T$ and a preliminary agreement of experiment with a theory of next nearest neighbor association is discussed.

The variation of activation energy for impurity ion movement with size in both NaCl and KCl is discussed and a theory of "directed relaxation" is advanced to account for this. The variation of the entropy of association with impurity ion radius is also discussed but only for the KCl matrix.

The luminescence of NaCl:Pb:Mn and KCl:Pb:Mn phosphors was studied. It was found that the size of a side band of the normal manganese emission grows upon annealing. The manganese emission in NaCl:Pb:Mn was found at 2.05 ev at room temperature and at 1.91 ev at 90 ± 3°K. In KCl:Pb:Mn it was found at 2.02 ev at room temperature and at 1.95 ev at 90 ± 3°K.

The quantum efficiency of NaCl:Pb:Mn was studied as a function of manganese concentration. The samples were quenched to insure that the impurities were randomly distributed and the luminescence due to precipitated phases and impurity pairs was minimized. The theory of Dexter for dipole-quadrupole resonance energy transfer was followed to a concentration of 1.5×10^{-4} mole fraction of manganese for which the quantum efficiency was found to be 0.1. This led to the deduction that the energy absorbed in the 4.28 ev band of lead is transferred to the manganese from the 2.76 ev emission band of

lead with an overlap of about $1/2\ ev^{-1}$. The luminescence of NaCl:Pb:Mn is at 2.05 ev for a total Stokes' shift of about 2.2 ev.

The theory of Dow in which the energy is thought to be transferred from impurity A to impurity B by means of excitons was examined here. Transfer of energy by excitons was found to be not very probably in NaCl:Pb:Mn or KCl:Pb:Mn because of the large energy separation between the lead absorption band and the lowest host exciton band.

BIBLIOGRAPHY

1. Allen, C. A. Diffusion, conductivity and spectral properties of mercury II ion in potassium chloride crystals. Ph. D. thesis. Corvallis, Oregon State University, 1969. 141 numb. leaves.

2. Allen, C. A., D. T. Ireland and W. J. Fredericks. Diffusion of Cd^{+2} ions in single-crystal sodium chloride. Journal of Chemical Physics 47:3068-3072. 1967.

3. Allen, C. A., D. T. Ireland and W. J. Fredericks. Diffusion of lead ions in sodium chloride. Journal of Chemical Physics 46:2000-2001. 1967.

4. Beaumont, J. H. and P. W. M. Jacobs. Energy and entropy parameters for vacancy formation and mobility in ionic crystals from conductivity measurements. Journal of Chemical Physics 45:1496-1502. 1966.

5. Boswarva, I. M. and A. B. Lidiard. The energy of formation of Schottky defects in ionic crystals. United Kingdom Atomic Energy Authority, Atomic Energy Research Establishment, Harwell, Didcot, Berks, 1966. 49 numb. leaves. (T. P. 232 Rev.)

6. Botden, Th. P. J. Transfer and transport of energy by resonance processes in luminescent solids. Philips Research Reports 6:425-473. 1951.

7. Botden, Th. P. J. and F. A. Kroger. Energy transfer in sensitized $Ce_3(PO_4)_2$-Ce-Mn and Ca Si O_3-Pb-Mn. Physica 14:553-566. 1948.

8. Burstein, E. et al. A note on the distribution of impurities in alkali halides. Physical Review 81:459-460. 1951.

9. Chemical Rubber Publishing Company. Handbook of chemistry and physics, ed. by C. D. Hodgeman, R. C. Weast and S. M. Selby. 40th. ed. Cleveland, 1959. 3456 p.

10. Chemla, M. Diffusion d'ions radioactifs dans des cristaux applications. Annales de Physique 1:959-1002. 1956.

11. Claffy, E. W. and C. C. Klick. Energy transport by cascade and reasonance processes in doubly activated phosphors. Journal of the Electrochemical Society 104:445-447. 1957.

12. Cotton, F. A. and G. Wilkinson. Advanced inorganic chemistry. New York, Interscience Publishers, 1962. 959 p.

13. Crank, J. The mathematics of diffusion. London, Oxford University Press, 1956. 347 p.

14. Curie, D. Luminescence in crystals, tr. by G. F. J. Garlick. New York, John Wiley and Sons, 1963. 332 p.

15. Dexter, D. L. A theory of sensitized luminescence in solids. Journal of Chemical Physics 21:836-850. 1953.

16. Dexter, D. L. and R. S. Knox. Excitons. New York, Interscience Publishers, 1965. 139 p.

17. Dow, J. D. Resonance energy transfer in condensed media from a many-particle viewpoint. Unpublished condensation of a Ph. D. thesis. Rochester, New York, University of Rochester, Dept. of Physics, 1968. 38 numb. leaves.

18. Dow, J. D. Resonance energy transfer in condensed media from a many-particle viewpoint. Ph. D. thesis. Rochester, University of Rochester, 1968. 238 numb. leaves. (microfilm)

19. Eisberg, R. M. Fundamentals of modern physics. New York, John Wiley and Sons, 1964. 729 p.

20. Etzel, H. W. and R. J. Maurer. The concentration and mobility of vacancies in sodium chloride. Journal of Chemical Physics 18:1003-1007. 1950.

21. Förster, Th. Versuche zum zwischenmolekularen Übergang von Elektronenanregungsenergie. Zeitschrift für Elektrochemie und angewandte Physikalische Chemie 53:93-100. 1949.

22. Förster, Th. Zwischenmolekulare Energiewanderung und Fluoreszenz. Annalen der Physik, ser. 6, 2:55-75. 1948.

23. Franck, J. and R. Livingston. Remarks on intra- and intermolecular migration of excitation energy. Reviews of Modern Physics 21:505-509. 1949.

24. Fredericks, W. J., F. E. Rostoczy and J. Hatchett. Investigation of crystal growth processes. Palo Alto, 1963. 24 numb. leaves. (Stanford Research Institute. Final report on SRI Project No. PAU-3523)

25. Fredericks, W. J., L. W. Schuerman and L. C. Lewis. An investigation of crystal growth processes. Corvallis, 1966. 78 numb. leaves. (Oregon State University, Department of Chemistry. Final reports on Air Force Contracts AF-AF OSR-217-63 and AF OSR-217-66)

26. Friedlander, G., J. W. Kennedy and J. M. Miller. Nuclear and radiochemistry. 2d. ed. New York, John Wiley and Sons, 1964. 585 p.

27. Fumi, F. G. and M. P. Tosi. Ionic sizes and Born repulsive parameters on the NaCl-type alkali halides. I. The Huggins-Mayer and Pauling forms. Journal of Physics and Chemistry of Solids 25:31-43. 1964.

28. Gie, T. I. and M. V. Klein. Infrared and ultraviolet OH bands in hydroxide-doped KCl, KBr, NaCl and NaBr. Bulletin of the American Physical Society 8:230. 1963.

29. Ginther, R. J. Luminescence of K_4MnCl_6 and KCl(Pb + Mn). Journal of the Electrochemical Society 98:74-81. 1951.

30. Ginther, R. J. Sensitized luminescence of CaF_2(Ce + Mn). Journal of the Electrochemical Society 101:248-257. 1954.

31. Howard, R. E. and A. B. Lidiard. Matter transport in solids. Report on Progress in Physics 27:161-240. 1964.

32. Iida, Y. and Y. Tomono. Diffusion coefficients of Co^{60} and Ni^{63} in NaCl crystals. Journal of the Physical Society of Japan 19:1264. 1964.

33. Kallman, H. and F. London. Über quantenmechanische Energieübertragung zwischen atomaren Systemen. Zeitschrift für Physikalische Chemie, Abteilung B, 2:207-243. 1929.

34. Keneshea, F. J. Jr. and W. J. Fredericks. The diffusion of cadmium ions in solid potassium chloride. Journal of Physics and Chemistry of Solids 26:501-508. 1965.

35. Keneshea, F. J., Jr. and W. J. Fredericks. The diffusion of lead in potassium chloride. Palo Alto. 1962. 33 numb. leaves. (Stanford Research Institute. Contract no. 19(604)-7231, project 5620, task 562001)

36. Keneshea, F. J., Jr. and W. J. Fredericks. Diffusion of lead ions in potassium chloride. Journal of Chemical Physics 38:1952-1958. 1963.

37. Keneshea, F. J., Jr. and W. J. Fredericks. Diffusion of lead ions in solid potassium chloride. Journal of Chemical Physics 41:3271-3272. 1964.

38. Khalilov, A. Kh. et al. Comprehensive investigation of the optical and thermooptical properties of polyactivated alkali-halide crystal phosphors. Bulletin of the Academy of Sciences of the USSR, physical series, 25:325-330. 1961. (Translated from Izvestiya Akademii Nauk SSSR.)

39. Kirs, J. and A. Niilisk. Luminescence of alkali halide phosphors activated with europium. Akademiia Nauk Estonian SSR, Instituta Fiziki i Astronomii Trudy 18:36-50. 1962. (Abstracted in Chemical Abstracts 58:6335h. 1963)

40. Kittel, C. Introduction to solid state physics. 2d. ed. New York, John Wiley and Sons, 1963. 617 p.

41. Klick, C. C. and J. H. Schulman. Luminescence in solids. Solid State Physics 5:97-172. 1957.

42. Kuwabara, G. and K. Aoyagi. Ultraviolet absorption of transition metal ions in alkali-halides. In: Proceedings of the Conference on Photographic and Spectroscopic Optics, Tokyo and Kyoto, 1964. Tokyo 1965. p. 627-630. (Japanese Journal of Applied Physics vol. 4, sup. 1. 1965)

43. Kyropoulos, S. Ein Verfahren zur herstellung grosser Kristalle. Zeitschrift für Anorganische und Allgemeine Chemie 154:308-313. 1926.

44. Lark-Horovitz, K. and V. A. Johnson (eds.). Methods of experimental physics. vol. 6. Solid State Physics. Part B. Electrical, magnetic and optical properties. New York, Academic Press, 1959. 416 p.

45. Lidiard, A. B. Impurity diffusion in crystals (mainly ionic crystals with the sodium chloride structure). Philosophical Magazine, ser. 7, 46:1218-1237. 1955.

46. Lidiard, A. B. Ionic conductivity. Handbuck der Physik 20:246-349. 1957.

47. Lure, B. G., A. N. Murin and R. F. Brigevich. Diffusion and electrolytic migration of manganese ions. Soviet Physics-Solid State 4:1432-1433. 1963. (Translated from Fizika Tverdogo Tela.)

48. Lushchik, N. E. An investigation of luminescence centers in NaCl phosphors activated by mercury-like ions. Akademiia Nauk Estonian SSR, Instituta Fiziki i Astronomii Trudy 10:68-96. 1959. (Abstracted in Chemical Abstracts 54:23776c, 1960.)

49. McClure, D. S. Electronic spectra of molecules and ions in crystals. Solid State Physics 9:399-525. 1959.

50. Mannion, W. A., C. A. Allen and W. J. Fredericks. Diffusion of lead ions in purified NaCl crystals. Journal of Chemical Physics 48:1537-1540. 1968.

51. Mantano, C. On the relation between the diffusion-coefficients and concentrations of solid metals. Japanese Journal of Physics 8:109-113. 1933.

52. Mapother, D., H. N. Crooks and R. Maurer. Self-diffusion of sodium in sodium chloride and sodium bromide. Journal of Chemical Physics 18:1231-1236. 1950.

53. Mellor, J. W. A comprehensive treatise on inorganic and theoretical chemistry. Vol. 12. New York, Longmans, Green and Company, 1932. 944 p.

54. Morlin, Z. The electrical conductivity and the phase transformation of cesium chloride. Acta Physica Academiae Scientiarum Hungaricae 21:137-147. 1966.

55. Murata, K. J. and R. L. Smith. Manganese and lead as coactivators of red fluorescence in halite. American Mineralogist 31:527-538. 1946.

56. Murin, A. N., S. N. Banasevich and Yu. S. Grushko. Diffusion of calcium ions in NaCl + $CaCl_2$ mixed crystals. Soviet Physics-Solid State 3:1762-1766. 1962 (Translated from Fizika Tverdogo Tela.)

57. Pauling, L. The nature of the chemical bond. 3d. ed. Ithaca, Cornell University Press, 1960. 644 p.

58. Pauling, L. and E. B. Wilson. Introduction to quantum mechanics. New York, McGraw-Hill Book Company, 1935. 468 p.

59. Perkin-Elmer Corporation. Instruction manual for Perkin-Elmer 450 spectrophotometer. Norwalk, Connecticut, 1966. 145 p.

60. Perkin-Elmer Corporation. Instruction manual for spectral fluorescence attachment 350-0196. Norwalk, Connecticut, 1963. 30 p.

61. Rothman, S. J., L. W. Barr, A. H. Rowe and P. G. Selwood. Diffusion and conductivity in the NaCl-$ZnCl_2$ system. Philosophical Magazine, ser. 8, 14:501-513. 1966.

62. Schulman, J. H., E. Burstein, R. J. Ginther, M. White and L. W. Evans. Sensitized luminescence of alkali-halide phosphors. Physical Review 76:178. 1949.

63. Schulman, J. H., L. W. Evans, R. J. Ginther and K. J. Murata. The sensitized luminescence of manganese-activated calcite. Journal of Applied Physics 18:732-739. 1947.

64. Schulman, J. H., R. J. Ginther and C. C. Klick. Some optical properties of lead-activated sodium chloride phosphors. Journal of the Optical Society of America 40:854-862. 1950.

65. Schulman, J. H., R. J. Ginther and C. C. Klick. A study of the mechanism of sensitized luminescence of solids. Journal of the Electrochemical Society 97:123-132. 1950.

66. Seevers, R. E. Electrical conductivity of additively colored crystals. Ph. D. thesis, Corvallis, Oregon State University, 1968. 128 numb. leaves.

67. Sheehan, W. F. Physical chemistry. Boston, Allyn and Bacon, 1961. 618 p.

68. Shvarts, K. K. and G. K. Vale. Sensitized luminescence of KCl:Pb:Mn phosphor. Bulletin of the Academy of Sciences of the USSR, physical series, 25:333-334. 1961. (Translated from Izvestiya Akademii Nauk SSSR.)

69. Soovik, Kh. A. Resonance migration of energy in polyactivated ionic crystals. Bulletin of the Academy of Sciences of the USSR, physical series, 29:390-394. 1965. (Translated from Izvestiya Akademii Nauk SSSR.)

70. Stasiw, V. O. and J. Teltow. Uber Fehlordnungsercheinungen in Silberhalogeniden mit Zusatzen. Annalen der Physik, ser. 6, 1:261-272. 1947.

71. Stewart, W. H. and C. A. Reed. Diffusion measurement of Mn^{+2} in single-crystal NaCl using electron spin resonance absorption intensity. Journal of Chemical Physics 43:2890-2892. 1965.

72. Tosi, M. P. and F. G. Fumi, Ionic sizes and Born repulsive parameters in the NaCl-type alkali halides. II. The generalized Huggins-Mayer form. Journal of Physics and Chemistry of Solids 25:45-52. 1964.

73. Watkins, G. D. Electron spin resonance of Mn^{+2} in alkali chlorides: association with vacancies and impurities. Physical Review 113:79-90. 1959.

74. Watkins, G. D. Motion of Mn^{+2}-cation vacancy pairs in NaCl: study by electron spin and dielectric loss. Physical Review 113:91-97. 1959.

APPENDICES

APPENDIX I. RAW DATA FOR DIFFUSION MEASUREMENTS

Table 5.1. Values used to calculate K in equation (3.1).

Temp. (°C)	Sample	V/V*	c' (mg/ml)	A (cm^2)	r (c/min)+	K x 10^8
NaCl host:						
449	104A	1/8	1.292	1.081	8.33×10^4	9.61
	B	1/8	1.292	1.069	8.33×10^4	9.72
502	87A	1/8	1.241	0.820	1.03×10^5	9.82
	B	1/8	1.241	0.563	1.03×10^5	14.3
537	85B	1/8	1.292	1.175	1.03×10^5	7.16
551	103A	1/8	1.292	1.077	8.85×10^4	9.09
	B	1/8	1.292	1.079	8.85×10^4	9.07
601	120A	3/8	1.491	0.635	1.25×10^5	37.9
	B	3/8	1.491	0.606	1.25×10^5	39.7
606	108A	1/8	1.292	1.307	1.22×10^5	5.46
656	116A	3/8	1.491	1.267	1.30×10^5	18.2
	B	3/8	1.491	1.240	1.30×10^5	18.6
KCl host:						
457	97A	1/8	1.292	1.737	1.00×10^5	6.94
	B	1/8	1.292	1.743	1.00×10^5	6.92
465	111A	1/8	1.292	1.719	1.21×10^5	5.81
	B	1/8	1.292	1.719	1.21×10^5	5.81
474	125A	1/6	1.513	0.952	1.05×10^5	18.9
	B	1/6	1.513	0.900	1.05×10^5	20.0
482	123A	1/4	1.491	1.059	1.13×10^5	23.3
	B	1/4	1.491	1.026	1.13×10^5	24.0
512	118A	1/4	1.491	1.107	1.29×10^5	19.5
	B	1/4	1.491	1.061	1.29×10^5	20.4
533	119A	1/4	1.491	1.298	1.26×10^5	17.0
	B	1/4	1.491	1.277	1.26×10^5	17.3
564	124A	1/6	1.513	0.868	1.08×10^5	20.1
	B	1/6	1.513	0.866	1.08×10^5	20.2
583	117A	1/4	1.491	1.141	1.30×10^5	18.8
	B	1/4	1.491	1.131	1.30×10^5	19.0
616	107A	1/8	1.292	1.270	1.21×10^5	7.86
	B	1/8	1.292	0.981	1.21×10^5	10.2
653	122A	3/8	1.491	0.977	1.15×10^5	37.1
	B	3/8	1.491	0.985	1.15×10^5	36.8

+ r is counts/minute for a 25 μl standard.

APPENDIX II

RAW DATA FOR LUMINESCENCE MEASUREMENTS

Percent transmittance of Perkin-Elmer reference screens as measured in P-E 450 spectrophometer.

Screen No.	Percent Transmittance
1	53. 1
2	31. 6
3	15. 0
4	7. 22
5	3. 3
6	1. 3

Figure (5. 1) is a curve of the experimental data of relative recorder deflection as a function of energy incident on the photomultiplier. Thus it is a measure of the relative detector sensitivity as a function of wavelength, i. e. "S" as defined in section 3.

Figure (5. 2) is a curve of relative F values as a function of wavelength which was calculated from equation (3. 16) with n, the number of reflections, equal to ten. This curve was used to relate the areas under the absorbance curves and emission curves for the quantum efficiency measurements.

Figure (5. 3) shows the reflectance spectra for various concentrations of activator for calculation of quantum efficiency. The area of the reflectance spectrum of a pure sample is shown in Figure (3. 4). Note the different scale factor.

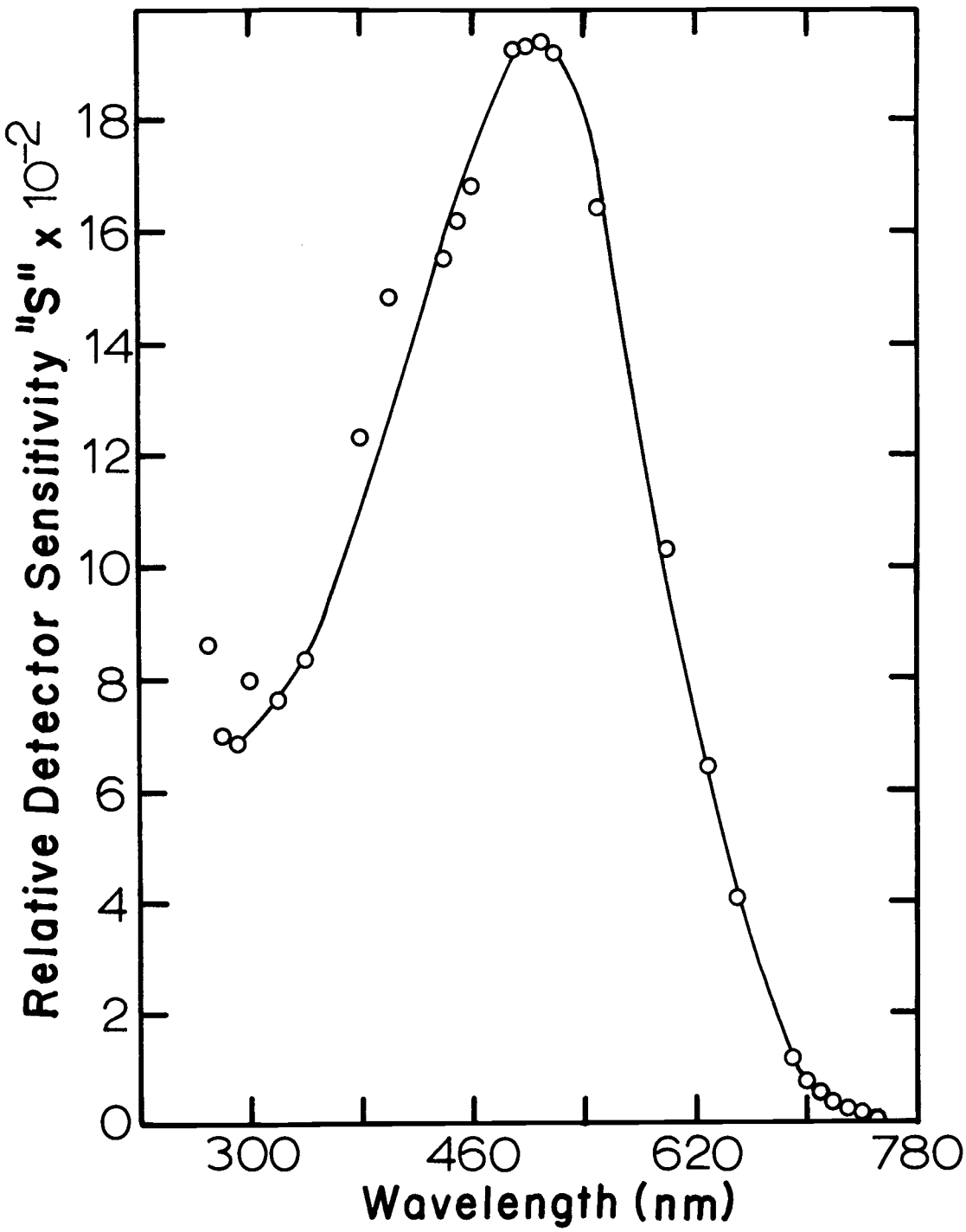

Figure 5. 1. Relative recorder deflection as a function of energy incident on the photomultiplier of the Perkin-Elmer 450 spectrophotometer.

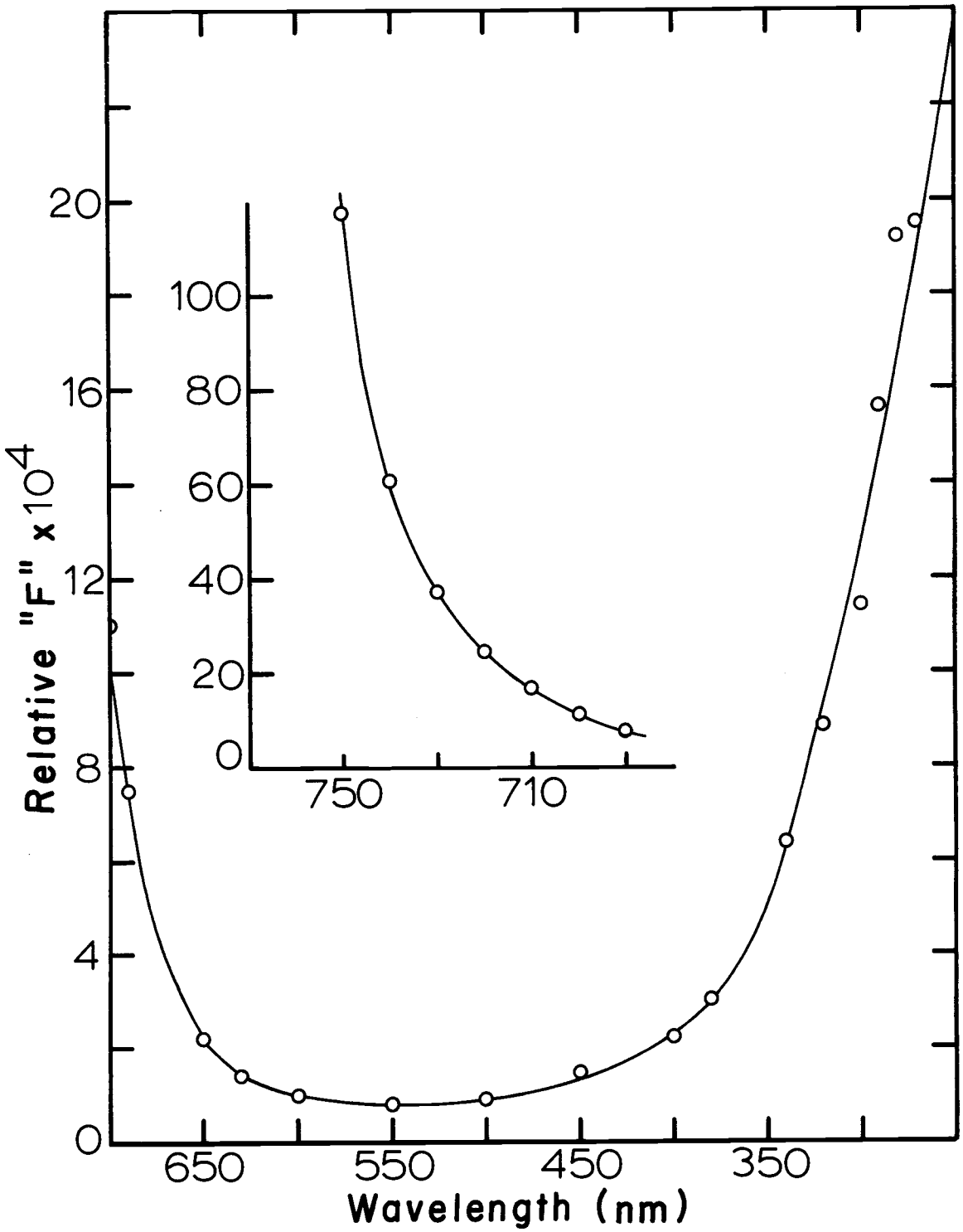

Figure 5. 2. Relative "F" as a function of wavelength. Inset has the same coordinates but different scales.

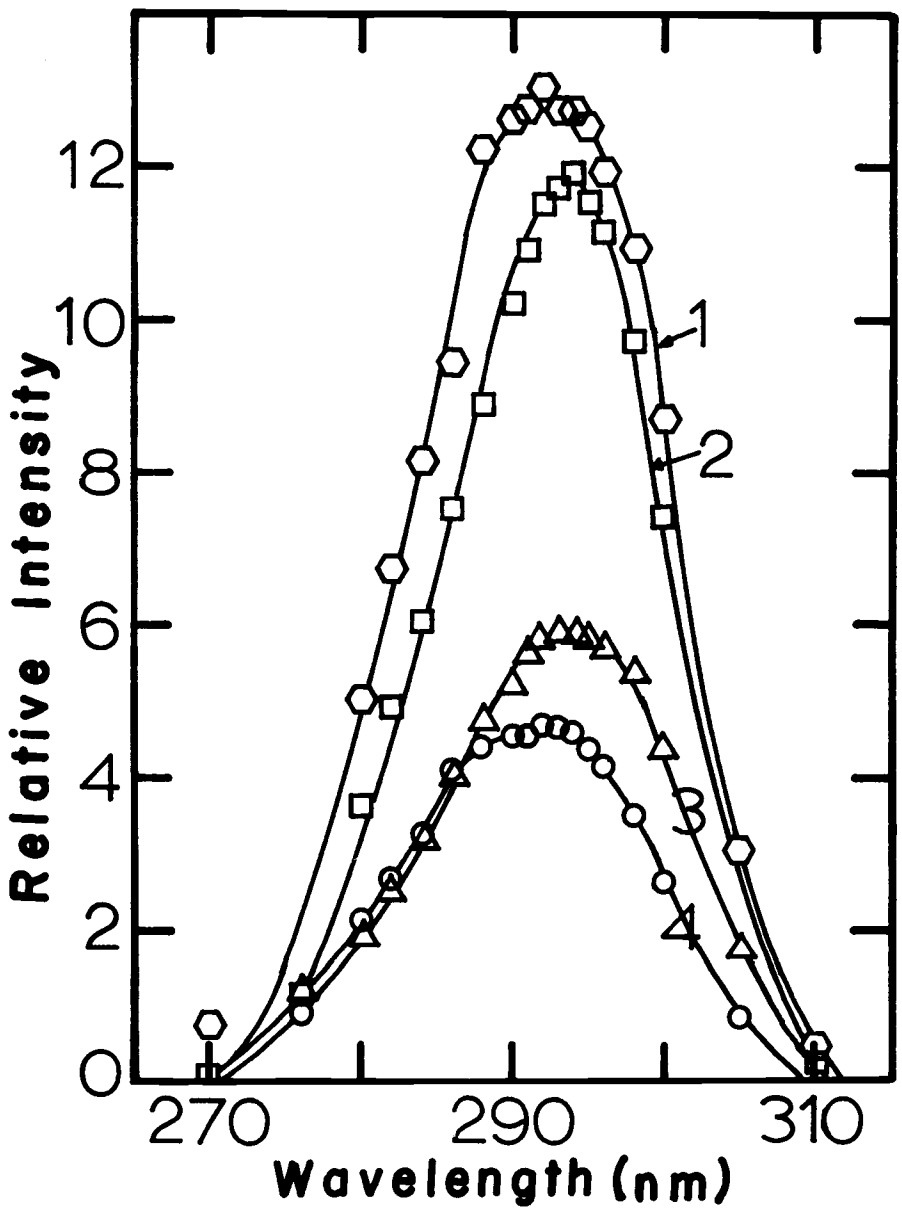

Figure 5.3. Reflectance spectra as a function of wavelength for various activator concentrations. 1:x_a = 1.5×10^{-4}; 2:x_a = 1.66×10^{-4}; 3:x_a = 5.8×10^{-4}; 4:x_a = 2.7×10^{-5}.

Figure (5.4) shows the emission spectra for the luminescence associated with the above reflectance (absorption) spectra for various x_a. Any emission on the short wavelength side of 550 nm is neglected in the measurement of the area under these luminescence curves.

The area of the reflectance spectrum for the pure NaCl is 696 R. I. -nm and this area is used for all the samples except $x_a = 2.7 \times 10^{-5}$. The area of this sample is to be subtracted from a pure reflectance spectrum of area 580 R. I. -nm because these measurements were made about six months prior to the other measurements.

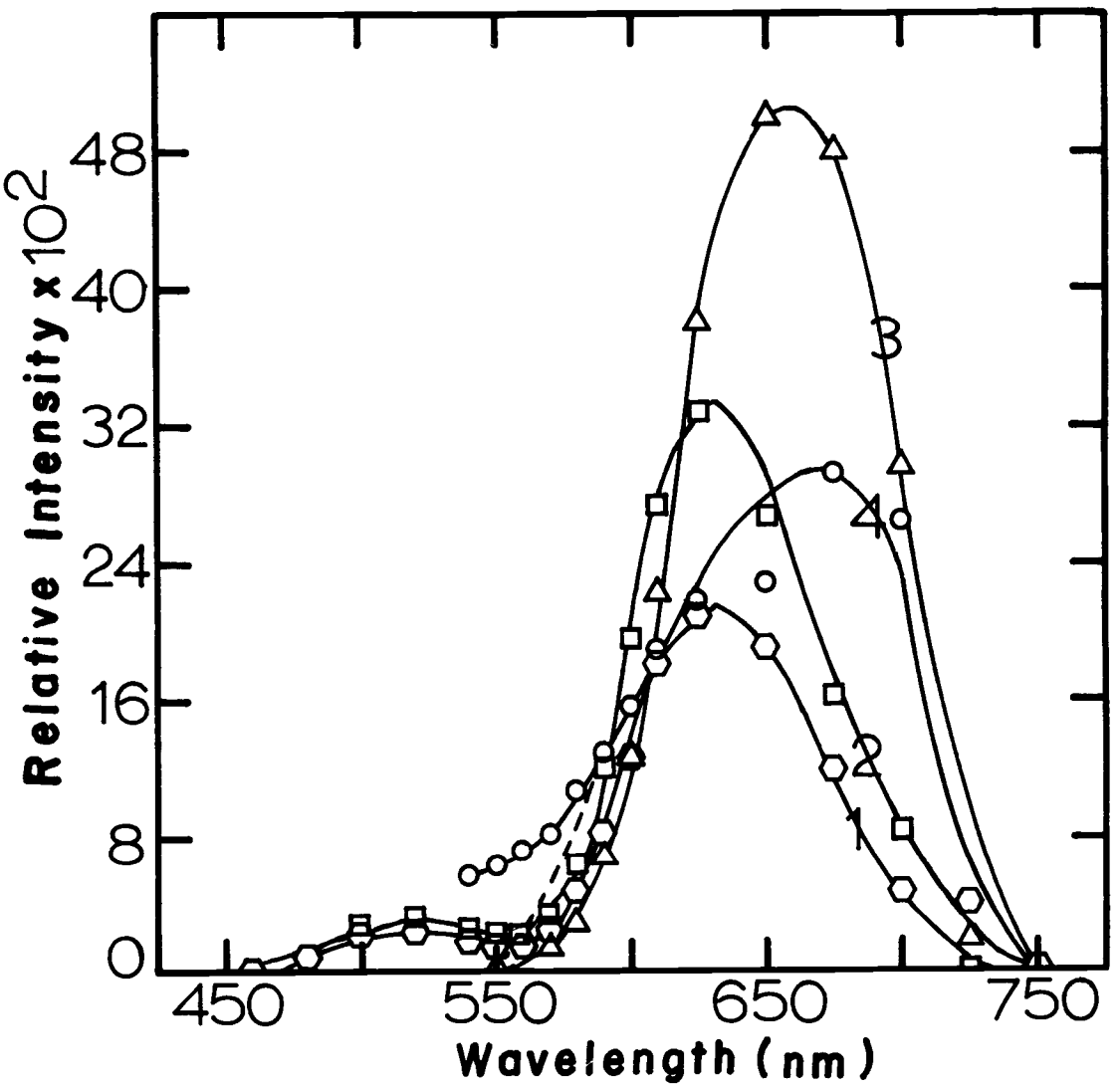

Figure 5.4. Emission spectrum as a function of wavelength for various activator concentrations. 1: $x_a = 1.5 \times 10^{-4}$; 2: $x_a = 1.66 \times 10^{-4}$; 3: $x_a = 5.8 \times 10^{-4}$; and 4: $x_a = 2.7 \times 10^{-5}$ (intensity multiplied by 10 to fit on scale).